THE INFLUENCE OF MANUFACTURING DEFECTS ON STRUCTURAL PERFORMANCE OF COMPOSITE OVERWRAPPED PRESSURE VESSELS

A THESIS SUBMITTED TO
THE GRADUATE SCHOOL OF NATURAL AND APPLIED SCIENCES
OF
MIDDLE EAST TECHNICAL UNIVERSITY

BY

KIVANÇ YURDAKUL

IN PARTIAL FULFILLMENT OF THE REQUIREMENTS
FOR
THE DEGREE OF MASTER OF SCIENCE
IN
METALLURGICAL AND MATERIALS ENGINEERING

FEBRUARY 2022

Approval of the thesis:

THE INFLUENCE OF MANUFACTURING DEFECTS ON STRUCTURAL PERFORMANCE OF COMPOSITE OVERWRAPPED PRESSURE VESSELS

submitted by **KIVANÇ YURDAKUL** in partial fulfillment of the requirements for the degree of **Master of Science** i**n Metallurgical and Materials Engineering, Middle East Technical University** by,

Prof. Dr. Halil Kalıpçılar
Dean, Graduate School of **Natural and Applied Sciences** _____

Prof. Dr. C. Hakan Gür
Head of the Department, **Met. and Mat. Eng., METU** _____

Prof. Dr. Rıza Gürbüz
Supervisor, **Met. and Mat. Eng., METU** _____

Examining Committee Members:

Prof. Dr. Bilgehan Ögel
Metallurgical and Materials Eng, METU _____

Prof. Dr. Rıza Gürbüz
Metallurgical and Materials Eng, METU _____

Prof. Dr. Cevdet Kaynak
Metallurgical and Materials Eng, METU _____

Prof. Dr. Ali Kalkanlı
Metallurgical and Materials Eng., METU _____

Prof. Dr. Bora Maviş
Mechanical Eng., Hacettepe University _____

Date: 04.02.2022

I hereby declare that all information in this document has been obtained and presented in accordance with academic rules and ethical conduct. I also declare that, as required by these rules and conduct, I have fully cited and referenced all material and results that are not original to this work.

Name: Kıvanç Yurdakul

Signature :

ABSTRACT

THE INFLUENCE OF MANUFACTURING DEFECTS ON STRUCTURAL PERFORMANCE OF COMPOSITE OVERWRAPPED PRESSURE VESSELS

Yurdakul, Kıvanç
Master of Science, Metallurgical and Materials Engineering
Supervisor : Prof. Dr. Rıza Gürbüz

February 2022, 107 pages

In this study, the influence of defects that are occurred in manufacturing operations of filament wound composite overwrapped pressure vessels on burst pressure is investigated experimentally. Firstly, material characterization methods such as tensile testing and fiber volume fraction testing of carbon/epoxy composite specimens are completed. Following determining of different layer configurations for small scale composite pressure vessels, manufacturing and burst testing of vessels are accomplished. Effect of composite layer configuration hence stress ratio on burst pressure and failure mode is observed. Then, two types of manufacturing defects are defined as delamination and spaced winding for two different layer configurations. Artificial delaminations are embedded to the samples during manufacturing and cured samples are subjected to hydrostatic burst testing. Likewise, gaps were deliberately left the in layers and the effects of these gaps on burst pressure and fracture mode were observed. Fracture behavior of burst vessels are investigated via high-speed camera images taken during testing. Finally, composite microstructure via optical microscope and fracture surfaces via scanning electron microscope (SEM) are examined.

Experimental and visual data obtained by this study is investigated and influence of manufacturing defects in composite overwrapped pressure vessels on burst pressure performance of vessels is evaluated within the design limits of small scale vessel.

Keywords: Composite Overwrapped Pressure Vessels, Filament Winding, Stress Ratio, Burst Pressure, Manufacturing Defects

ÖZ

ÜRETİM HATALARININ KOMPOZİT SARGILI BASINÇLI TANKLARIN YAPISAL PERFORMANSINA ETKİSİ

Yurdakul, Kıvanç
Yüksek Lisans, Metalurji ve Malzeme Mühendisliği
Tez Yöneticisi: Prof. Dr. Rıza Gürbüz

Şubat 2022, 107 sayfa

Bu çalışmada, kompozit sargılı basınçlı kapların üretim proseslerinde meydana gelen hataların patlama basıncına etkisi deneysel olarak araştırılmıştır. İlk olarak, karbon/epoksi kompozit numunelerin çekme testi ve elyaf hacim oranı testi gibi malzeme karakterizasyon yöntemleri tamamlanmıştır. Küçük ölçekli kompozit basınçlı tank için farklı katman dizilimlerinin belirlenmesinin ardından tankların imalat ve hidrostatik patlatma testleri gerçekleştirilmiştir. Kompozit katman diziliminin dolayısıyla gerilme oranının patlama basıncı ve arıza modu üzerindeki etkisi gözlemlenmiştir. Daha sonra, iki farklı katman konfigürasyonu için delaminasyon ve boşluklu sarım olmak üzere iki tip üretim hatası tanımlanmıştır. Üretim sırasında numunelere yapay delaminasyonlar yerleştirilmiş ve olgunlaşmış numuneler patlatma testine tabi tutulmuştur. Aynı şekilde filaman sarım işleminde kasıtlı olarak katmanlarda boşluklar bırakılmış ve bu boşlukların patlama basıncı ve kırılma modu üzerindeki etkileri gözlemlenmiştir. Test sırasında alınan yüksek hızlı kamera görüntüleri ile basınçlı kapların kırılma modları gözlemlenmiştir. Son olarak, optik mikroskop ile kompozit mikroyapı ve taramalı elektron mikroskobu (SEM) ile kırılma yüzeyleri incelenmiştir.

Bu çalışma ile elde edilen deneysel ve görsel veriler değerlendirilmiş ve kompozit sargılı basınçlı tanklardaki üretim hatalarının patlama basıncı performansına etkisi küçük ölçekli kompozit tank tasarım sınırları içinde değerlendirilmiştir.

Anahtar Kelimeler: Kompozit Sargılı Basınçlı Tanklar, Filaman Sarım, Gerilim Oranı, Patlama Basıncı, Üretim Hataları

To My Precious Family&Friends

ACKNOWLEDGEMENTS

I would like to thank Prof. Dr. Rıza Gürbüz for his encouragement, guidance and support during tough times of COVID-19 pandemic.

I would like to express my deepest gratitude to my colleagues Mr. Emre ÖZASLAN and Mr. Gökberk DEMİROK because this study could not be accomplished without their enthusiasm and contribution.

I am deeply thankful to my other colleagues; Mr. Cihan TALEBİ, Mr. Yiğit Kemal ÖKTEN and Mr. Utku OLGUN they did their best in the time of need.

Above all, I offer my sincere thanks to my family and friends for their support and courage to finish this thesis with their deepest love.

TABLE OF CONTENTS

LIST OF TABLES

TABLES

LIST OF FIGURES

FIGURES

LIST OF ABBREVIATIONS

COPV	Composite Overwrapped Pressure Vessel
NDI	Non-Destructive Inspection
CNC	Computerized Numerical Control
CNG	Compressed Natural Gas
IM	Insensitive Munitions
TDS	Technical Data Sheet
ASTM	American Society for Testing and Materials
CFRP	Carbon Fiber Reinforced Polymer Composite
CLT	Classical Lamination Theory
X	Helical Filament Winding Layer
O	Hoop Filament Winding Layer
XOX	Winding Layer Configuration (First Letter Indicates Inner Layer)
OXOX	Winding Layer Configuration (First Letter Indicates Inner Layer)
XOXOO	Winding Layer Configuration (First Letter Indicates Inner Layer)
PTFE	Polytetrafluoroethylene
PMMA	Polimetil Metakrilat
DC	Artificial Delamination, Circumferential
DLS	Artificial Delamination, Local Square
SW	Spaced Winding
SWX	Spaced Winding of Helical Layer

SWO	Spaced Winding of Hoop Layer
SWXO	Spaced Winding of Both Helical and Hoop Layers
SEM	Scanning Electron Microscope
BP	Burst Pressure
EPDM	Ethylene Propylene Diene Monomer

LIST OF SYMBOLS

$\boldsymbol{N_{\varphi}}$: Longitudinal unit load

$\boldsymbol{N_{\theta}}$: Circumferential unit load

$\boldsymbol{\alpha}$: Winding angle

$\boldsymbol{R}$: Radius

$\boldsymbol{\sigma_{\alpha}}$: Helical fiber stress

$\boldsymbol{\sigma_{h}}$: Hoop fiber stress

$\boldsymbol{\sigma_{f:}}$ Tensile stress of fiber material

$\boldsymbol{\sigma_{m:}}$ Tensile stress of matrix material

$\boldsymbol{t_{\alpha}}$: Helical laminate (layer) thickness

$\boldsymbol{t_{h}}$: Hoop laminate (layer) thickness

$\boldsymbol{E_{f}}$: Elastic Modulus of fiber material

$\boldsymbol{V_{f}}$**:** Fiber volume fraction

$\boldsymbol{P}$**:** Pressure

$\boldsymbol{T_{g}}$: Glass transition temperature

ε: Strain

CHAPTER 1

INTRODUCTION

The reason for quick development in utilization and acceptance of composite materials in a wide variety of engineering applications is that they provide superior material properties in terms of strength to weight ratio, corrosion resistance, damage tolerance and toughness. Cylindrical structures such as CNG tanks and hydrogen storage tanks are the applications where composite materials are highly preferred for pressure vessels.

In this study, laminate configuration of composite overwrapped pressure vessels and the effect of manufacturing defects are investigated.

1.1 Motivation

Although composite materials have increasing popularity, the fact that their complex mechanical behavior is still not fully understood is a serious problem for engineers and researchers. This issue is even more crucial for filament wound pressure vessels due to their mechanical nature and variability in the manufacturing process. The motivation of this study is to observe the effect of manufacturing defects such as gaps and delamination on the structural performance of composite overwrapped pressure vessels.

1.2 Aim of the Work and Original Contribution

Composite pressure vessels are widely manufactured by filament winding method. Different layer (laminate) configurations may arise in the design stage of composite

pressure vessel. In the variety of layer configurations, burst pressure and failure modes are affected. Firstly, effect of stress ration is investigated by manufacturing 3 different layer configurations. In addition, some defects may occur during manufacturing operations and these defects may influence the structural performance these vessels.

The representative small scale carbon/epoxy composite overwrapped pressure vessels are planned to be manufactured with artificial defects such as delamination and gaps in a single layer. Overwrapped term comes from the most widely used manufacturing technique for composite pressure vessels, filament winding. Manufacturing defects in composite could be detected by a special NDT method called C-Scan ultrasonic inspection technique or X-Ray radiographic technique.

Pressure vessels with artificial manufacturing defects such as delamination and spaced winding are going to be subjected to burst test (Figure 1.1).

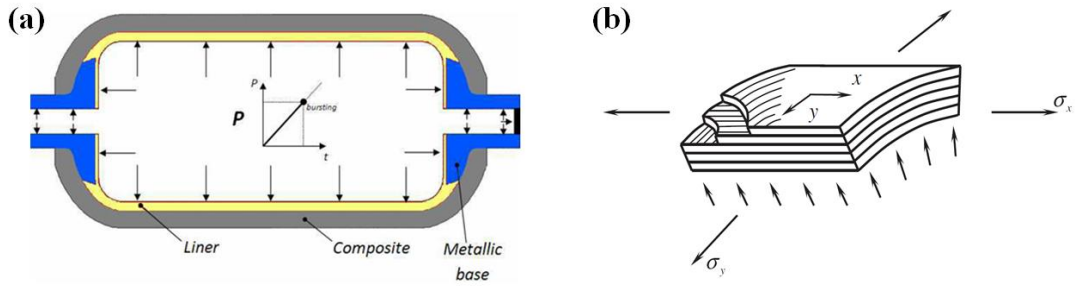

Figure 1.1 (a) Illustration of COPV (1) (b) Free body of composite pressure laminate when internal pressure applied (2).

Although the manufacturing parameters such as winding tension, winding time, bandwidth etc. have been widely discussed, investigation of the defects such as delamination and gaps, which may occur during manufacturing process, is very limited in literature. In this study, an experimental study was performed to investigate the effects of manufacturing defects on the bursting behavior of composite overwrapped pressure vessels with various stress ratios. Firstly, three pressure vessels with different number of helical and hoop windings were studied to characterize the bursting behavior of the vessels with different stress ratio. Then, two

of the tested vessels were selected to investigate the effect of manufacturing defects, which were delamination and spaced winding, on the bursting behavior. The strain gage measurement and high-speed camera were utilized to interpret bursting behavior in detail.

The aim of this thesis topic is to provide experimental data to identify manufacturing defect to structural analysis tools and specify quality control acceptance criteria for manufacturing defects in composite overwrapped pressure vessels.

CHAPTER 2

LITERATURE REVIEW

2.1 Filament Winding Process

Filament winding is considered to be most efficient method for manufacturing of composite pressure vessels. It has many advantages such as process automation, high fiber volume fraction, relatively low cost when compared with other composite manufacturing techniques. Alongside its benefits, the disadvantages of filament winding method could be listed as it is not suitable for concave part manufacturing and mandrel extraction could be challenging for parts with closed geometries (3).

Filament winding process consists of winding continuous rowing of resin impregnated fibers onto a rotating mandrel in predetermined angles and patterns. There are mainly two types of winding which are wet winding and dry winding. In wet filament winding, dry fiber spools are impregnated with resin in resin bath during manufacturing process. Nevertheless pre-impregnated fibers called towpreg is used in dry filament winding process. The wound part shall be cured in room temperature or in an oven depending on type of the resin system. The rotation of wound part must be continuous during curing since resin drippage of resin due to gravity may cause nonhomogeneous resin distribution throughout the composite material.

2.1.1 Filament Winding Machine Components

Therefore, a resin unit is not included in dry filament machines. Generally, filament winding machines could be used for both wet and dry winding with the necessary

tooling. In this study, wet filament winding process is chosen for the manufacturing of samples.

Primary wet filament winding units shall be listed as; multiple axes CNC-managed fiber positioning control unit, creel unit, resin bath unit and fiber delivery unit (Figure 2.1). CNC positioning unit shall have at least 2-axes of control which are rotation axis of mandrel and carriage axis. Simple cylindrical geometries may be wound with 2-axes filament winding machines. Depending on complexity of part geometry, control unit axes may increase up to 6 axes.

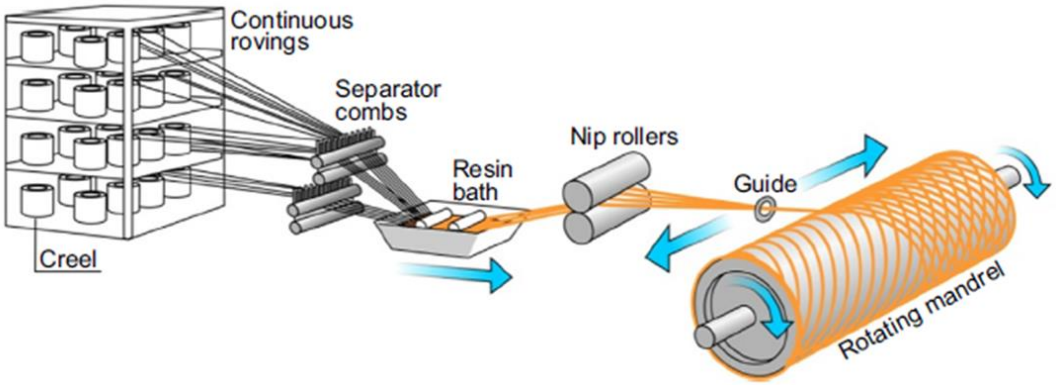

Figure 2.1 Filament winding process (4)

Fiber spools are positioned in creel unit in which pneumatic or servo motors provides necessary winding tension for the process. Since there are lots of spools, separator comps are used in order to prevent fiber tangling. On the other hand, comb surfaces shall be smooth for not causing any damage to the fibers. When the fibers are guided with separator combs, they are dipped to the resin bath for impregnation. There are many types of designs for resin bath section however the drum-type of resin bath is the one that is widely used. In this type of resin bath, a drum is rotating in the bath and a special tool called “Doctor blade” peels of the excess resin to adjust impregnation process. For spreading of the impregnated fibers special apparatus are used such as nip rollers or D-Shaped delivery tools. The last section where the impregnated fibers leave the fiber delivery unit is called as delivery eye. If the surface of delivery eye contains notch or it has relatively high roughness values, the fibers

shall be damaged and strength of the composite material may decrease due to the damage.

2.1.2 Filament Winding Mandrels

Many of composite manufacturing process require a mould in order to shape final geometry of composite part. In filament winding process, mandrel is considered to be the mould to conduct the winding. There are several types of mandrel available in the market depending on composite part geometry. For a simple cylindrical part, metal mandrels are used generally. After curing of the part, mandrel shall be extracted by using hydraulic pusher. Composite overwrapped pressure vessels are designed with the liner material which acts as a mandrel and do not require any removal operation. However, some composite overwrapped pressure vessels have flexible liner or no liner at all; in this case liners shall not be used as mandrels. Since the dome parts have smaller diameter than the cylindrical section a special mandrel design is required for the removal of mandrel. Mandrels that are used in filament winding are given in Figure 2.2.

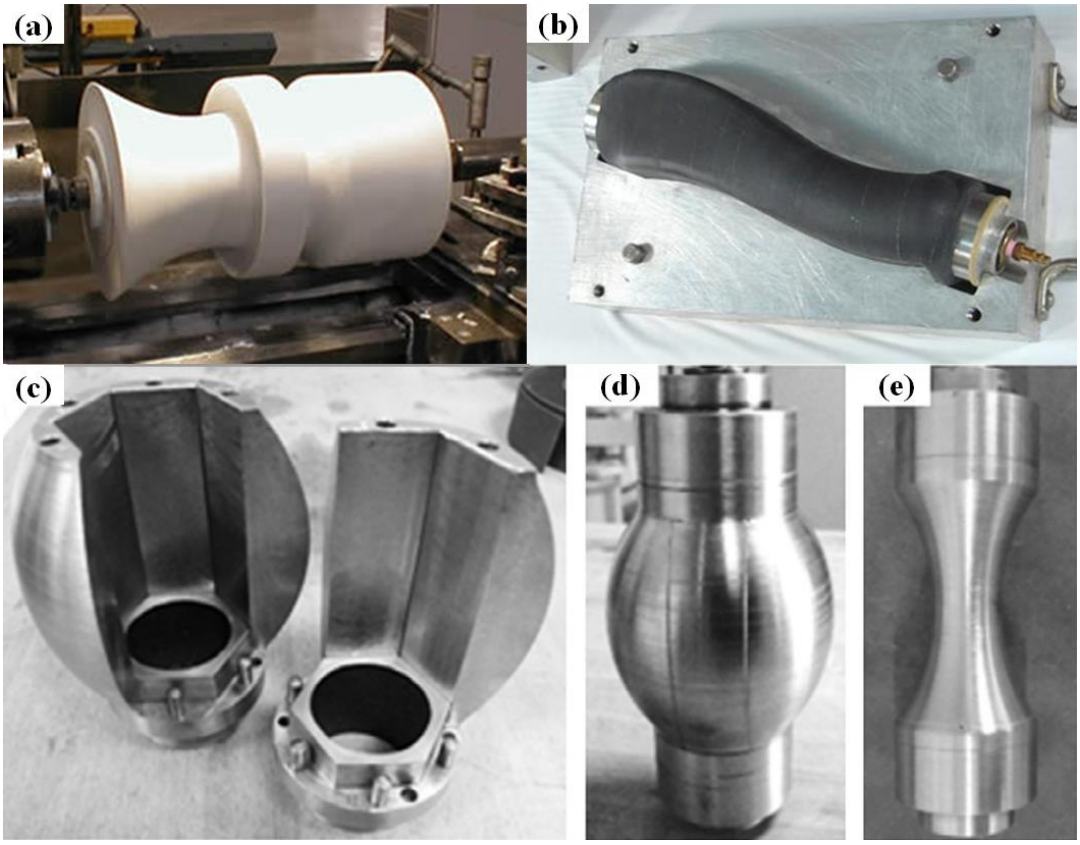

Figure 2.2 Filament winding mandrel types (a) water-soluble mandrel (b) Rubber bladder mandrel (c) half-assembled segmented mandrel (d) full assembled segmented mandrel (e) Shaft of segmented mandrel (5)

For the small-scale pressure vessels, rubber or silicon based bladder mandrel is suitable for manufacturing. Pressurized air is introduced to the bladder mandrel for winding and curing process. After curing of composite part is completed, air is released from the mandrel and mandrel shrinks. Another alternative mandrel solution for small-scale pressure vessels is called as water soluble mandrel. A mixture of ceramic based powder mixed with a special resin is poured to a mould and cured in an oven. After curing, preform becomes rigid and machined to the desired geometry. Following winding and curing of composite part, the mandrel is removed by using water. However for the bigger pressure vessel geometries such as large pressurized gas containers, bladder mandrel or water soluble mandrel solutions are not applicable. Mandrel is designed to be segmented in the radial section, in order to be

removed from larger dome openings. A shaft and segments shall be made from steel or aluminum alloys depending on weight or coefficient of thermal expansion requirement of the part to be manufactured.

2.1.3 Filament Winding Process Parameters

Filament wound parts consist helical and hoop (90^o) winding layers. When the winding pattern is designed between 10-89^o of angle it is called as helical winding. Helical layers contain two woven sub-layers with positive and negative winding angles. On the other hand, as name gives the idea, if there is a need to increase strength for the internal pressure which is also called as hoop strength; 90^o of 'hoop' winding is required. During designing of filament wound part, a balanced number of helical and hoop layers shall be chosen in order to achieve optimum strength on both longitudinal and radial axes.

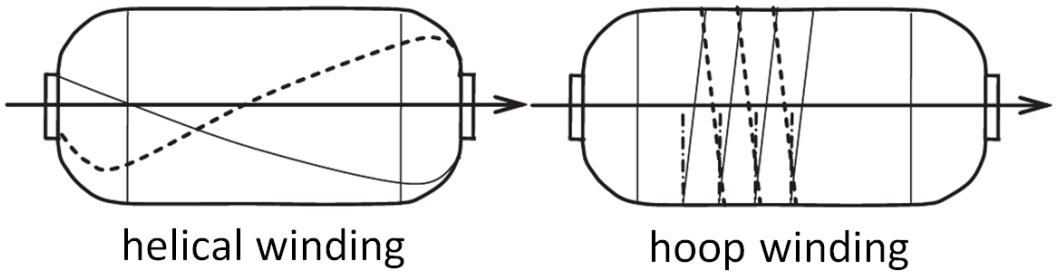

Figure 2.3 Helical and hoop winding illustrations in filament winding process (6)

Although filament winding process is an automated process, the quality of manufactured part is effected by many process parameters such as resin viscosity, fiber tension, winding speed, stacking sequence, fiber wetting etc. (7). Resin viscosity is related with resin type and resin bath temperature. Moreover, pot life of resin shall effect wetting of fibers due to the change in viscosity during process. For that reason, resin viscosity shall change from layer to layer in longer process time (8). Due to the fact that resin impregnation is critical parameter for composite manufacturing, custom-made resin impregnation units are being studied in the

literature. Simulation of impregnation has been carried out to determine the design of resin bath unit to achieve better quality product (9). Winding tension is another critical parameter for wet winding which have direct influence on the thickness of a layer and fiber/volume fraction. There is an optimum tension value for each type of fiber and it is determined by winding trials (10).

The main conclusion of the statistical analysis is that stacking sequence, winding tension, winding tension gradient, winding time and the interaction between winding tension gradient and winding time had a significant effect on strength of the composite overwrapped pressure vessel. The main reason for increasing the strength of the vessel is the increase of the fiber volume fraction, especially at the first hoop ply. Rousseau et al. (11) performed an experimental study by keeping all manufacturing parameters constant except for the winding pattern to investigate the winding pattern effect on the damage behavior under various loadings. They found a negligible effect in the case of off-axis loadings. However, it was observed that in the case of dense winding patterns, the presence of the undulation regions causes damage growth for the closed-ended internal pressure case. Mertiny and Ellyin (12) studied the influence of winding tension on strength of tubular composites under different biaxial loading ratios. The interesting finding of this study is that the strength of the tubular specimen is improved by increasing the winding tension under fiber-dominated loadings, whereas under matrix-dominated loadings failure pressure is improved by reducing the fiber tension. Zhang et al. (13) performed an experimental study to understand the effects of carbon fiber micromorphology on pressure vessels manufactured from wet spinning process fiber (HB) and dry-jet spinning process fiber (SC). They observed that HB vessels burst at about 10% lower than expected from the dome region, whereas SC vessels burst at about 10% higher than expected from the cylindrical region. In addition, the conversion ratios, which were defined as fiber breaking strength at burst pressure over tensile strength of fibers, for HB and SC vessels, were 72% and 92.3% respectively. Cohen et al. (14) detailed Cohen's previous study (7) to better examine the effect of the fiber volume fraction on strength and to develop a model to predict the fiber volume fraction in

the wet wound vessels. They confirmed the positive relationship between fiber volume fraction and strength and validated their model to predict fiber volume fraction. Zu et al. (15) studied the effect of the number of the tangent points and bandwidth parameters of pressure vessels with non-geodesic trajectories. It is concluded that decreasing the bandwidth increases the layer thickness of the dome region, while increasing the number of the tangent points reduces fiber overlap and enables smooth thickness distribution along the circumferential direction. Rafiee et al. (16) performed a stochastic analysis considering manufacturing variability to predict burst pressure of composite overwrapped pressure vessels exposed to internal pressure. Fiber volume fraction, winding angle and mechanical/strength properties were selected as random parameters to investigate the manufacturing uncertainties. The importance of stochastic analysis that takes into account manufacturing uncertainties in the prediction of burst pressure is emphasized. Harada et al. (17) investigated the burst pressure of type III composite overwrapped pressure vessels taking into account the inhomogeneity of fiber packing. It is shown that winding of glass epoxy layers over carbon epoxy layers may increase burst pressure by 20% due to dense fiber packing. In addition to manufacturing variables, another important issue that needs to be considered for a safe design is stacking sequence. Although Rousseau et al. (18) suggested to have hoop layers after helical layers to achieve better consolidation for composite structures, Nebe et al. (19) investigated the effect of stacking sequence on burst pressure of composite overwrapped pressure vessels experimentally. It is revealed that the burst pressure may differ 67% in pressure vessels with different stacking sequences. The pressure vessel with high angle plies stacked in the innermost had the lowest burst pressure, while the pressure vessel with high angle plies stacked in the outermost had the highest burst pressure. The main reason for this finding was that a preliminary failure occurs in the cylinder-dome transition region due to delamination between low angle and high angle layer groups.

2.2 Composite Overwrapped Pressure Vessels

Recently, composite materials are been used in many application areas. Except from its high specific strength and better environmental resistance advantages when compared with the metallic materials, composite materials are safer. For that reason, the earlier metallic pressure vessels are being replaced by the design of composite overwrapped pressure vessels. At the time of burst, the shell fragments of metal pressure vessels are far more dangerous than the fragments of composite overwrapped pressure vessels (20). Pressure vessels are classified in terms of materials in order to standardize the design, manufacturing and test activities.

2.2.1 Classification of Pressure Vessels

Typical pressure vessels, which have one cylindrical part and two dome regions are designed to withstand high internal pressures. ISO 11439 - An international standard for high pressure on-board CNG storage cylinders - (21) classifies pressure vessels into 5 types in terms of materials used. These types and their differences can be seen in Figure 2.4. Type IV is chosen as the pressure vessel sample in this study.

Composite overwrapped pressure vessels with polymer liner, called Type IV, are mostly manufactured by the wet filament winding method. The composite structure consists of helical and hoop windings. Metal end bosses on both side are attached to a mandrel and resin impregnated fiber tapes are wound to fully cover the mandrel in desired fiber orientations. The helices are wound along the whole vessel including the dome region whereas the hoop layers are wound only the cylindrical region. The axial load is carried by the helices and circumferential loads by the hoop layers. Composite overwrapped pressure vessel is abbreviated as ‘COPV’ or ‘vessel’ and hereupon these abbreviations shall be used.

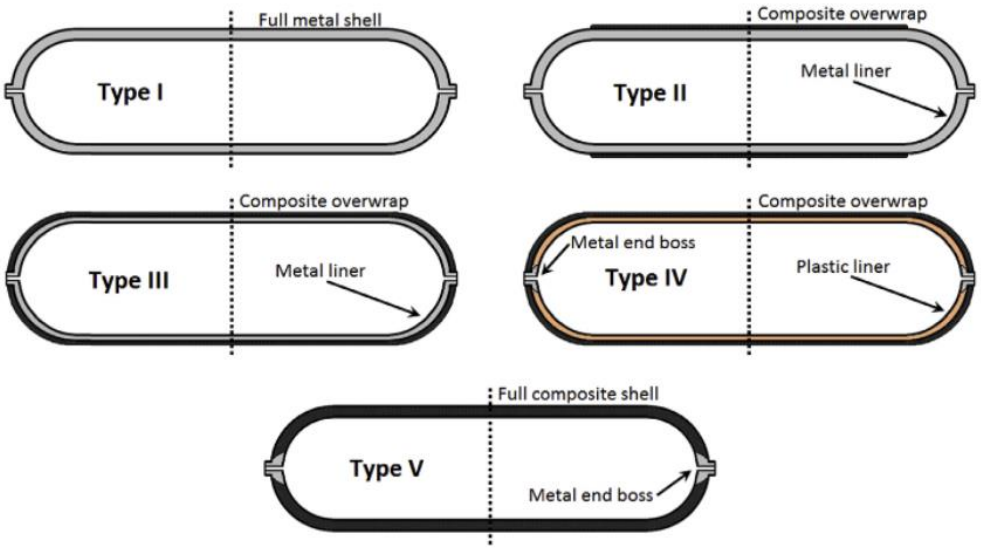

Figure 2.4 Classification of pressure vessels, Type IV is selected for this study (22)

2.3 Effect of Composite Layer Configuration in COPVs

The mechanical performance of a composite overwrapped pressure vessel is completely dependent on the stress ratio, which is defined as the ratio of helical to hoop fiber stress in the cylindrical region of the pressure vessel (4). Changes in the layup, load condition or boundary conditions affect the stress ratio and accordingly, the mechanical performance of the pressure vessel. Therefore, the effects of stress ratio on the pressure vessels were studied in literature by changing these conditions. Martins et al. (23), (24) investigated the effect of stress ratio, which was defined in this study as the ratio of hoop stress to axial stress, on the fracture morphology of filament wound composite tubes. One essential finding of this study is that when the stress ratio is greater than about 3 or in the case of pure hoop stress (1 hoop stress / 0 axial stress) fracture occurs in two planes. However, in cases where the stress ratio is 2 or less, fracture occurs in one plane. Ellyin et al. (25) performed an experimental study to inspect the behavior of multidirectional filament wound composite tubes under various biaxial loading ratios. They concluded that stress ratio has a great effect on the failure mode and damage progression as well as stiffness. Meijer and

Ellyin (26) studied the first failure behavior of +/-60° filament wound composite tubes under fourteen different stress ratios. They observed five different failure modes: axial failure along a helical crack under axial tension dominant stress ratios, weepage at the constrained end under 2:1 Hoop:Axial stress ratio, local leakage under 4:1 and 5:1 stress ratios, burst under hoop dominated stress ratios and finally axial break under compressive axial loads. Krishnan et al. (27) investigated the effect of winding angle on the failure behavior of glass epoxy composite tubes with various winding angles under different load ratios. They observed that each winding angle has the best strength under different loading conditions: +/-55° for pure hydrostatic loading, +/-45° for 1:1 hoop:axial loading and +/-63° for 4:1 loading. Hamed et al. (28) conducted a study to understand the effect of winding angle on the failure behavior of filament wound tubes under three different load conditions namely, pure hoop pressure, hydrostatic pressure and biaxial pressure with axial compressive loading. These authors found that winding of 55° shows the best performance for hydrostatic pressure, 75° for pure hoop loading and 85° for biaxial loading with axial compression.

2.4 Influence of Defects in COPVs to Burst Pressure

Although composite materials have increasing popularity, the fact that their complex mechanical behavior is still not fully understood is a serious problem for engineers and researchers. This issue is even more crucial for filament wound pressure vessels due to their mechanical nature and variability in the manufacturing process.

Many researchers are focusing on simulating the complex mechanical behavior, especially damage characterization, of filament wound structures numerically. Afrathim et al. (29) performed a finite element analysis to evaluate the first ply failure pressure of a pressure vessel. After validating their analysis with experimental results, they checked the applicability of basalt fiber reinforced composite for usage in pressure vessels using their validated finite element model. The study affirmed that the basalt epoxy composites could be used as an alternative material to

conventional composite materials such as carbon, glass, and Kevlar fiber based composites. Lin et al. (30) developed a progressive failure analysis involving matrix cracking, fiber fracture and interlaminar failure for Type III composite overwrapped pressure vessels during hydraulic burst tests. They predicted the blasting position on the cylindrical section as observed in the actual tests. Illustration of failure mode types in laminated polymer composites is given in Figure 2.5. Rafiee et al. (31) compared ply-discount and continuum damage methods for material degradation of progressive failure analysis of glass fiber reinforced composite tubes in internal pressure. They concluded that the continuum damage method predicts the burst pressure accurately, while the ply-discount method underestimates the burst pressure. Wu et al. (32) stated that the maximum strain criterion is capable of predicting the burst pressure of composite overwrapped pressure vessels for their numerical analysis.

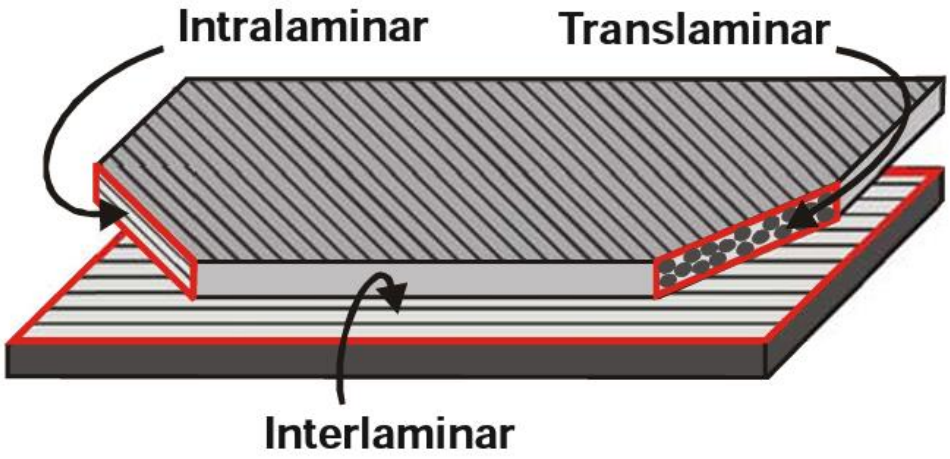

Figure 2.5 Failure modes classification in laminated polymer composites (33)

There are some studies that investigate the residual strength of composite overwrapped pressure vessels. Vannet (34) studied the residual burst pressure performance of various composite overwrapped pressure vessels exposed to mechanical impacts on their cylindrical part. It is found that the absorbed energy parameter, which can be found with several tests, is a threshold parameter to describe the severity of impacts. Perillo et al. (35) performed numerical and experimental

investigation of the impact effects on filament wound pressure vessels. Both interlaminar and intralaminar damages were considered. The impact damage was numerically over-predicted due to inaccuracy of the material and geometrical parameters and the used stiffness matrix degradation model. In this study, impact damage is considered as manufacturing defect since the part may subject impact during transportation between manufacturing operations.

CHAPTER 3

MANUFACTURING AND TESTING OF COPV SAMPLES

Before manufacturing of COPV samples, matrix and fiber materials are selected. Geometry of the sample is determined by considering design requirements of a product and manufacturing process time. Design, manufacturing and burst testing operations are explained in detail in this section.

Total number of 41 composite overwrapped pressure vessel (COPV) samples is manufactured and subjected to burst testing. Three repetitions are used for each configuration except from the calibration COPV sample and XXO vessel.

- 9 samples: Reference (no artificial defect) XOXOO, OXOX and XOX layer configurations of the composite overwrapped pressure vessels (COPVs) in order to observe the effect of stress ratio to burst locations.
- 30 samples: XOXOO and XOX layer configurations with 2 types of artificial delamination as interlaminar defect and 3 types of spaced winding as intralaminar defect.
- 1 sample: calibration COPV sample to validate the monitoring of embedded artificial delamination defects via NDI method called ultrasonic C-Scan inspection.
- 1 sample: COPV with XXO layer configuration to verify the effect of delamination in XOX.

3.1 Matrix and Fiber Materials of COPV Sample

Due to their specific strength and good environmental resistance carbon fiber and epoxy resin system is widely used as reinforcement and matrix materials in composite overwrapped pressure vessels, (36). In addition to this, carbon fiber has excellent insensitive munitions (IM) properties to be used in composite pressure vessels for aerospace applications (37). In wet filament winding process, fiber and matrix materials are selected by considering some critical process parameters such as fiber bandwidth and resin viscosity. When mechanical properties and process parameters are considered together, the most suitable fiber and resin combination are determined for this study from the available material database.

3.1.1 Carbon Fiber Material

Standard modulus and high strength continuous carbon fiber spool is selected to be used in the manufacturing of COPV Sample. The bandwidth of the fiber is defined as 3 mm in the technical data sheet of the material. Mechanical properties of the carbon fiber material are given in Table 3.1.

Table 3.1 Mechanical properties of (12K) carbon fiber material

Tow Size	***Tensile Strength (MPa)***	***Tensile Modulus (GPa)***	***Maximum Tensile Strain (%)***	***Density (g/cm3)***	***Yield (g/1000m)***
12K	4200	240	1.8	1.78	800

3.1.2 Epoxy Resin System

High modulus, low viscosity epoxy (thermoset) resin system with 3 components is selected as matrix material which fulfills the requirements in MIL-HDBK-17F (38). The components are;

- Epoxy resin

- Anhydride hardener
- Imidazole accelerator

Some basic mechanical and chemical properties of epoxy resin system that is used in this study are given in Table 3.2.

Table 3.2 Basic mechanical and chemical properties of epoxy resin system

Components	***Parts by weight***	***T_g (C^o)***	***Tensile strength (MPa)***	***Interlaminar shear strength (MPa)***
Epoxy resin	100			
Hardener	90	125-128	83-93	75-77
Accelerator	0.5			

3.1.3 Liner Material

Since epoxy resin systems have limited impermeability properties at high pressures, carbon/epoxy composite material requires a sealing material at the inner section of the COPV.

EPDM liner material is used in the COPV samples in order to provide liquid and gas impermeability in this study. It is known that elastomeric liner materials have no contribution to the burst strength of COPV samples. That is why their mechanical properties are not included to the context of this study.

3.1.4 Material Characterization Testings of Carbon/Epoxy Composite

Although the mechanical properties of carbon fiber and epoxy resin system are given in the Technical Data Sheet (TDS) by supplier, composite material properties needs to be tested and determined by the same manufacturing method that is planned to be used in the production of the part. For that cause, the coupons for tensile testing shall be manufactured by filament winding method. Weerts et. al. (39) suggests special

mandrel geometry according to ASTM D3039 (40) which is illustrated in Figure 3.1. Similar mandrel geometry is used for the manufacturing of both longitudinal and transverse tensile coupons. Two batches of composite plates are manufactured for longitudinal tensile testing coupons.

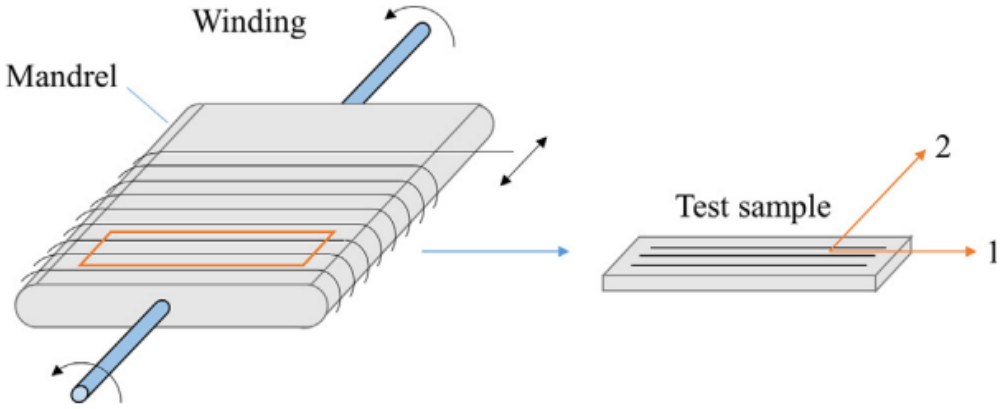

Figure 3.1 Special mandrel design for tensile test coupon manufacturing (39)

Three characterization testing are planned to be covered in this study. These are arranged as; longitudinal (0^o, fiber direction) tensile testing, transverse (90^o, perpendicular to fiber direction) tensile testing and fiber volume fraction determination testing. Fiber reinforced polymeric materials have bigger variation in testing results when they compared metallic materials testing. Main parameters causing the variation shall be sorted as fiber/matrix surface phenomena, manufacturing operations and even mechanical testing parameters (41). The mechanical properties of CFRP were generally determined experimentally using small coupon tests. Among the other mechanical properties, the fiber strength trends initiate from defects or other weak points in the materials. Therefore, fiber strength can be expected to reduce with the increasing volume of the material being tested. This is called the size effect on fiber strength (42).

Longitudinal tensile stress and fiber volume fraction is required for the calculations of COPV layer configuration. Although the transverse tensile strength is not going to be used in the calculations in this study, transverse tensile testing is covered in this

study. As Adams et. al. (43) describes; the process flow of mechanical testing coupon manufacturing could be sorted as; filament winding, curing, rough cutting, tabbing, fine cutting respectively which are shown in Figure 3.2.

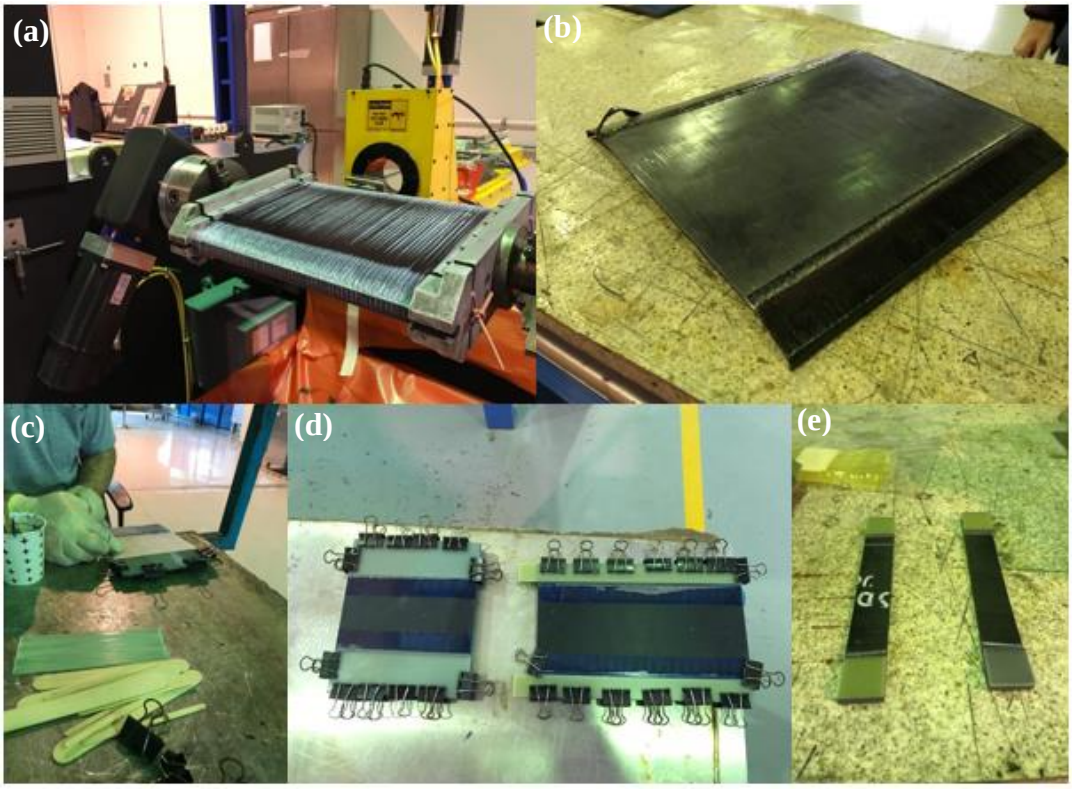

Figure 3.2 Manufacturing operations of carbon/epoxy mechanical testing coupons (a) winding (b) rough cutting (c) tabbing (d) curing (e) fine cutting

The conducted tests are listed below.

- ASTM D3039 (40) - Test Method for Tensile Properties of Polymer Matrix Composite Materials: It is required to determine Ultimate Tensile Stresses and Elastic Modulus values at the fiber direction (0^o) and transverse direction (90^o).
    - For longitudinal (0^o) tensile strength testing, 15 coupons with the dimension of 250 mm (l) x 15 mm (w) x 1 mm (t) are tested.
    - For transverse (90^o) tensile strength testing, 10 coupons with the dimension of 175 mm (l) x 25 mm (w) x 2 mm (t) are tested.

Instron testing machine with 20 tons capacity is used for the tensile testing. Class 0.5 load cell is used and crosshead speed is determined as 2mm/min. Tensile testing setup of 90^{o} carbon/epoxy coupon is given in Figure 3.3.

Figure 3.3 Transverse tensile testing setup of carbon/epoxy coupons

- ASTM D 3171, Test Method 1, Procedure B (44) - Test Methods for Constituent Content of Composite Materials. This test is conducted to determine the fiber/matrix volume hence the weight fraction of carbon/epoxy composite material. Before starting to the test, density of composite material is determined by following steps in ASTM D1505 - Density of Plastics by the Density-Gradient Technique (45).

  In fiber volume fraction determination, a nitric acid digestion is used in order to dissolve matrix resin content. By this way, there is only fiber material is left. Density of carbon fiber material is measured by ASTM D1505 as it is applied to composite material. Then, fiber volume fraction is calculated by making a proportion with the composite weight at the start using density and weight values of both fiber and composite material.

3.2 Geometrical Properties and Layer Configuration Calculation of COPV Sample

Typically, conventional pressure vessel geometries have dome opening diameter to cylinder diameter ratio is around 0.1-0.2. However, this ratio could become as large as 0.5-0.6 (46) in some aerospace applications. In this study, both polar openings are determined to be 94 mm hence the polar opening to cylindrical diameter ratio is 0.644. Design constraints including some geometrical parameters of the COPV sample except from the composite layers are given below in Table 3.3. In addition, cross-section and 3-D model of the COPV sample is given in Figure 3.4.

Table 3.3 Dimensions of COPV sample

Dimensions	***Value (mm)***
Composite Part Length	160
Total Part Length (40 mm of metal polar bosses)	200
Mandrel Diameter (Including liner material)	146
Opening Diameters (equal)	94
Liner Thickness	3

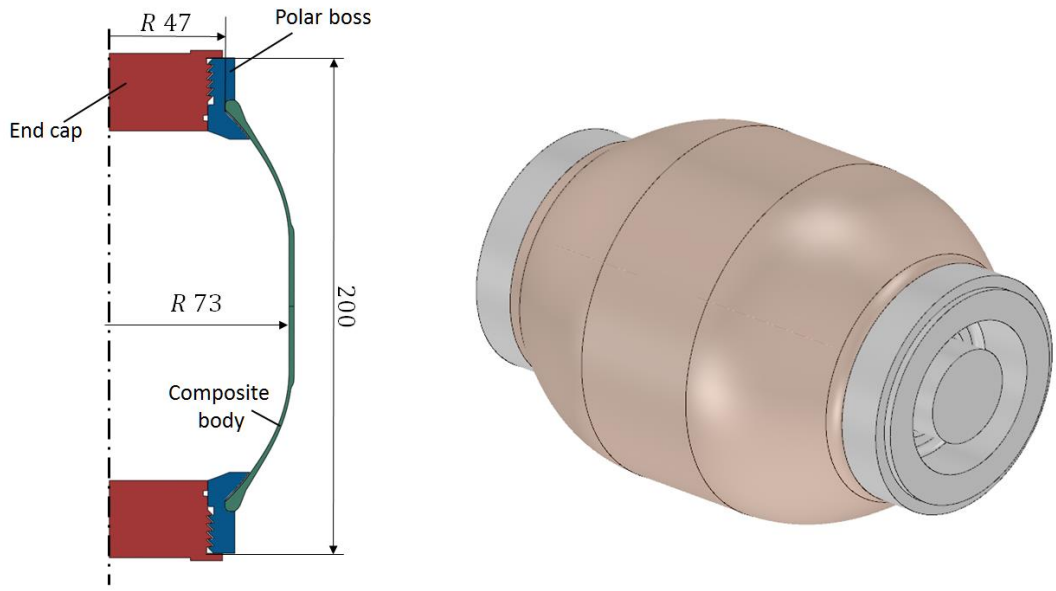

Figure 3.4 Cross-section and 3-D model of COPV sample

As the opening diameter to cylinder diameter increases, the winding angle in the cylinder section of the part increases (Figure 3.5). This situation could be explained by an equation which is called Clairault's Relation (47).

$$r \cdot \sin \alpha = Constant$$

The mandrel diameter at the cylinder section (including liner material thickness) is defined as 146 mm and both polar openings are 94 mm. When Clairault Relation is applied, the winding angle (α) in the cylindrical section is calculated as 40°. The points on the dome geometries are also calculated by using Clairault Relation. The calculated length and radius values corresponding to winding angle for the COPV sample is given in Annex-A.

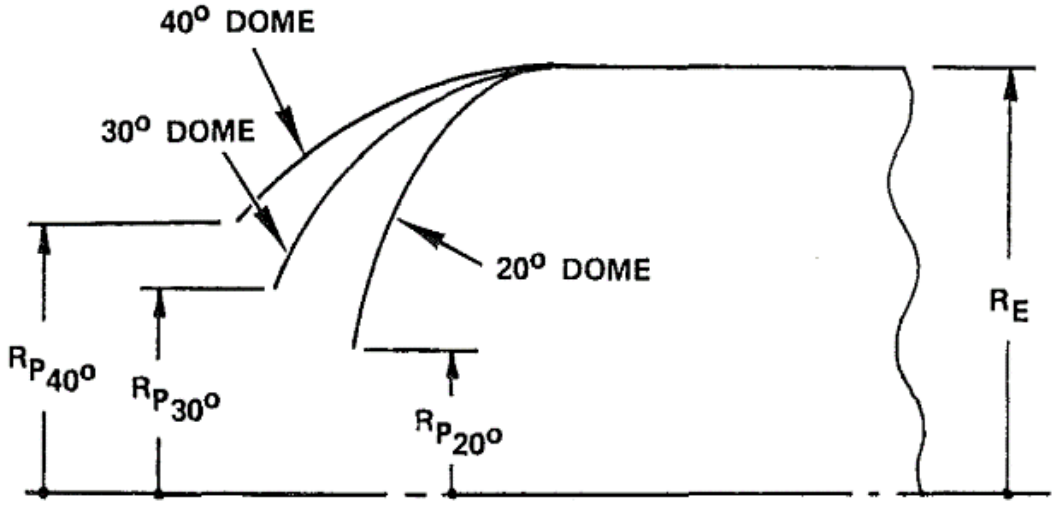

Figure 3.5 Polar opening radius vs. winding angle relation (48)

The required thickness of COPV sample laminate is calculated by following netting theory (18). In the netting theory, it is assumed that the only load carrier component in the composite is fiber and matrix contribution to the structure is neglected. In addition, each layer is assumed to be isotropic and the calculation of the layer thicknesses is carried out by this assumption.

During burst testing of pressure vessels, matrix cracking at the earlier pressure level is expected due to the low strength of epoxy resin material when compared with the fiber's strength. To prevent leakage before burst pressure, it is recommended to adapt liner material to the pressure vessel to see the potential highest pressure level that the COPV may reach (49). For that reason EPDM liner material is used in COPV samples for the impermeability for liquid and gas for this study. It is assumed that EPDM liner has no load carrying capacity it just acts as a sealant material in the burst testing. Where Camanno et. al. (50) defines matrix cracking non-catastrophic damage and prefers not to allow matrix cracks in the pressure vessels, Vasiliev et al. (2) states that it depends on the application of the pressure vessel product. If the pressure vessel is not subjected to fatigue load, it is convenient to neglect the effect of matrix cracking.

Pressure vessels with various stress ratios were discussed firstly to understand stress ratio effect on the bursting behavior. Stress ratio is calculated in composite overwrapped pressure vessel design in order to decide whether failure occurs at the cylinder or dome section of the vessel at the burst test. It is defined as the proportion of fiber stress in helical windings to fiber stress in hoop windings.

$$Stress\ ratio = \frac{\sigma_\alpha}{\sigma_h}\ (Equ. 1)$$

The pressure vessels are conceived with the stress ratio values from 0.60 to 0.80 (51). Peters et. al. (4) states that stress ratio is recommended from 0.60 to 0.85 to achieve hoop - dominated failure for composite pressure vessels.

Fibers in hoop and helical windings are the load carrying components for composite overwrapped pressure vessels according to the netting theory. The stress calculation is made in cylindrical geometry because hoop winding is only able to wound to the cylindrical section of the COPV sample. In the literature, it is suggested to apply hoop layers after helical layers for better consolidation (52). Therefore, the free body diagram of cylindrical section with radius R under internal pressure loading P is given in the Figure 3.6 (a). When hoop winding is considered to be in circumferential direction, helical winding makes an angle with longitudinal axis which is called as winding angle α. Since in the netting theory, the load carrying structural member is the fiber; the relation between the load components of the fibers in hoop and helical winding are shown in terms of pressure vessel's circumferential and longitudinal loading directions, respectively in Figure 3.6 (b).

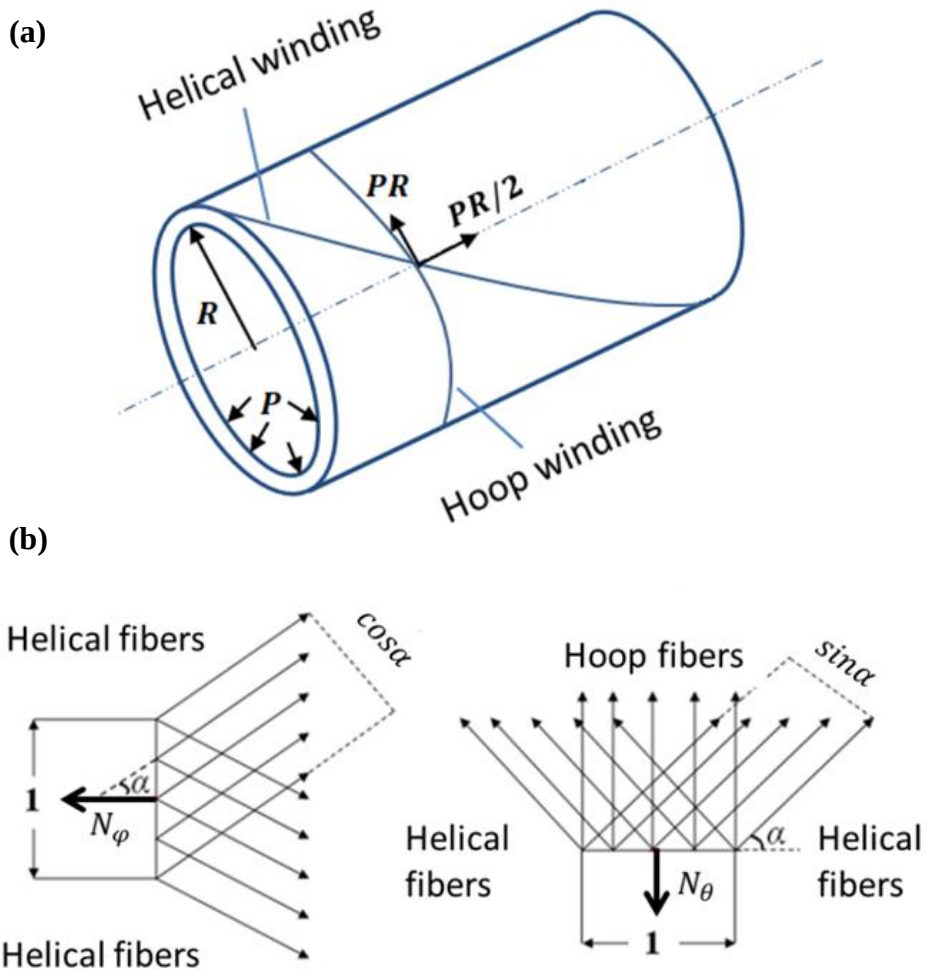

Figure 3.6 Free body diagram of cylindrical section (b) load components of the fibers in hoop and helical winding (53)

In a cylindrical pressure vessel free body diagram, circumferential and longitudinal load equilibriums related with helical and hoop winding parameters are given below (54);

$\boldsymbol{N_\varphi}$: Longitudinal unit load

$\boldsymbol{N_\theta}$: Circumferential unit load

$\boldsymbol{\alpha}$: Winding angle

$\boldsymbol{R}$: Radius

$\boldsymbol{\sigma_\alpha}$: Helical fiber stress

$\boldsymbol{\sigma_h}$: Hoop fiber stress

$\boldsymbol{t_\alpha}$: Helical laminate thickness

$\boldsymbol{t_h}$: Hoop laminate thickness

$$N_\varphi = \frac{P \cdot R}{2} = \sigma_\alpha \cdot t_\alpha \cdot \cos^2 \alpha \ (Equ. 2)$$

$$N_\theta = P \cdot R = \sigma_\alpha \cdot t_\alpha \cdot \sin^2 \alpha + \sigma_h \cdot t_h \ (Equ. 3)$$

When the longitudinal and circumferential load equations are solved for the stress ratio equation according to classical lamination theory, CLT (55), the derived stress ratio in terms of thicknesses of both helical and hoop layers is given below;

$$Stress\ ratio = \frac{\sigma_\alpha}{\sigma_h} = \frac{t_h}{t_\alpha(2\cos^2 \alpha - \sin^2 \alpha)} \ (Equ. 4)$$

Three different vessels with various number of helical and hoop windings were used to investigate the effect of stress ratio phenomena on bursting behavior. Table 3.4 shows the tested pressure vessels for stress ratio comparison, where X stands for helical windings and O stands for hoop windings. The pressure vessels with different stress ratios were obtained by changing the number of hoop windings. The XOXOO winding with 0.99 stress ratio was selected for expectation of an unsafe failure mode at dome region, whereas the XOX winding with 0.33 stress ratio was chosen to obtain a safe failure mode at cylindrical region. In addition to two vessels with extreme stress ratios, the OXOX winding with a 0.66 stress ratio was tested to investigate the effect of the stress ratio on the failure mode in a wide range. From the micrographs of filament wound part containing same carbon fiber and epoxy resin combination, the thickness of one helical layer is measured around 0.60 mm and the thickness of one hoop layer is measured around 0.30 mm. It should be noted that, thickness values could change up to 10-15% in a single layer due to the variation of filament winding process parameters such as fiber tow bandwidth and resin viscosity.

Table 3.4 COPV sample configuration with different stress ratios and their layer properties

Layer Configuration	*Total X Thickness [mm]*	*Total O Thickness [mm]*	*X Winding Angle [°]*	*O Winding Angle [°]*	*Stress Ratio (Theoretical)*
XOXOO		0.90			0.99
OXOX	1.20	0.60	40	90	0.66
XOX		0.30			0.33

σ_f is the carbon/epoxy composite tensile strength in longitudinal direction (0^o) which is the result of mechanical characterization coupon testing explained in Section 3.1.4.

While the coupon manufacturing composite batches have average of 0.57 fiber volume fraction value, COPV samples have 0.62 fiber volume fraction. For that reason, Tensile Strength and Elastic Modulus values are normalized according to fiber volume fractions before calculation.

Rule of mixtures equation (56) is applied with tensile stress values that are taken from carbon and epoxy supplier's technical data sheets. As explained before it is not convenient to use these data without mechanical characterization of the composite material. However it is calculated for comparison with the tensile testing results. Since tensile testing manufacturing batches has an average fiber volume fraction of 0.57, V_f is taken as 0.57.

$$\sigma_c = \sigma_f \cdot V_f + \sigma_m \cdot (1 - V_f) \; (Equ. 5)$$

- $Rule\ of\ Mixtures\ \ Results$; σ_f: 2432,8 MPa
- $Tensile\ Testing\ Results$; σ_f: 1977,5 MPa,
- $Normalized\ Tensile\ Testing\ Results$; σ_f: 2189,9 MPa,

Peters et. al. (4) and TCR Company which is a carbon fiber producer (57) states that, typical fiber performance in a pressure vessel may decrease up to 20% depending on

the brand. When the normalized tensile strength is compared with the theoretical strength (with same fiber volume fraction), it is seen that %19 of drop is detected in tensile testing result which is acceptable considering the brand of the fiber.

$$P = \frac{2 \cdot \sigma_\alpha \cdot t_\alpha \cdot \cos^2 \alpha}{R} \quad (Equ. 6)$$

$$P = \frac{\sigma_\alpha \cdot t_\alpha \cdot \sin^2 \alpha + \sigma_h \cdot t_h}{R} \quad (Equ. 7)$$

σ_f is assumed to be equal to σ_h because hoop layers are carrying the load caused by internal pressure. When calculations are done with the equations above in order to obtain theoretical burst pressure values in terms of helical and hoop laminate thicknesses and stresses, burst pressure values for each layer configuration are given in Table 3.5.

Table 3.5 Theoretical burst pressures of COPVs for each layer configuration

Layer Configuration	***Theoretical Stress Ratio***	***Theoretical Burst Pressure (psi)***
XOXOO	0.99	4460
OXOX	0.66	3229
XOX	0.33	1975

3.3 COPV Sample Manufacturing Process

There are 5 main operations in the COPV manufacturing process. First of them is the production of water soluble mandrel. After that, liner material is applied to the mandrel. Wet filament winding, curing and the removal of the mandrel are the remaining operations. These operations are required for the manufacturing of COPV samples that contains no artificial defects. That is why; embedding of artificial delamination defects and manufacturing of spaced winding in COPV samples are

explained as well. To sum up, all the details related with the manufacturing of 41 COPV samples are covered in this section.

3.3.1 Manufacturing of Water Soluble Mandrel

For the manufacturing of a composite part with a cylindrical geometry a single part mandrels are used. However if the mandrel needs to be removed from the COPV after the manufacturing process without damaging the part, it is not convenient to use a single piece mandrel. There are some solutions for removal of the mandrel after curing process of COPV such as segmented mandrel, rubber bladder mandrel or water soluble mandrel (58). Each one of them has advantages and drawbacks however water soluble mandrels are cost effective if the composite part dimensions are not bigger than 200 mm and the production rates are not so much. That is why for the manufacturing of COPV Samples, water soluble mandrel is used in this study. The water soluble mandrel material is a mixture of ceramic based powdered material which is mixed with water and poured to a mould in green state. For the COPV Samples, mould with 250 mm of length and 160 mm of diameter cylindrical geometry is used (Figure 3.7).

For the machining and assembly of the mandrel, a metal shaft with 20 mm of diameter is placed in the center axis of the mandrel. Once the mixture is prepared it should be delivered to the mould in 5 minutes. After that, it kept in a dry place at room temperature to decrease the moisture for a week. Before machining the mould is released and the green state of water soluble mandrel is exposed to heat treatment at 135 ^{o}C for 72 hours for drying process. Then, it is machined to its final geometry just before the liner adhesion operation.

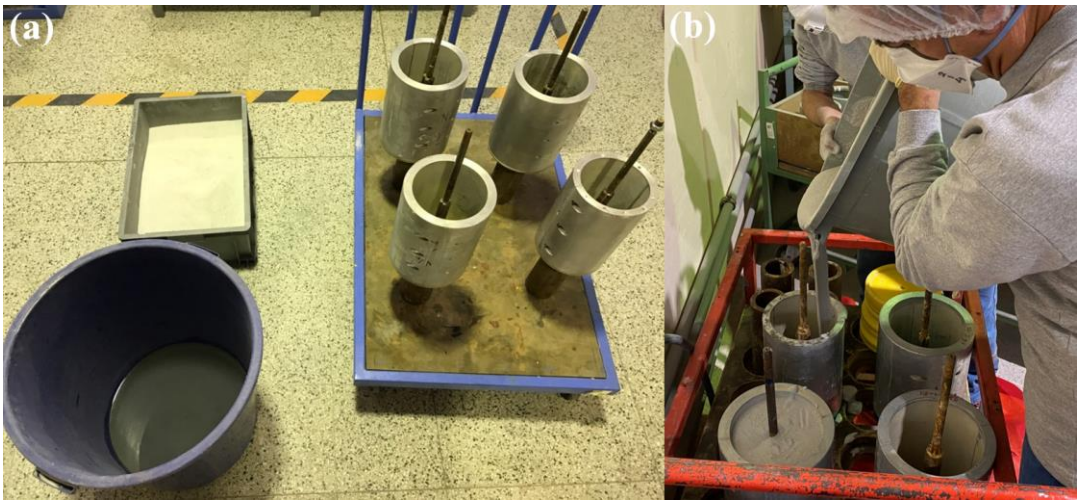

Figure 3.7 (a) Water soluble mandrel mould preparation (b) Pouring of soluble mandrel to moulds

3.3.2 Adhesion Process of Liner Material

Composite overwrapped pressure vessels have a liner material on their structures in order to provide gas and liquid impermeability. In COPV Samples, two cured EPDM liner materials are attached together by the use of an epoxy based adhesive material (Figure 3.8).

Adhesion process is applied on the water soluble mandrel and the epoxy based adhesive material is cured for 3 hours at 60 ^{o}C under -0.80 bar vacuum pressure applied. After curing of the adhesive, the residuals are being removed with grinding to achieve smooth surface before filament winding process.

Figure 3.8 Adhesion of EPDM liner on the mandrel

3.3.3 Filament Winding Process of COPV Samples

Filament winding process is conducted on a 4-axis CNC controlled filament winding machine. Before starting to the filament winding process, some setup operations are required. The schematic illustration of filament winding process design is given in Figure 3.9.

Firstly, at the winding software the mandrel generation shall be done. Since the mandrel has an axisymmetric geometry, the mandrel geometry is defined with radius, length positions and the winding angle at these positions that are defined in the design stage of the COPV sample. After geometrical parameters are defined to the software, it is required to specify the fiber bandwidth.

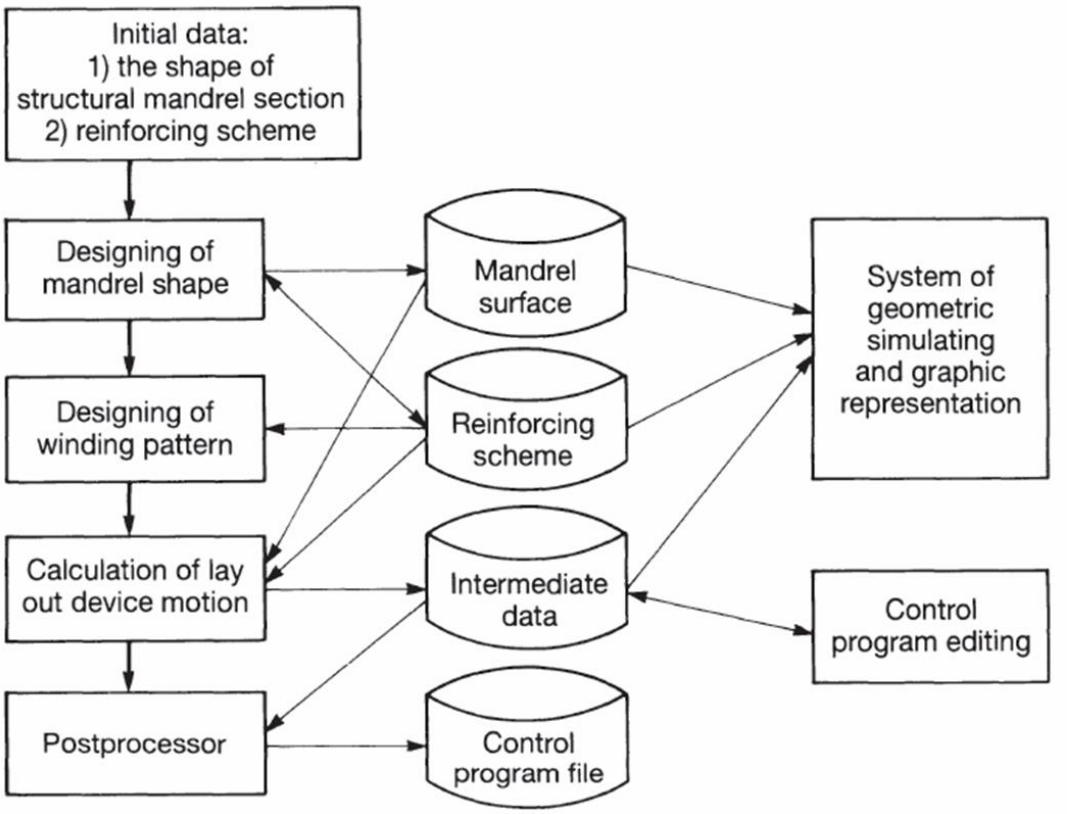

Figure 3.9 Filament winding process design steps (10)

In the literature, fiber bandwidth is recommended to be 2 to 4 % of the cylindrical diameter of the pressure vessel part (4). For COPV sample, since the cylindrical diameter with the liner is 146 mm, the recommended fiber bandwidth is calculated between 2.92 to 5.84 mm. When one carbon fiber spool is used for filament winding, the fiber bandwidth is measured between 3.0-3.5 mm depending on the resin content. For that reason, it is determined to use single carbon fiber spool for COPV sample and specify the fiber bandwidth as 3 mm. When mandrel dimensions, winding angle and the fiber bandwidth parameters are defined in the winding software, winding patterns are calculated and listed. Generally, it is not possible to achieve exact 100% mandrel coverage with the parameters identified to the software. Calculated patterns from the software have the coverage above 100% in order to make sure there are no gaps in the layer. From the past experiences, it is better to choose pattern numbers which are not greater than 10 due to prevention of unnecessary kinking of the fibers.

When the pattern number increases, the layer becomes more interwowen and fiber undulation in the structure increases. In addition to this, the void content increases and the fiber/resin ratio decreases. All of these parameters cause reduction in strength for the structure (4). In this study, the first calculated winding pattern number which is 5 with 116 circuit number, is determined as a helical winding pattern.

In COPVs, hoop winding is only possible to implement to the cylindrical section of the product. In the dome sections, resin content causes fiber slippage that is why especially in wet winding it is not possible to cover dome geometries with hoop winding. In the COPV sample geometry, except from the domes there is only 54 mm on the axial axis has a cylindrical geometry. The hoop winding is applicable to this cylindrical section. In the winding software, the parameters such as cylinder diameter, fiber bandwidth, cylinder starting and cylinder endpoint are identified as input data for hoop winding generation. It is relatively easy to handle when it is compared with the helical winding pattern generation. All of the hoop layers are planned to be wound with the same winding program.

Following the winding pattern is selection, machine parameters shall be adjusted in order to start winding process. From this point, the COPV mandrel is mounted to the headstock and the tailstock of the machine. The reference coordination of the mandrel with respect to the headstock surface should be measured and noted in order to provide input to the machine software to specify the exact mandrel location. Finally, the machine parameters are calculated by the software with respect to the selected winding pattern and the location of the mandrel.

When the mandrel is mounted to the filament winding machine, resin mixture is prepared and poured to the resin bath unit of the machine. Resin bath is heated to 35^{o}C to achieve the recommended viscosity value for filament winding proves. Resin amount is adjusted with the special apparatus which is called Dr. Blade. It is driven by a servo motor for setting the gap between the values of 0.08 mm to 1.00 mm to dose the resin content for impregnation.

As mentioned above, one carbon fiber spool is used for the process. It is mounted to the servo-controlled fiber creel unit and passed through fiber delivery path which includes several pulleys, resin bath and delivery eye. Fiber creel unit provides the designated tension force to the carbon fiber spool. Delivery path is designed to achieve minimum friction because friction may cause fiber damage which reduces the strength of the final product.

The surface of the liner material is grinded with 180 grit sandpaper in order to increase the surface energy. By this way, the adhesion between the EPDM liner material and the epoxy is improved.

For the winding of 5 layers with the sequence of XOXOO starting from the inner side of the composite is wound by using a single helical winding program for two helical layers and a single hoop winding program for three hoop layers. Same programs are used for the winding of OXOX and XOX layer configurations. The program is selected from the filament winding machine and the machine axes move to the starting point of the first helical layer. Resin impregnated fiber is pulled by hand and fastened to the left polar opening by circling around 3 times before starting to winding process. The winding process of first helical layer takes approximately 10 minutes with the 20 rpm of mandrel speed and the fiber tension is set to 2 kg of load. In order to achieve complete coverage of the helical layer, the machine travels 116 circuits. After finishing the helical layer, the impregnated fiber cuts and the ending of the fiber is attached to the left opening by the tackiness of the resin. Helical layer winding for COPV is shown in Figure 3.10.

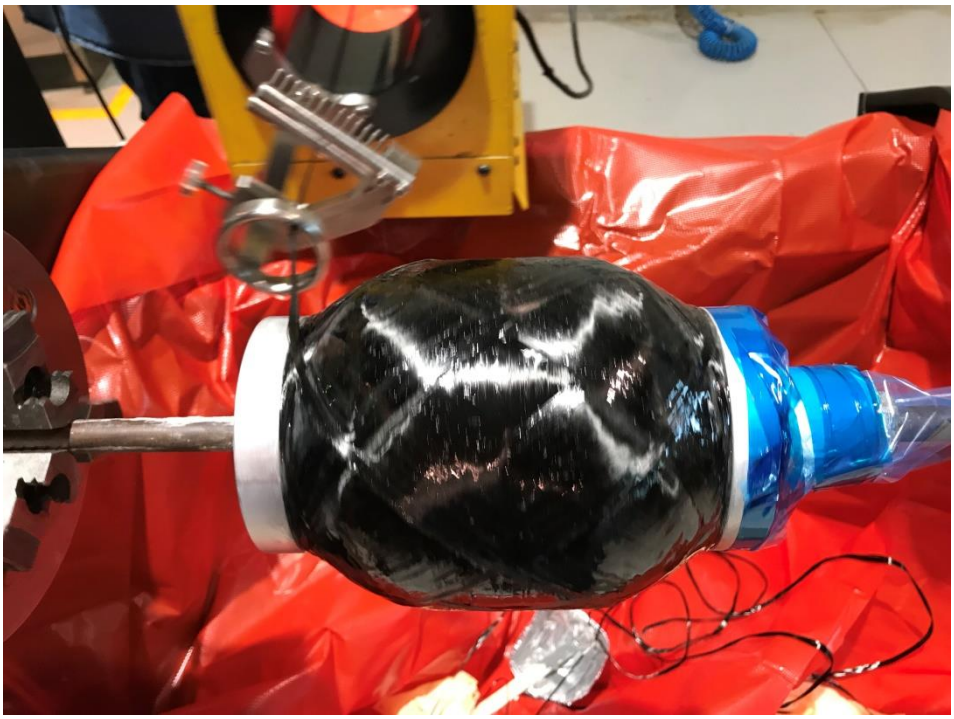

Figure 3.10 Helical layer winding process of XOXOO COPV sample

Afterwards, the hoop layer program is chosen from the winding software and the filament winding machine moves to the starting position for the hoop winding. The resin impregnated fiber is circled around the cylindrical section of the mandrel 3 times and the winding program is started. It takes approximately 1 minute to complete a single layer of hoop winding with the 20 rpm of mandrel speed and the fiber tension is set to 1 kg of load. At the end of the hoop winding, similar to the helical winding, the impregnated fiber is cut and attached to the end position of the cylindrical region by the help of the tackiness of the resin. By following the routes explained above, layers are completed for each layer configuration such as XOX, OXOX and XOXOO before curing process.

3.3.4 NDI of Artificial Delamination in COPV Calibration Sample

3.3.4.1 Preparation and Embedding of Artificial Delamination Defects

Lauder et. al. (59) states that an interlaminar delamination could be simulated with using PTFE tapes between the composite laminates. Single sided PTFE tapes are selected to simulate the delamination defects between the wound layers. First the calibration COPV Sample is manufactured for validating the ultrasonic C-Scan inspection method. Four different square size of delamination are determined and prepared. The properties of the each artificial defect that are prepared for the manufacturing of calibration COPV Sample are given below in Table 3.6.

Table 3.6 Dimensions of artificial PTFE delaminations with square geometry for calibration COPV Sample

Delamination Code	***DEL-5***	***DEL-10***	***DEL-15***	***DEL-20***	***DEL-40***
Square Edge Length (mm)	5	10	15	20	40

Preparation of DEL-40 is explained as an example. It is aimed to prepare an envelope with the trapped air inside of this envelope. First, 40mm x 90 mm of PTFE tape is cut with a razor blade on a glass table. Then it is folded with the adhesive side out to the dimensions of 40 mm x 40 mm. Then a second tape is cut with the dimensions of 50 mm x 120 mm. This tape is folded by covering the opening of first folded tape with adhesive side in in order to trap the air inside and avoid adhesion in the envelope. The thickness of DEL-40 is measured with digital caliper and result is changing between 0.15-0.25 mm. Other artificial delaminations are measured in the same range.

Embedding of the artificial defects during filament winding process of calibration COPV Sample is shown in Figure 3.11.

Figure 3.11 Embedding of PTFE delamination defects to calibration COPV sample

During winding of the second helical layer, the artificial defects manually attached on the hoop layer to the predetermined locations by the help of the tackiness of the epoxy resin. Sometimes during winding of the helical layer, artificial defects may separate from the surface. By carefully handling of the artificial defect, mandrel speed set to the value of 1-2 rpm and the tensioned fiber holds the defect at some point.

3.3.4.2 Nondestructive Testing of COPV Calibration Sample

The monitoring of the artificial defects in composite materials could be conducted with non-destructive inspection (NDI) ultrasonic and radiographic techniques. Manually driven ultrasonic A-Scan method is more effectible on cylindrical composite parts than the dome generated composite parts. That is why automated ultrasonic C-Scan method is chosen for composite COPV parts. Ultrasonic waves are generated and transmitted to the composite part to detect voids, delaminations or any other defect by analyzing the reflection wave characteristics (60). For accurate results, the calibration sample manufacturing and detection is required in all NDI

techniques. A calibration COPV part is a sample which contains possible artificial defects with different dimension for simulation of delamination in the part.

Rotational inspection was emulated by performing a 3D contour following inspection around the calibration COPV Sample piece using automated ultrasonic C-Scan testing machine software. Artificial delaminations have been successfully detected between two carbon/epoxy composite laminate. In addition, potential delaminations originated during process have also been identified between the composite layers. The inspection map of the calibration COPV sample is given in Figure 3.12. By evaluating the results, it can be said that embedded artificial defects which simulates delamination in the composite laminates are detected successfully. In other words, the manufacturing method of COPV Samples with artificial defects is verified by ultrasonic C-Scan inspection.

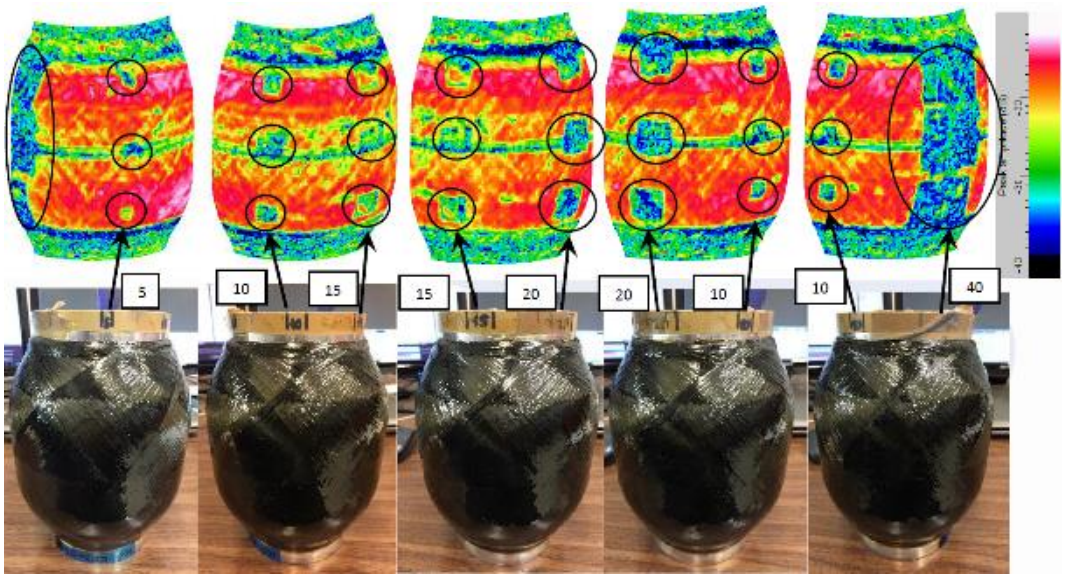

Figure 3.12 C-Scan ultrasonic inspection result of a COPV calibration sample

3.3.5 Manufacturing of COPV Samples with Artificial Delamination Defects

After manufacturing and NDI inspection of COPV calibration sample, even 5 mm edge of PTFE artificial delamination defects are being able to be monitored. Since

there is no technology to simulate real delamination in desired dimensions, in this study it is assumed that artificial delamination defects behave as real delamination. Failures in the burst testing may occur in cylindrical or dome section depending on stress ratio equation calculated for COPV. Effects of delamination to the burst pressure are investigated for both cases. It means that, XOXOO and XOX layer configurations are selected to introduce artificial PTFE delaminations to observe their effects to burst pressure of COPV samples. Skaar el. al. (61) claims that delamination caused by impact damage occurs near to the damaged area. Considering the impact damage location, outer surface of composite overwrapped pressure vessels may be subjected to impact damage during transportation between the manufacturing operations. That is why; the artificial delaminations are located under the last composite layer in this study. Two types of delamination sizes are determined to be introduced to COPV samples. First one is named as circumferential delamination and designated as DC. It has 40 mm of width and 460 mm of length. The second artificial delamination is designated as DLS and it has a square geometry with 40 mm of edge length. Both delamination types are considered to be embedded under last layer of the composite and to the middle section of the winding pattern. Delaminated COPV sample configuration is given in Table 3.7.

Table 3.7 Configuration of COPV samples with embedded artificial delaminations

Layer Configuration	***Delamination Type***	***Delamination Size (mm)***	***Abbreviation***	***Sample Repetition***
XOXOO	Circumferential	40 mm x 460 mm	XOXOO DC	3
	Local Square	40 mm x 40 mm	XOXOO DLS	3
XOX	Circumferential	40 mm x 460 mm	XOX DC	3
	Local Square	40 mm x 40 mm	XOX DLS	3

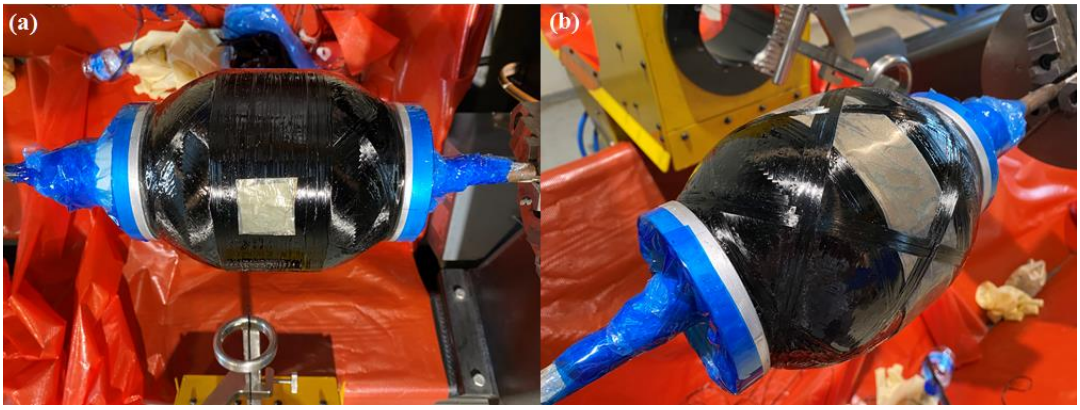

Figure 3.13 (a) Manufacturing of XOX DLC COPV sample (b) Manufacturing of XOXOO DC COPV sample

Artificial delamination is prepared with same method used in manufacturing of COPV calibration sample. During winding of both XOXOO and XOX layer configurations, DC and DLC artificial delaminations are embedded under the last layer of composite, as it is shown in Figure 3.13. Although the artificial defects are not clear to be seen as they are in ultrasonic C-Scan inspection, they could also be detected by X-Ray radiographic inspection method. The certified technicians could observe the artificial defects in COPV sample. The X-Ray radiograph of COPV sample with 40 mm x peripheral artificial delamination, which has XOX DC abbreviation, is given in Figure 3.14.

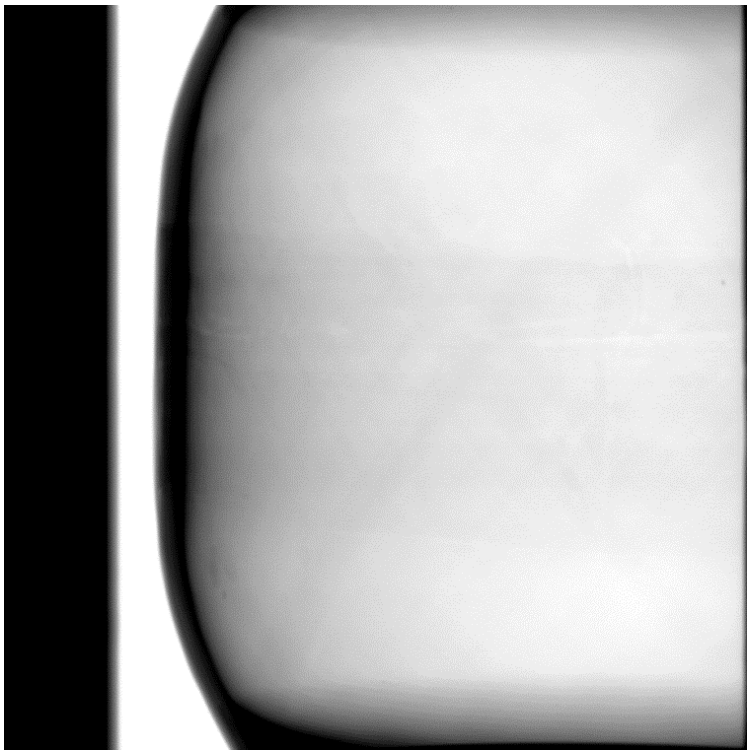

Figure 3.14 X-Ray radiographic inspection of a XOX DC COPV sample

3.3.6 Manufacturing of COPV Samples with Spaced Winding

In the filament winding process, resin impregnated fiber bundles ought to be laid to the neighboring filament without any gap. However due to the some parameters such as variation of fiber bundle throughout the length and filament winding machine fiber delivery tooling geometry, gaps/openings may be observed between fiber bundles on the wound part. Although it may be observed at the first layer dues to the contrast between liner material or mandrel, it is not possible to detect gaps after first layer. This situation creates an uncertainty for the product's quality. In this study, the gaps in composite overwrapped pressure vessels layers defined as spaced winding and their effect to the burst pressure is investigated. As in COPV samples with delaminations, XOX and XOXOO layer configurations are determined to apply spaced winding to COPV samples. In the range between 1.0-1.5 mm of gaps are targeted to achieve because there is a variation not only in the bandwidth of fiber

itself but also in the winding path. As explained earlier, X is designated as helical layer and O is designated for hoop layer in the layer configuration. When spaced winding applied for the X layer, it is called as spaced winding X aka SWX. Same logic for the abbreviations is valid for the other spaced wound COPV samples. The spaced winding COPV sample configuration is given in Table 3.8. There are 18 spaced winding COPV samples are manufactured in total.

Table 3.8 Spaced winding COPV sample configuration

Layer Configuration	***Spaced Winding Type***	***Gap Size (mm)***	***Abbreviation***	***Sample Repetition***
XOXOO	Gaps in X layers	1.0-1.5 mm	XOXOO SWX	3
	Gaps in O layers	1.0-1.5 mm	XOXOO SWO	3
	Gaps in X&O layers	1.0-1.5 mm	XOXOO SWXO	3
XOX	Gaps in X layers	1.0-1.5 mm	XOX SWX	3
	Gaps in O layers	1.0-1.5 mm	XOX SWO	3
	Gaps in X&O layers	1.0-1.5 mm	XOX SWXO	3

For the COPV samples that has no gap, the bandwidth is chosen as 3 mm as explained in the generating winding program for COPV. When single layer is completely wound, there are no gaps observed with 3 mm bandwidth. In order to observe 1.0-1.5 mm gaps between each fiber bundle, the bandwidth is selected between 4.5 mm. The winding software calculated the pattern as 5 with 78 circuits when bandwidth is defined as 4.5 mm. As it can be seen from Figure 3.15, the helical and hoop layers with spaced winding are achieved by using defined methodology.

Figure 3.15 (a) 1.0-1.5 mm spaced winding of helical layer in COPV (b) spaced wound helical layer (c) 1.0-1.5 mm spaced winding of hoop layer in COPV (d) completed spaced wound XOX COPV sample

The fiber weight of a single helical layer is directly proportional to the circuit number. In other words, while creating gaps between fiber bundles with increased bandwidth value, the fiber hence composite material weight decreases as expected. However the aim of this study is to observe if there is an additional drop down at the burst pressure not only by virtue of the decrease at the weight but also caused by local stress concentrations that occur due to the gaps between bundles.

3.3.7 Curing Process of COPV Samples

Following the filament winding process, the wet composite part should be cured in a composite curing furnace with a rotation system. If the mandrel is not rotated during curing process, significant amount of resin is going to be dripped because of

the gravitational force until the resin gelation stage is completed. By rotating the mandrel during curing process, homogeneous distribution of the epoxy resin in the composite is acquired. COPV sample is mounted to the chuck inside of the furnace from the metal shaft and the rotation is started. After filament winding operation, COPV samples are placed in an oven with rotation system as it can be seen from Figure 3.16.

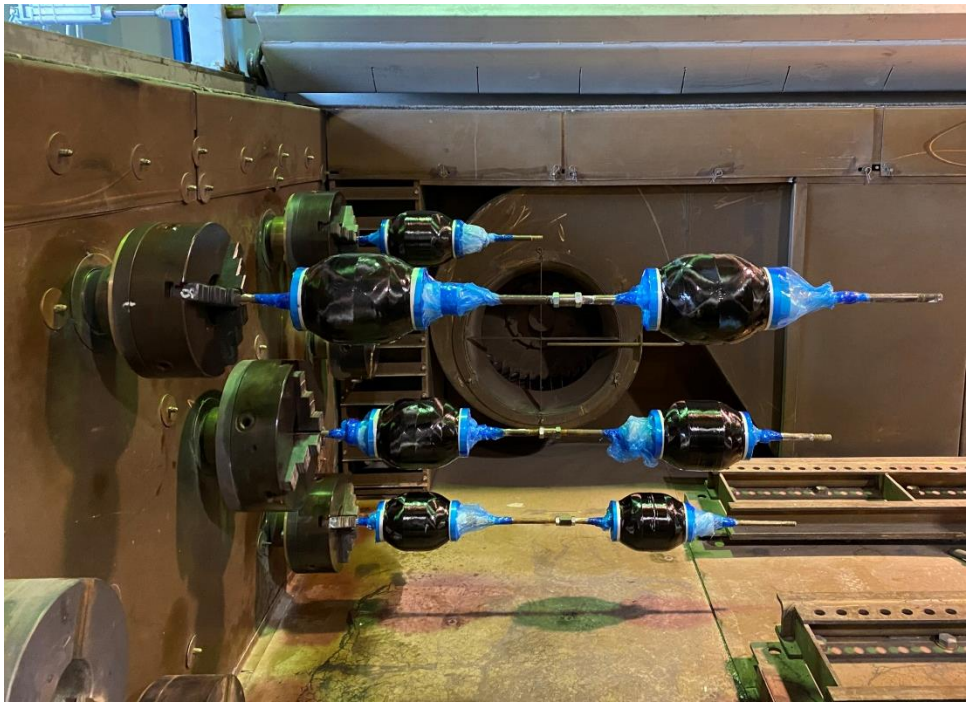

Figure 3.16 Rotating of COPV samples before curing operation

Curing profile is determined from the recommended curing profiles in TDS of the resin system. For the complete gelation of the resin system, recommended curing cycle in TDS of resin system is applied. From the past experiences and literature; heating rate is set to 3 ^{o}C/min (62) and after the curing is completed, the sample is cooled in the furnace cooling condition to avoid thermal stresses at the composite part.

3.3.8 Mandrel Removal of COPV Samples

After the curing process is completed, water soluble mandrel is removed from the COPV Sample. It is subjected to pressurized RT water for approximately 15 minutes. The mandrel is torn apart into pieces however since these pieces are not in the dust form, they may blockage the drainage hole. That is why a 10 grit metal mesh is placed at the entry of the drainage hole. When most of the pieces are detached from the COPV part, the metal shaft is loosened and it can be taken out from the part by hand. There are some residuals of water soluble mandrel especially at the liner adhesion areas nevertheless they could be removed by using sandpaper.

3.4 Hydrostatic Burst Testing of COPV Samples

3.4.1 Hydrostatic Burst Testing Setup of COPV Samples

COPV Samples are subjected to hydrostatic burst tests to observe burst strength performances. The vessels were placed in a rectangular prism test chamber that had an aluminum sigma profile chassis and transparent PMMA windows on three sides to observe inside of the chamber as it can be seen in Figure 3.17 (c). A mirror was also placed on the remaining side of the chamber to make visible the backside of the vessel. Finally, the top of the chamber was closed with a thick steel plate. The steel plate had two holes for the pressurization pipes and for strain gauges cables which are connected to COPV sample caps in Figure 3.17 (a). A water pressurization system with capacity of 9500 *psi* was utilized. The vessels were pressurized with a rate of 150 *psi*/s. Internal pressure data was monitored and collected by the pressurization system which is shown in Figure 3.17 (b).

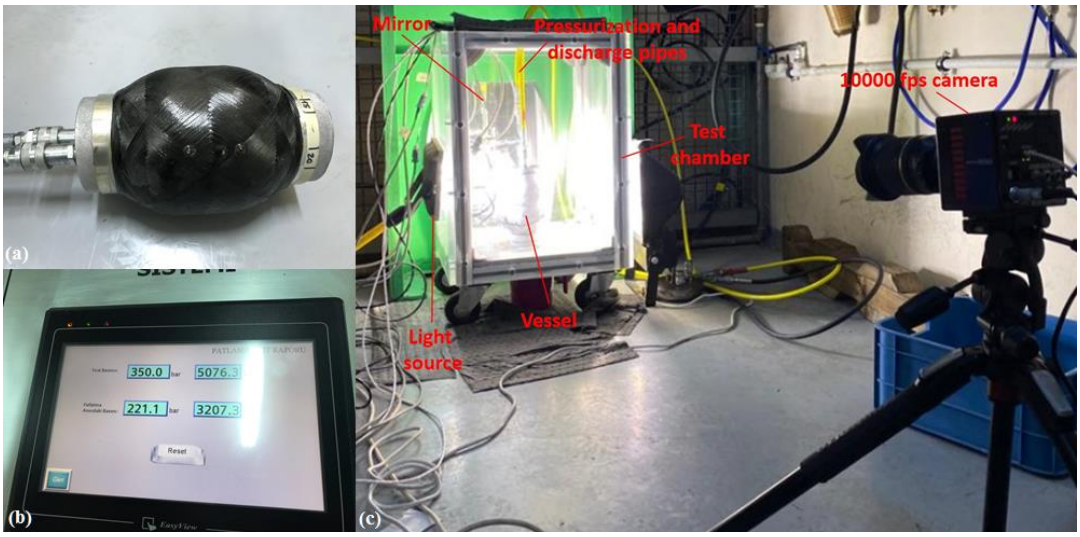

Figure 3.17 (a) COPV burst testing apparatus and connection (b) burst testing machine interface (c) COPV burst testing setup

Before the burst tests, the vessels are controlled for any sign of leakage. This is done by first pressuring the vessels at 300 *psi* and waiting for a minute at that pressure. If no sign of leakage is observed then the pressure is released and the burst test begins afterwards. For both the leakage and the burst tests the internal pressure of vessel were increased at a rate of 150 *psi*/s.

A high-speed camera was placed directly on the opposite side of the mirror-side wall of the chamber. The chamber was lit up from the other two sidewalls by external light sources. The camera was placed such that between its own view coverage and the reflection from the mirror, to make visible most of the COPV samples. This corresponds to around 300° of the circumference of the vessels. The data collected by the high-speed camera was at 10000 frames per second, which was deemed enough to observe the damage initiation occurring during the burst event.

3.4.2 Strain Gauge Application to COPV Samples

Hoop strains on the cylindrical region of the vessels were monitored by unidirectional strain gauges with a gauge length of 3 mm and 350-ohm resistance.

To track any deviation from axisymmetric behavior of the vessel 3 strain gauges were placed 100 mm away from the ends of COPV sample, which corresponds to the mid-section of the part. The strain gauges were spread along the circumferential direction with 120° angle between them. Strain measurement was taken at a rate of 10000 data per second.

Burst pressures and maximum hoop strain readings per COPV sample are recorded. Strains recorded from each sample were in agreement with each other with a coefficient of variation less than 5%. Hence, for better readability, maximum hoop strain measured for each vessel will be presented in the results and discussions section.

CHAPTER 4

RESULTS AND DISCUSSION

4.1 Material Characterization Results of Carbon/Epoxy Composites

4.1.1 Fiber Volume Fraction Testing Results

For each tensile testing coupon, two batches of composite plate manufacturing have been completed. During cutting operation, 3 specimens are collected from two different batches to specify fiber volume fraction. Fiber/resin weight ratio is calculated as explained in section 3.1.4 according to ASTM D 3171, Method B. Fiber volume fraction results of two manufacturing batches are given in Table 4.1.

Table 4.1 Fiber volume fraction results of two manufacturing batches for coupons

Batch number	***Specimen-1***	***Specimen-2***	***Specimen-3***	***Average fiber volume fraction***
1	0,575	0,552	0,560	0,56
2	0,593	0,571	0,585	0,58

MIL-HDBK-17F (38) states that fiber volume between 0.55-0.65 has been nominated to allow consistent measurement of normalized fiber properties for carbon fiber laminates. It can be seen that, the results of 0.56 and 0.58 for two batches of composite plate are in between 0.55-0.65 fiber volume fraction range.

4.1.2 Longitudinal Tensile Testing Results of Carbon/Epoxy Coupons

Two batches of manufacturing have been completed for 15 coupons of longitudinal tensile testing (0^o direction). Although there is a slight difference in the fiber volume fractions of batches (0.56 and 0.58) batch-to batch variability is assumed to be negligible. Total number of 15 tensile testing coupons is prepared and tested according to ASTM D3039 (40). Tensile testing results are given in Table 4.2. Longitudinal tensile stress-strain curve is given in Figure 4.1.

Table 4.2 Longitudinal tensile testing results of carbon/epoxy coupons

Coupon Number	***Longitudinal Tensile Strength (MPa)***	***Poisson's Ratio (ν_{12})***	***Elastic Modulus (MPa)***	***Strain (%)***
1	1954	0.33	131200	1,49
2	1849	0.32	132235	1,40
3	1901	0.33	130974	1,45
4	2045	0.34	132616	1,54
5	2032	0.33	128488	1,58
6	2131	0.33	134584	1,58
7	-	-	-	-
8	1259	0.30	121354	1,04
9	1947	0.34	124196	1,57
10	1862	0.32	135216	1,38
11	1446	0.32	119258	1,21
12	1927	0.33	135673	1,42
13	1983	0.33	129018	1,54
14	2085	0.33	130974	1,59
15	2016	0.34	128257	1,57

Coupon 7 had an earlier failure at the start of testing due to the mistake in mounting of the specimen that is why testing data cannot be taken. In addition to this, there were early failures occur from tab termination regions at testing of Coupon 8 and 11, the tensile strength of these coupons were calculated as 1259 MPa and 1446 MPa respectively. The failure images of the tab termination region failure and first six coupons are given in Figure 4.2.

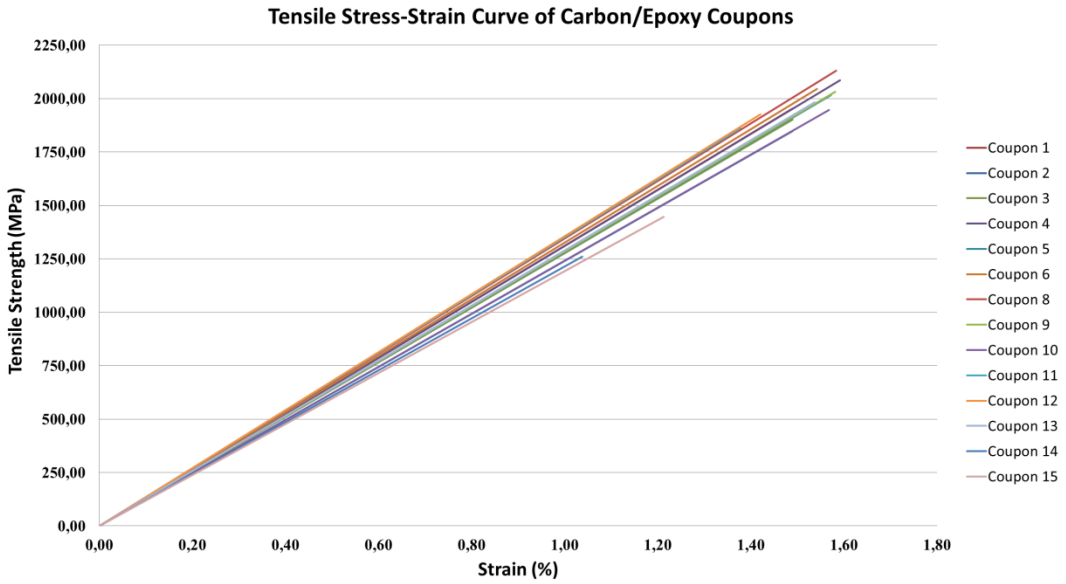

Figure 4.1 Longitudinal tensile stress-strain curve of carbon/epoxy coupons

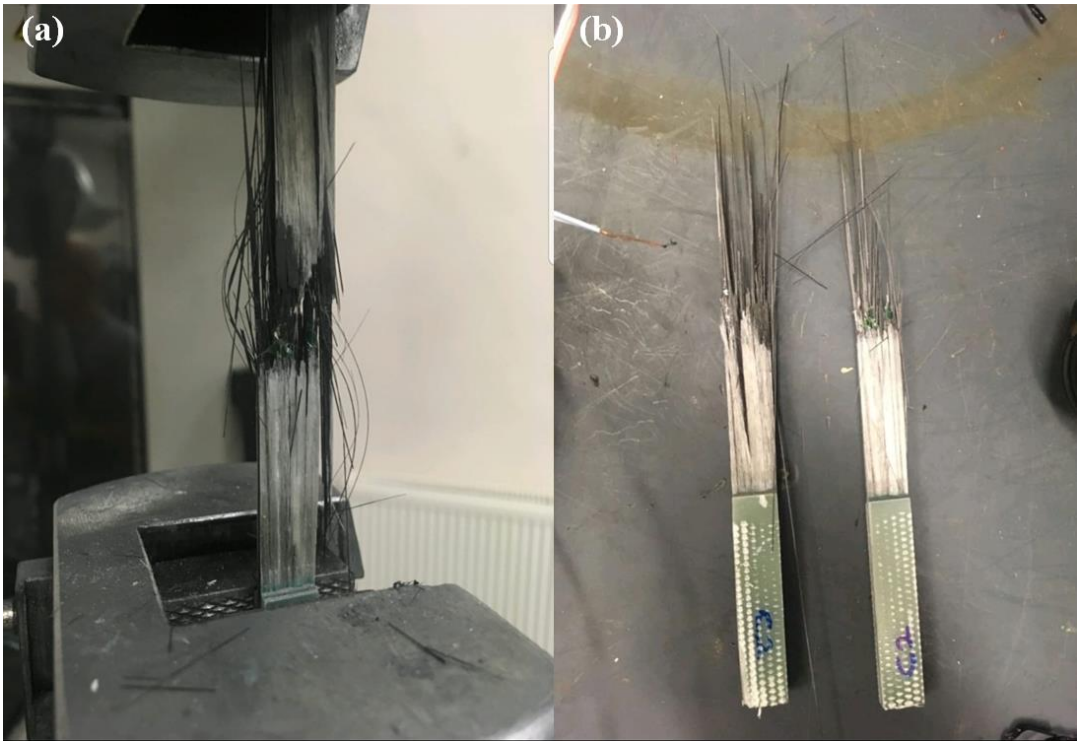

Figure 4.2 (a) Failure of longitudinal tensile specimen (b) Fracture surface of Coupon 2.

The mechanical properties obtain from tensile testing results are given in Table 4.3. Due to the early failures of Coupon 7,8 and 11, these specimens are not included to statistical calculations of tensile strength. At it can see from Table 4.3, coefficient of variance values of Elastic Modulus and Tensile Strength values are calculated as 2.52 and 4.41 respectively. Romano et. al. (63) states that coefficient of variance values between 2.44 and 7.95 is considered to be intermediate statistically. It may be concluded that, longitudinal tensile testing results are applicable to be used in the design of COPV sample since the scattering in the data is acceptable.

Table 4.3 Statistical outcomes of Longitudinal Elastic Modulus and Tensile Strength results

	Average Value	***Standard Deviation***	***Coefficient of Variance***
Elastic Modulus (GPa)	131	4.99	3.80
Longitudinal Tensile Strength (MPa)	1978	87.20	4.41

4.1.3 Transverse Tensile Testing Results of Carbon/Epoxy Coupons

Although there is no need of transverse tensile strength for the calculation of layer configuration according to netting theory (18), transverse testing of carbon/epoxy coupons are completed. Total number of 10 coupons is prepared according to ASTM D3039 (40) for testing however Coupon 2 and Coupon 3 could not be successfully tested due to the early damaging during testing. Transverse tensile testing results are given in

Table 4.4.

Table 4.4

Transverse tensile testing results of carbon/epoxy coupons

Coupon Number	***Transverse Tensile Strength (MPa)***	***Poisson's Ratio (ν_{21})***	***Elastic Modulus (MPa)***	***Strain (%)***
1	52,12	0,016	8741,82	0,596
2	-	-	-	-
3	-	-	-	-
4	50,65	0,017	8205,47	0,617
5	48,08	0,019	8581,72	0,560
6	47,85	0,014	7994,80	0,599
7	47,52	0,014	7747,05	0,613
8	42,39	0,013	7747,93	0,547
9	44,36	0,020	7738,10	0,573
10	45,91	0,014	7110,05	0,646

When the results are statistically evaluated (Table 4.5), it is seen that coefficient of varience is in the intermediate region as well. It is expected to observe transverse tensile strength is less than the tensile strength of resin due to the limited interface strength between resin and fiber. Transverse stress-strain curve is given in Figure 4.3.

Table 4.5 Statistical outcomes of Transverse Elastic Modulus and Tensile Strength results

	Average Value	***Standard Deviation***	***Coefficient of Variance***
Elastic Modulus (GPa)	7983	523,3	6,55
Transverse Tensile Strength (MPa)	47,4	3,2	6,68

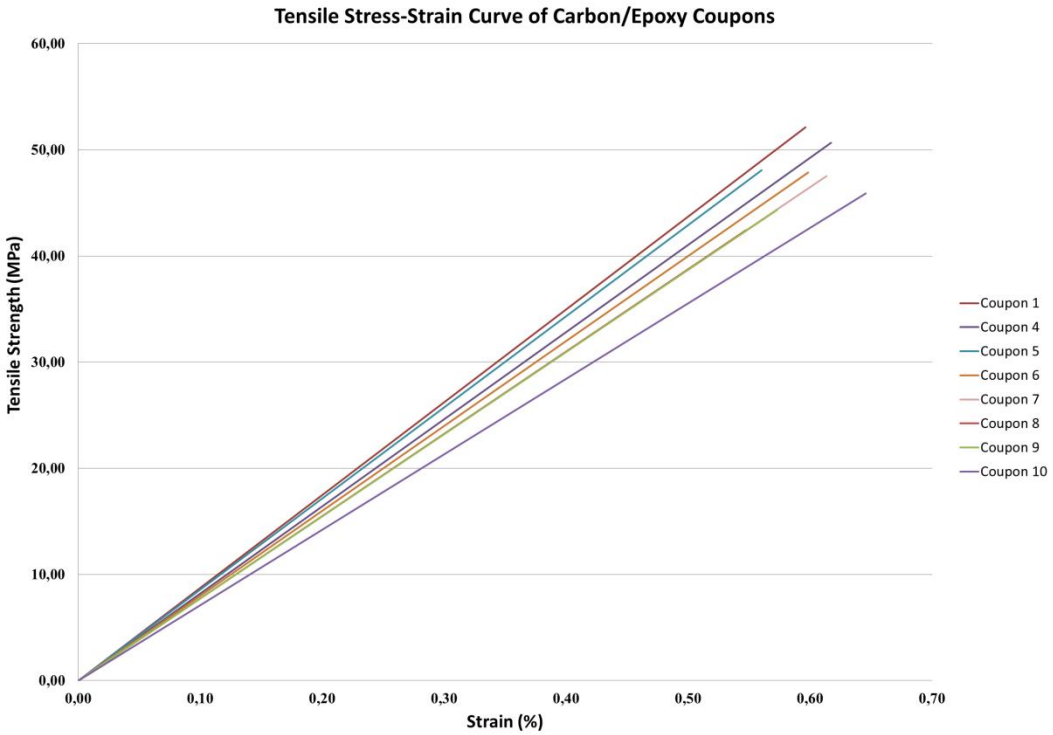

Figure 4.3 Transverse tensile stress-strain curve of carbon/epoxy coupons

4.2 COPV Fiber/Resin Volume Fraction Testing Results

Specimens from tested COPV samples are cut for some purposes such as determining fiber/resin fraction and investigation of microstructure. In order to observe the differences between COPV sample configurations, specimens are taken from cylindrical and dome sections. It is seen from Figure 4.4, COPV sample on the left side is with XOX layer configuration and COPV sample on the right side is XOXOO layer configuration.

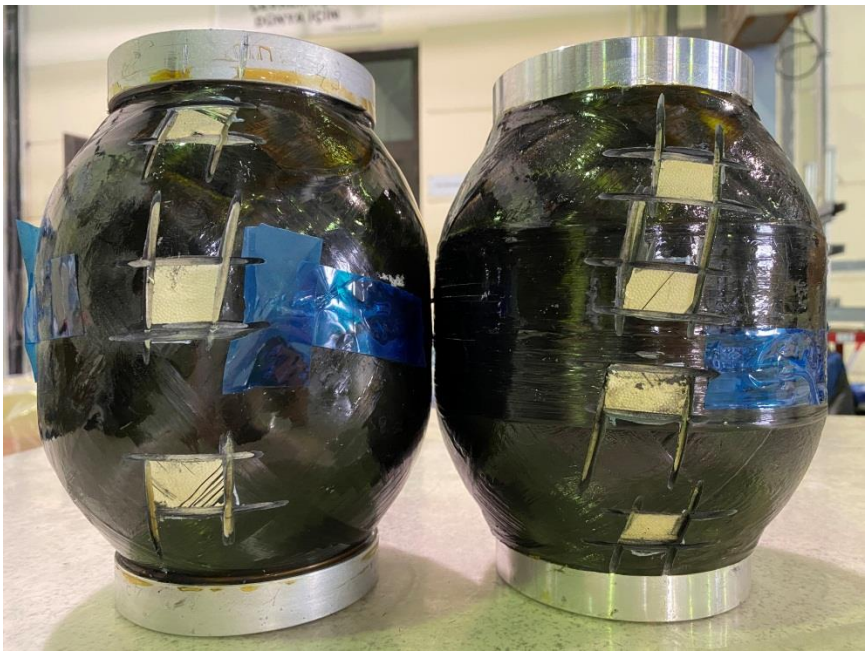

Figure 4.4 XOX COPV layer configuration on the left side, XOXOO COPV layer configuration on the right side

Specimens are taken from ten COPV samples. In order to validate the fiber volume fraction variation, four of stress ratio specimens are chosen which are XOXOO-1, XOXOO-2, XOX-1, XOX-2. In addition, one for each spaced winding COPVs are selected to observe if spaced winding have an effect on fiber volume fraction in the composite. Fiber/resin weight ratio is tested according to ASTM D 3171 (Method B), Test Methods for Constituent Content of Composite Materials Fiber as it is applied to coupon composite parts in Section 3.1.4. Fiber/resin volume fraction test results of COPV samples are given in Table 4.6. The average fiber volume ratio is 0.61, which is in the expected range for wet filament wound parts (64). When the results are evaluated, it is seen that cylindrical sections have a larger fiber volume fraction than the come section have. This is most probably caused by the rotation of COPV samples during curing. Wet resin tends to migrate from the cylindrical sections to the dome sections due to the gravitational force before glass transition temperature (T_g) and this situation causes dome section to have higher resin content.

Table 4.6 Fiber volume fraction test results of COPV samples

Sample Name	*Specimen Location*	*Average Fiber Volume Fraction*
XOXOO-1	Dome	0.58
XOXOO-1	Cylinder	0.62
XOXOO-2	Dome	0.56
XOXOO-2	Cylinder	0.61
XOXOO SWXO-3	Dome	0.53
XOXOO SWXO-3	Cylinder	0.59
XOXOO SWO-2	Dome	0.56
XOXOO SWO-2	Cylinder	0.61
XOXOO SWX-2	Dome	0.55
XOXOO SWX-2	Cylinder	0.62
XOX-2	Dome	0.56
XOX-2	Cylinder	0.62
XOX-3	Dome	0.60
XOX-3	Cylinder	0.63
XOX SWXO-1	Dome	0.53
XOX SWXO-1	Cylinder	0.61
XOX SWO-2	Dome	0.60
XOX SWO-2	Cylinder	0.63
XOX SWX-2	Dome	0.54
XOX SWX-2	Cylinder	0.60

4.3 Burst Testing Results of COPV Samples

4.3.1 Burst Testing Results of COPV Layer Configuration Samples

Total number of 39 COPV samples is subjected to hydrostatic burst testing in this study. As introduced before, there are 9 COPV samples are subjected to burst pressure to observe the effect of stress ratio. These COPV samples are labeled as XOXOO, OXOX and XOX with 3 repetitions. The burst pressure results and failure areas of these samples are given in Table 4.7. In order to clarify the burst pressure result and fracture behavior of DC XOX sample, only one sample of XXO layer

configuration is manufactured and tested. The motivation shall be explained in Discussion section in detail.

Table 4.7 Burst pressure results, strain values and failure areas of COPV layer configuration samples

Serial Number	*Layer Configuration*	*Theoretical Burst Pressure (psi)*	*Burst Pressure (psi)*	*Max. Hoop Strain (%)*	*Failure Location*
XOXOO-1	XOXOO	4460	3542	1.04	Dome
XOXOO-2	XOXOO		3256	0.96	Dome
XOXOO-3	XOXOO		2904	0.87	Dome
OXOX-1	OXOX	3229	3518	1.46	Dome + Cylinder
OXOX-2	OXOX		3331	1.39	Dome + Cylinder
OXOX-3	OXOX		3116	1.28	Dome + Cylinder
XOX-1	XOX	1975	2176	1.56	Cylinder
XOX-2	XOX		2297	1.62	Cylinder
XOX-3	XOX		2453	1.70	Cylinder
XXO-1	XXO		1640	1.30	Cylinder

4.3.2 Burst Testing Results of COPV Samples with Delaminations

COPVs with manufacturing artificially embedded delamination defects were manufactured and tested in order to observe burst pressure and failure locations. Two types of delaminations introduced to the both XOXOO and XOX COPV layer configurations. First type of delamination is a circumferential delamination which has dimensions of 40 mm x 460 mm and it designated as DC. Second one is a local square delamination with 40 mm of edge length and it is called DLS. When the layer configuration and 3 repetitions are considered, 12 COPV samples are manufactured and tested. The results of COPV samples with delaminations are given in Table 4.8.

Table 4.8 COPV samples with delaminations burst pressure results, strain values and failure areas

Serial Number	*Layer Configuration*	*Delamination Dimensions*	*Burst Pressure (psi)*	*Max. Hoop Strain (%)*	*Failure Area*
DC-1	XOXOO	40mm x Peripheral	2979	0.95	Dome
DC-2	XOXOO	40mm x Peripheral	2996	0.96	Dome
DC-3	XOXOO	40mm x Peripheral	3062	1.00	Dome
DLS-1	XOXOO	40x40 mm square	3207	1.03	Dome
DLS-2	XOXOO	40x40 mm square	3324	1.06	Dome
DLS-3	XOXOO	40x40 mm square	3074	0.99	Dome
DC-1	XOX	40mm x Peripheral	2062	1.44	Cylinder
DC-2	XOX	40mm x Peripheral	1869	1.40	Cylinder
DC-3	XOX	40mm x Peripheral	1897	1.34	Cylinder
DLS-1	XOX	40x40 mm square	2277	1.53	Cylinder
DLS-2	XOX	40x40 mm square	2345	1.60	Cylinder
DLS-3	XOX	40x40 mm square	2195	1.49	Cylinder

4.3.3 Burst Testing Results of Spaced Winding COPV Samples

Spaced wound COPV samples are manufactured with setting fiber bandwidth to 4.5 mm instead of 3 mm in no defect COPV manufacturing. As mentioned before, SWX stands for spaced winding in helical layer, SWO stands for spaced winding in hoop layer. When there are gaps in both helical and hoop layers, vessel sample is designated as SWXO. All three types of spaced winding are introduced for XOXOO and XOX layer configurations, and the corresponding results of 18 spaced winding COPV samples are given in Table 4.9.

Table 4.9 Spaced winding COPV samples burst pressure results, strain values and failure areas

Serial Number	*Layer Configuration*	*Imperfection Type*	*Burst Pressure (psi)*	*Max. Hoop Strain (%)*	*Failure Area*
SWXO-1	XOXOO	Gaps in all layers	2361	1.21	Dome
SWXO-2	XOXOO	Gaps in all layers	1834	0.94	Dome
SWXO-3	XOXOO	Gaps in all layers	2089	1.07	Dome
SWO-1	XOXOO	Gaps in O layers	3088	1.58	Dome
SWO-2	XOXOO	Gaps in O layers	2938	1.51	Dome
SWO-3	XOXOO	Gaps in O layers	3332	1.70	Dome
SWX-1	XOXOO	Gaps in X layers	2463	0.80	Dome
SWX-2	XOXOO	Gaps in X layers	2403	0.79	Dome
SWX-3	XOXOO	Gaps in X layers	2545	0.83	Dome
SWXO-1	XOX	Gaps in all layers	1358	1.58	Cylinder
SWXO-2	XOX	Gaps in all layers	1410	1.61	Cylinder
SWXO-3	XOX	Gaps in all layers	1440	1.62	Cylinder
SWO-1	XOX	Gaps in O layers	2339	1.81	Cylinder
SWO-2	XOX	Gaps in O layers	2330	1.79	Cylinder
SWO-3	XOX	Gaps in O layers	2255	1.75	Cylinder
SWX-1	XOX	Gaps in X layers	1540	1.19	Dome
SWX-2	XOX	Gaps in X layers	1620	1.26	Dome
SWX-3	XOX	Gaps in X layers	1740	1.35	Dome

4.4 Examination of COPV Specimen Microstructures in Optical Microscope

4.4.1 Optical Examination of COPV Winding Layers

Ozaslan et. al (65) describes route to prepare filament wound carbon/epoxy composite specimen for getting optical images. Some of the operations are applied

at the specimen preparation process. First composite specimens are cut in the dimensions of 25 mm (l) x 10 mm (w) from the undamaged section of burst COPV samples. Although it is recommended to use Bakelite cast resin for the specimens to be placed, it is not used in this study. Specimens are grinded with 250-grit, 1200-grit and 4000-grit sandpaper respectively for at least 30 second each. It is critical to apply the load vertically to sandpaper in order to get equal contrast from the surface. Then, specimens are polished with 3 microns of diamond suspension. The optical analysis is conducted with a NIKON Eclipse LV100MD microscope.

Figure 4.5, 50x optical micrograph of XOXOO layer configuration with no defect can be seen. The image is taken from the radial section of the composite thickness which means hoop layers can be observed as long strips. In the micrograph, first X layer is cannot be seen on the bottom. However, starting from the down-side thicknesses of first O layer, second X layer and last two O layers can be seen clearly. The thickness values measured for the O and X helical layers are very close to the theoretical ones that are used in the calculations which are X layer: 0.60 mm and O layer: 0.30 mm.

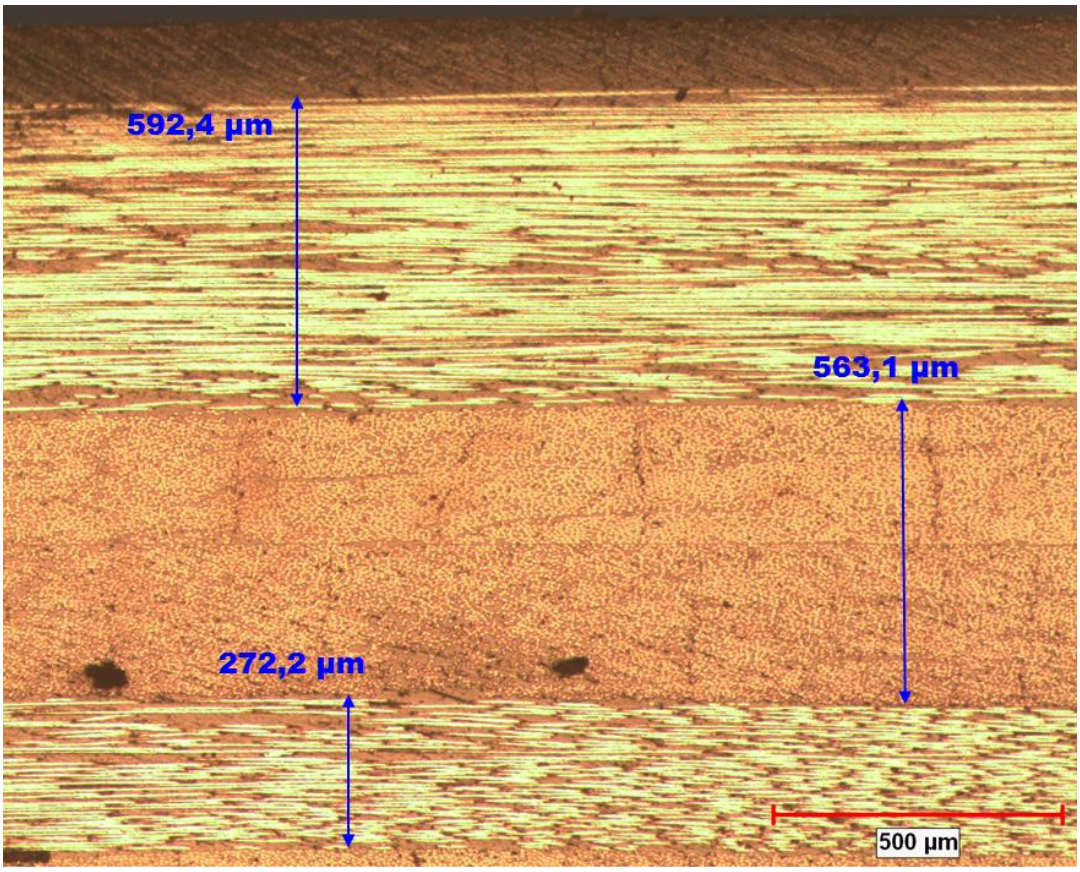

Figure 4.5 50x micrograph of XOXOO COPV sample with no defect

XOXOO SWXO vessel specimen (spaced winding of both X and O layers) is investigated with optical microscope in order to see the effects of spaced winding. In Figure 4.6, 50x magnification of XOXOO SWXO image with first two layers can be seen. Since helical layers contain two woven sub-layers with $+40^{o}$ and -40^{o} winding angle, the interface between them is observed clearly in the micrograph. During the scanning of the surface in the microscope, it is realized that there are no actual spaces in the structure. Due to the residual tension in the fibers after filament winding process and shrinkage of resin system during curing, fibers tend to migrate to the vacancies. In other words, optical evaluation reveals that spaced winding method do not cause large resin-rich areas in the microstructure; it causes a certain decrease in the layer thickness.

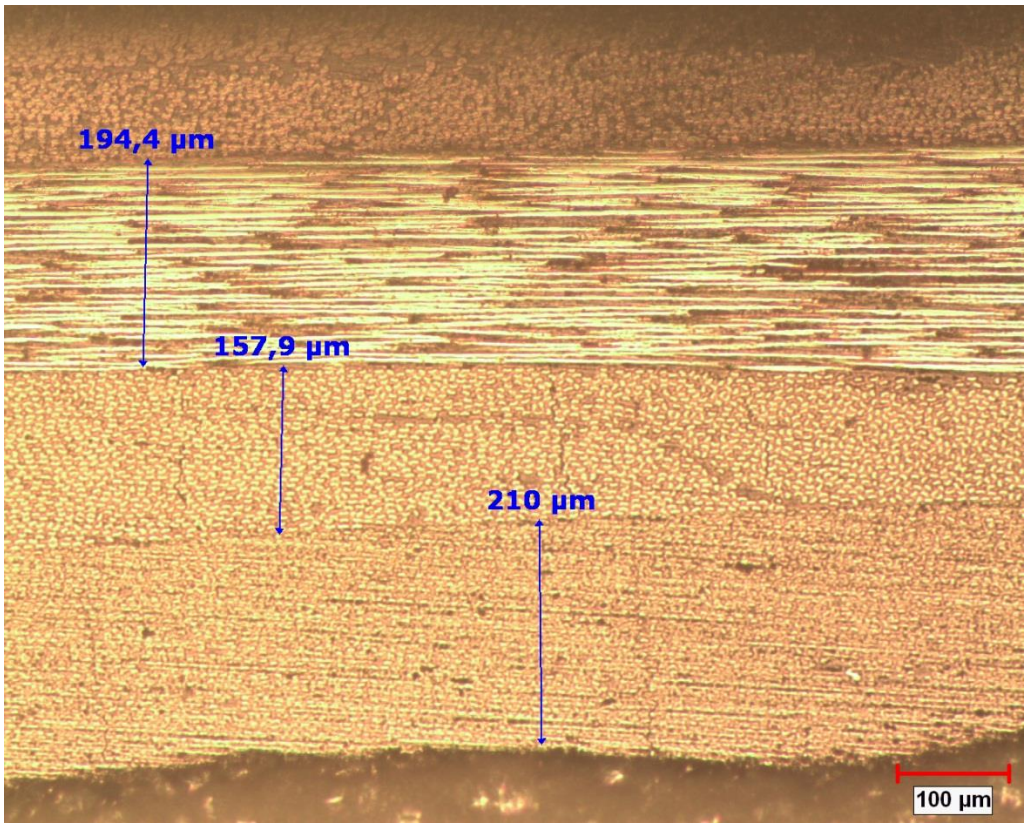

Figure 4.6 50x micrograph of XOXOO SWXO COPV

As mentioned before when the bandwidth is set to 3 mm (actual fiber bandwidth), winding software generates 116 circuit winding program for a complete X layer. On the other hand, when the bandwidth is set to 4.5 mm for spaced winding, software generates 78 circuit winding program. Circuit number is proportional with the length hence weight of the carbon fiber used. For that reason, circuit number is proportional with the thickness of X layer as expected.

$$\frac{Circuit\ number\ of\ X\ (1.5\ mm\ gap)}{Circuit\ number\ of\ X\ (no\ gap)} = \frac{78}{116} = \frac{X\ thickness\ (1.5\ mm\ gap)}{X\ thickness\ (no\ gap)}$$

When the calculation is made, 78/116= 0.67 value is found. The calculated theoretical thickness values and measured thickness values are given in Table 4.10. Same calculation is applied for the O layer for XOXOO layer configuration. When optical image of the XOX SWX (spaced winding at X layers) is evaluated, measured thickness values are similar with the ones in XOXOO layer configuration. It should

be noted that, thickness values of layers may change due to dimensional variation in fiber material and filament winding process parameters such as resin viscosity. Bandwidth of fiber tows may change from batch to batch. In addition, as the viscosity increases, the spreading of the fibers will decrease.

Table 4.10 Theoretical and measured thickness values of X and O layers

	XOXOO COPV with no defect		***XOXOO SWXO COPV***	
Layer Type	***Average of Measured Thickness (µm)***	***Theoretical Thickness (µm)***	***Average of Measured Thickness (µm)***	***Expected thickness, no gap (µm)***
X layer	560	600	360	403
O layer	280	300	190	201

X and O layer intersection area is viewed with 1000x of magnification in vertical cross-section. In Figure 4.7 (a) X and O interface can be seen clearly. Since the cross-section is vertical, hoop fibers have a shape which is close to a circle. Sharp et. al. (66) states that due to the change in the viewing angle of the fibers, geometry of fiber cross-section changes. Since helical layers have 40^{o} of angle with the vertical-view, the fibers have a bean-like shape (Figure 4.7(a)).

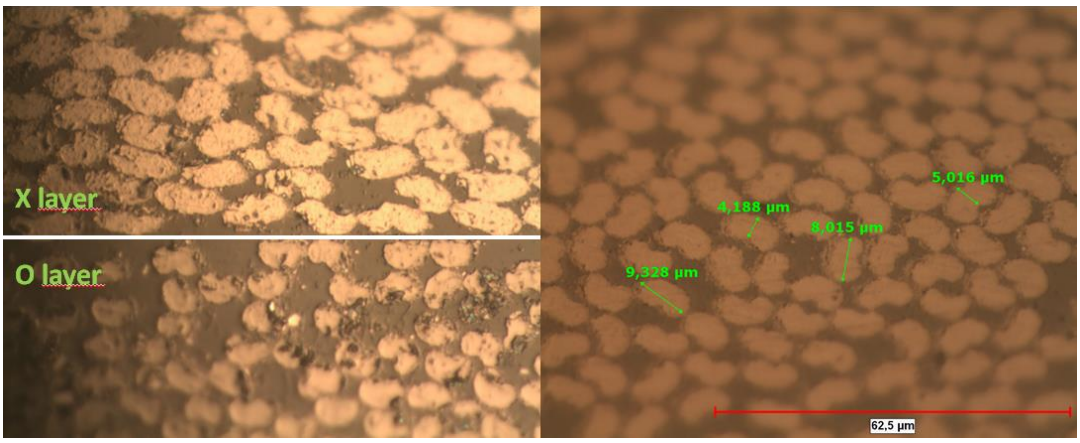

Figure 4.7 1000x magnification (a) X-O interface (b) bean shaped fibers

Last specimen that is examined in the optical microscope is XOX DLS COPV sample which has artificial local square delamination with 40 mm of edge. In chapter

to it is mentioned that artificial delamination thickness has been measured between 0.15-0.25 mm. This value is measured as 0.184 mm in the Figure 4.8. Moreover, there is a resin-rich rectangle at the tip of the delamination whose longer edge is around 1 mm. This may cause stress concentration effect when the vessel is subjected to burst pressure. However, there is no specific failure mode that proofs as COPV sample with delamination burst close to the tip of the delamination in this study.

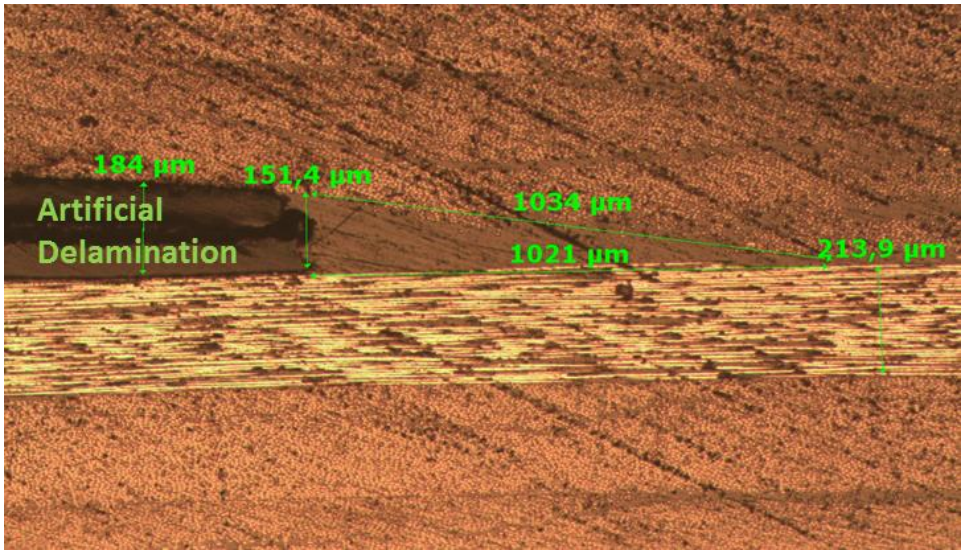

Figure 4.8 50x micrograph of XOX DLS COPV

4.5 Evaluation Fracture Surfaces of COPV Samples in SEM

Scanning electron microscope specimen is obtained near to one of the burst XOX COPV sample. As it can be seen from the macro images of the fracture surface, it is no possible to detect crack initiation area after burst (Figure 4.9). There is a shiny area at the outer layer due to high-resin concentration such as resin coating. However, there is a dull surface at the inner sections of part where the SEM specimen

is cut from. Since epoxy resin is nonconductive in carbon/epoxy composites, specimen is coated with 25 nm of gold before SEM imaging.

Figure 4.9 Macro image of XOX COPV (with no defect) failure surface.

Shin et. al (67) investigates SEM images of carbon/epoxy sample double cantilever beam mode II fracture surfaces, there are epoxy bridges and imprints of bulk debonding of fibers from the epoxy surface. Likewise, Kadlec et. al. (68) examines the fracture surface of carbon/epoxy composite, riverlines and cusps marks on the epoxy surfaces shows that composite has interlaminate shear failure. Fracture surfaces of XOX COPV obtained by SEM are given in Figure 4.10. Similar fracture surfaces are monitored in SEM images XOX COPV sample when compared with the ones in the literature. In Figure 4.10 (a) and (b), the epoxy bridges can be seen

clearly. In addition to that, some fibers are pulled-out with the effect of pressure at some level.

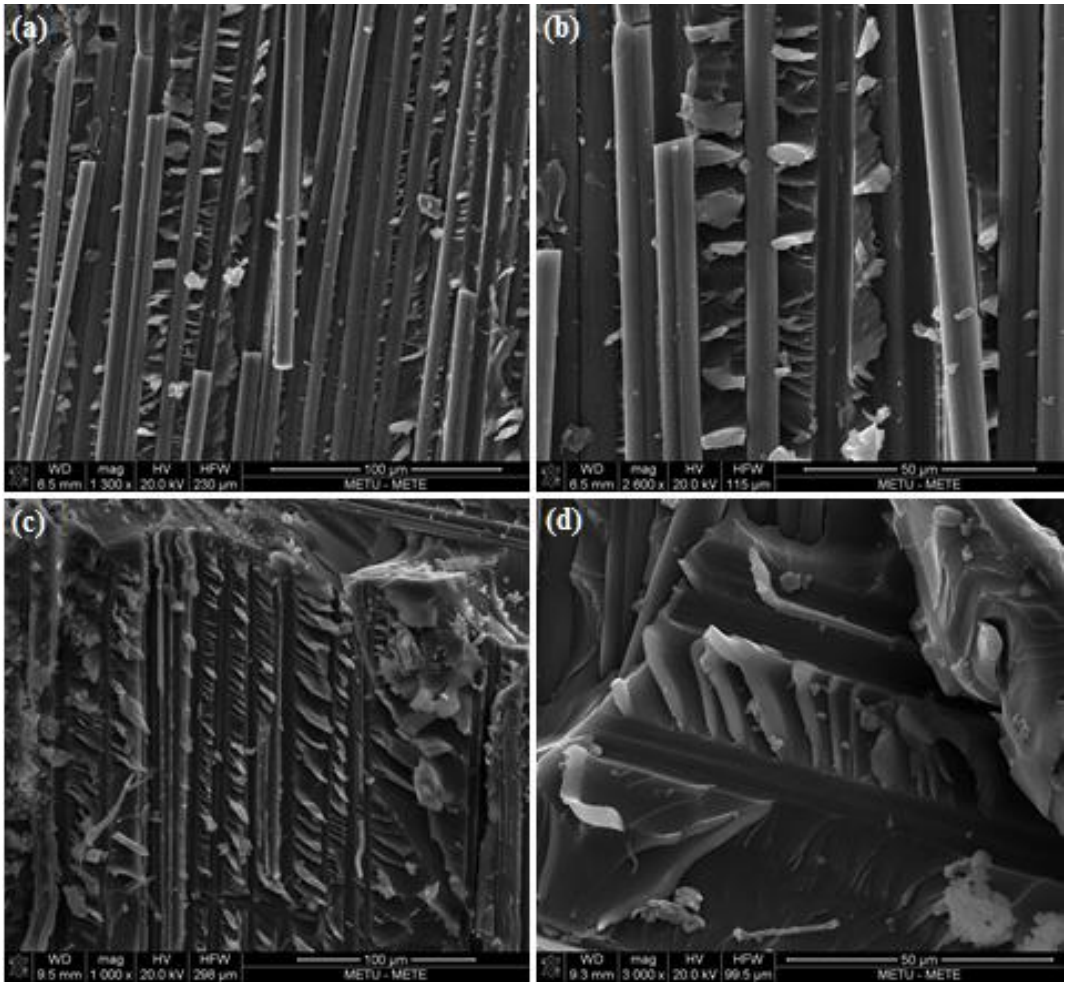

Figure 4.10 SEM images of XOX COPV fracture surface (a) epoxy bridges (b) fiber pull-out (c) riverline and fibers imprints of epoxy (d) epoxy cusps

As internal pressure increases, COPV tends to extend in radial and longitudinal directions where resin cracks are expected. During the extension, due to the difference in displacement of carbon fiber and epoxy resin creates riverline and cusp marks on epoxy layer (Figure 4.10 (c)). At the burst pressure, fibers tend to separate

collectively from the bottom epoxy surface and create fiber cavities on the epoxy surface as well (Figure 4.10 (d)).

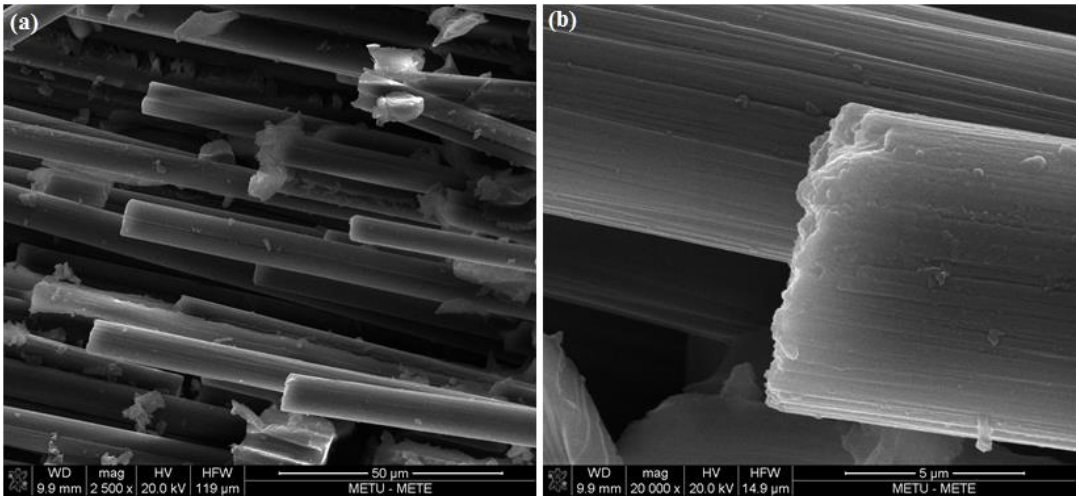

Figure 4.11 SEM images of XOX COPV fiber failure (a) x2,5k magnification (b) x20k magnification

In Figure 4.11 SEM images of fiber failure can be seen. Naito et. al. (69) investigates the fractures surfaces of carbon fibers in SEM. Carbon fiber failure surfaces are similar with the ones that has tensile failure in Naito's study. It means that fibers has tensile failure mode at the burst pressure as expected.

4.6 Discussion of COPV Burst Test Results

4.6.1 Effect of stress ratio on bursting behavior

Burst pressures and measured maximum hoop strains obtained from the COPVs with different stress ratios are presented in Figure 4.12. The XOXOO, OXOX and XOX windings burst at pressures between 2900 – 3600 *psi*, 3100 – 3500 *psi* and 2150 – 2500 *psi*, respectively. The theoretical burst pressures are 4460 *psi*, 3229 *psi* and 1975 *psi* respectively. It can be clearly seen that reducing the hoop winding by 1/3 (from XOXOO winding to OXOX winding) did not change the burst pressure on average. However, the burst pressure of the XOX winding was decreased

approximately by 28.6% on average relative to the XOXOO winding. According to Figure 4.12, highest hoop strain was measured from XOX winding, whereas lowest was measured from XOXOO winding. In addition, according to the results of the maximum hoop strain, it is seen that the most loaded hoop layer was in the XOX winding configuration.

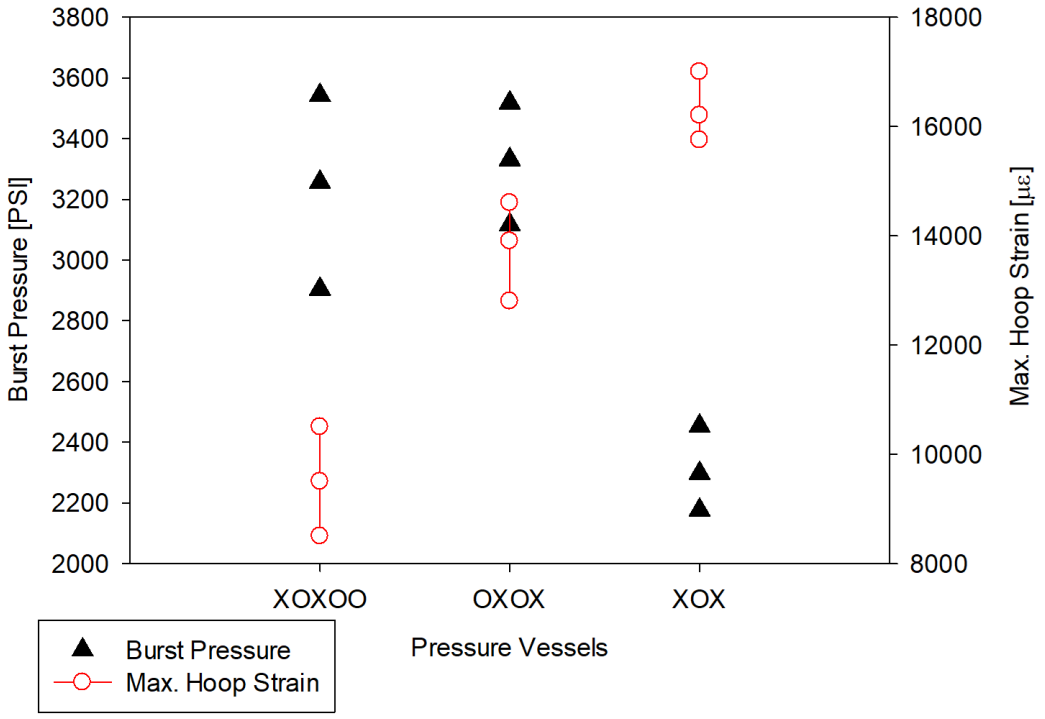

Figure 4.12 Burst pressures and maximum hoop strains for XOX, OXOX and XOXOO layer configurations

The fact that reducing number of the hoop layers by one for the XOXOO winding did not affect the burst pressure indicates that the burst mode of the XOXOO winding was not a hoop failure at the cylindrical region. Also measuring maximum 1.05% strain, which was lower than the fiber strength assumed in previous section, is additional evidence that the burst did not initiate due to fiber tensile failure at the hoop layers according to maximum allowable strain criteria (50). Having considerably lower measured hoop strain value than composite's maximum allowable strain shows that the hoop layers did not reach the fiber tension strength for the XOXOO winding. There may be two reasons the COPV bursts before the

fibers in the hoop layers reach their strength: bursting occurs in a region that is not related to the hoop layers or matrix-induced failure, which causes a failure before the layer reaches fiber direction tension strength, occurs in the hoop layer.

The OXOX winding has a lower dispersion than the XOXOO winding in terms of the burst pressure as seen in Figure 4.12. However, with a measured maximum 1.46% maximum hoop strain, the OXOX winding is at the lower bound of assumed fiber strength. It is not clear from the measured maximum hoop strain whether the hoop layers reached the fiber strength. This demonstrates that the burst mode of the OXOX winding cannot be figured out by evaluating only the burst pressure and maximum hoop strain presented in Figure 4.12. Therefore, high-speed camera data and visual inspection after the test are needed to explain the bursting behavior of the OXOX winding clearly.

According to Figure 4.12, measured 1.64% maximum hoop strain on average is a clue that the most probable burst mode of the XOX winding is a fiber tension failure in the hoop layer. Therefore, it seems that reducing the number of hoops by 2/3 (comparing XOXOO winding with XOX winding) may cause a burst induced by the hoop layer. This finding needs to be confirmed by the high-speed camera data and visual inspection of fracture surfaces of the XOX winding.

The fracture surfaces of COPV samples after tests are shown in Figure 4.13. The failure mode of the XOXOO winding with 0.99 stress ratio is clearly seen as pure dome damage in Figure 4.13 (a). The helical layers located in the dome region seem to be damaged whereas the hoop layers in the cylindrical region seems to be undamaged. In Figure 4.13 (b), the fracture surface of OXOX winding with 0.66 stress ratio shows an axial split mode unlike the pure dome failure of the XOXOO winding. Both of the helices and hoops were damaged in this type of failure. The XOX winding with 0.33 stress ratio has a failure mode in which only the helices and hoop positioned in the cylindrical region were damaged as it can be seen in Figure 4.13 (c). Thus, three different failure modes were observed for the three different pressure vessels with various stress ratios.

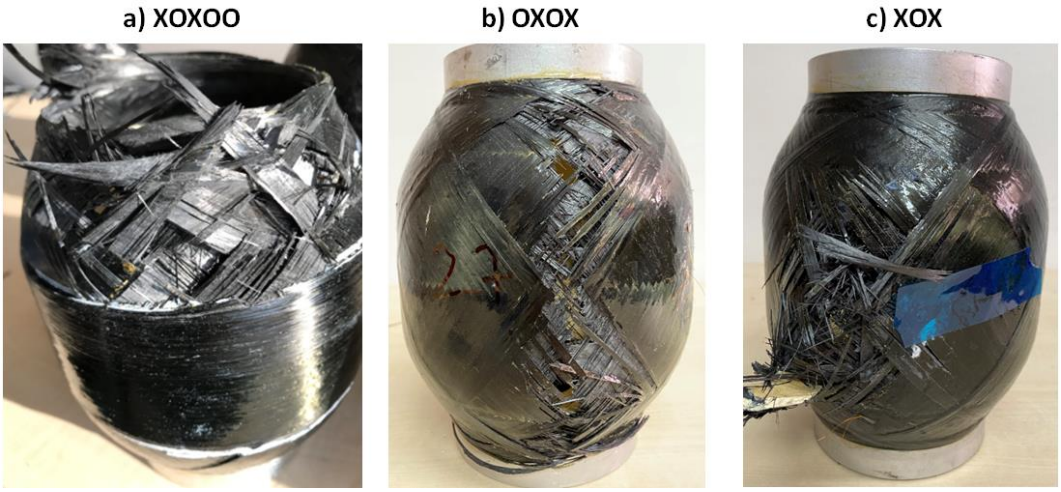

Figure 4.13 Fracture surfaces of COPV layer configurations of (a) XOXOO (b) OXOX (c) XOX

It is obviously seen that burst initiates at the dome region due to helical failure for the XOXOO winding when the post-test views (pure dome damage), the burst pressures, and the measured maximum hoop strains (1.05%) are evaluated together. Moreover, high-speed camera images presented in Figure 4.14 confirm that the burst initiates in the helical windings in the dome region for the XOXOO winding. Therefore, it is concluded that the XOXOO winding with pure dome damage has an unsafe failure mode.

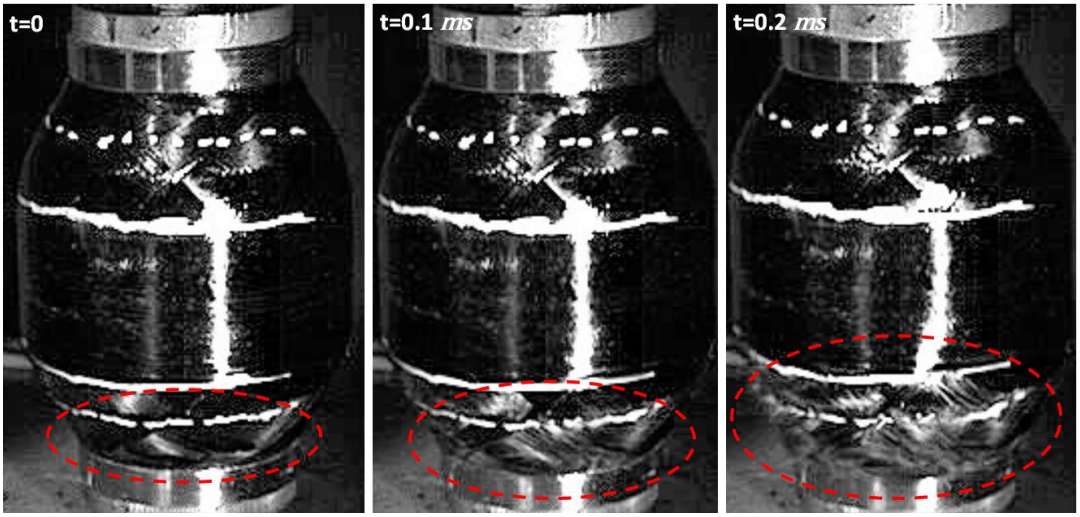

Figure 4.14 High-speed camera images of the XOXOO COPV Sample

It is not apparent from the post-test views for the OXOX winding where the failure was initiated due to observing damage at both of the cylindrical and dome regions. Then, in Figure 4.15, high-speed camera images were analyzed to find out the location of the burst initiation. However, bursting behavior of the OXOX winding cannot be clearly characterized with the high-speed camera images because burst did not initiate at within sight of the camera for all tests. Even so, from the high-speed camera frames presented in Figure 4.15, observing first water leakage at the top region of the COPV gives rise to thought that the location of the burst initiation was in the dome region. After approximately 2.7 ms from the first water leakage at the top of the vessel, progression of the water leakage through bottom of the vessel indicates that failure propagated from the dome region to the cylindrical region. Therefore, it is concluded that although the OXOX winding had more hoop strain (maximum 1.46%) than the XOXOO winding due to having less hoop, the main cause of the burst modes of these windings were similar. The main difference of the failure modes between the XOXOO and OXOX windings is the axial progression of the failure through the vessel for the OXOX winding. It is evaluated that having high hoop strain (1.46%) enabled to propagate of failure through the hoop layers in the cylindrical region for the OXOX winding. Then, it is determined that the OXOX winding has an unsafe failure mode as seen in the XOXOO winding. Although Peters et. al. (4) recommended the stress ratio between 0.6 to 0.85 causes a safe failure mode, the OXOX winding exhibited an unsafe failure mode with 0.66 stress ratio. However, Peters et al. (4) also states that the helical stress in fiber direction should be selected appreciably lower than the hoop stress to prevent the dome failure due to bending loads created by the discontinuities in this region. Therefore, it can be concluded that choosing the stress ratio range in 0.60-0.85 does not guarantee the safe failure mode. The failure mode according to the stress ratio ought to be confirmed by burst test. However, investigation of this issue in detail is not within the scope of this paper.

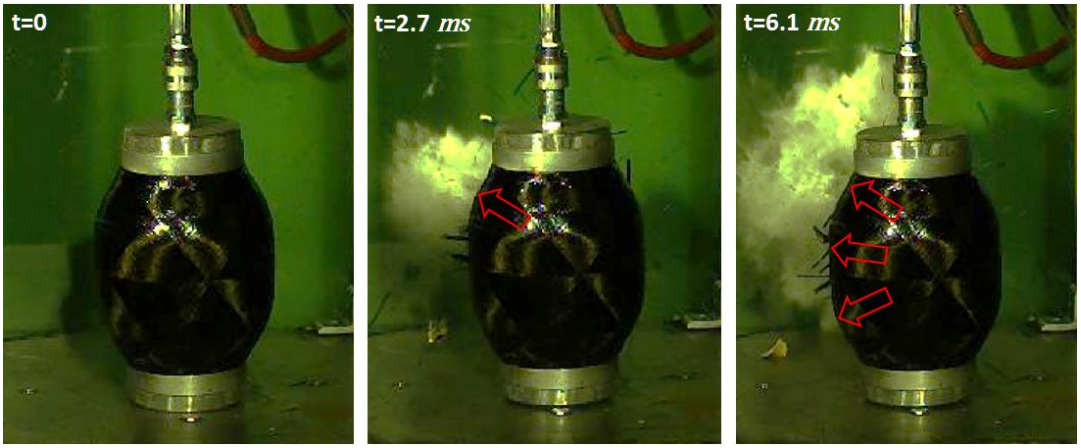

Figure 4.15 High-speed camera images of the OXOX COPV Sample

In addition to the maximum hoop strain measured from the XOX winding (1.64%) and the post-test views (cylindrical region damage), high-speed camera images presented in Figure 4.16 confirm that the failure occurred first in the hoop layer for the XOX winding. Thus, it is clearly showed that the failure mode of the XOX winding with pure cylindrical region damage is a safe mode.

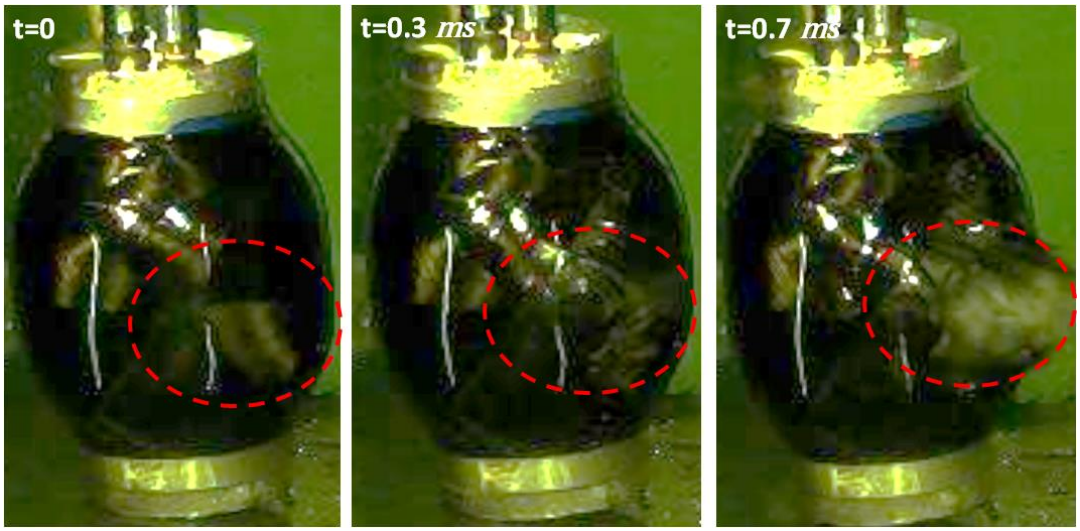

Figure 4.16 High-speed camera images of XOX winding configuration

Considering all the findings obtained from the measurements, it is concluded that having a stress ratio of 0.99 (XOXOO winding) causes an undesired dome failure, which is an unsafe failure mode. The OXOX winding exhibits an unsafe failure mode

despite having 0.66 stress ratio. A stress ratio of 0.33 (XOX winding) induces a safe failure mode that initiated with hoop failures in the cylindrical region. This type of failure is safe and predictable. Therefore, it is concluded that the stress ratio should be selected to design a pressure vessel with safe and predictable failure mode.

4.6.2 Effect of manufacturing defects on bursting behavior

In this section, effect of delamination and spaced winding on the bursting behavior of COPVs is presented. The bursting behavior is evaluated by considering burst pressure, maximum hoop strain measured, and high-speed camera images. XOXOO and XOX windings were selected to investigate the effects of these manufacturing defects on bursting behavior. The main idea behind choosing these layer configurations is that one of them (XOX) has a safe failure mode (pure cylindrical region damage) and the other one (XOXOO) has an unsafe failure mode (pure dome damage). However, the burst mode of the OXOX winding is a mixed mode in which both of dome and cylindrical regions were damaged. Therefore, it is considered that using OXOX winding with mixed-mode bursting mode may cause misinterpretation of the manufacturing effects. In addition, further investigation of OXOX winding is considered redundant, because XOXOO and XOX windings already cover the possible burst mode spectrum of the COPV.

4.6.2.1 Effect of delamination on the bursting behavior

4.6.2.1.1 Evaluation of XOXOO DC and DLS burst testing results

The defect type of delamination is studied firstly. Burst pressures and maximum hoop strains measured in the cylindrical region are given in Figure 4.17 for the XOXOO winding. It is clearly seen from Figure 4.17 that COPVs with both circumferential (DC) and local square (DLS) delamination burst at a pressure similar with the COPV with no defect. In addition, no remarkable difference was observed

between the no defect and the delaminated COPVs in terms of maximum hoop strain. This was expected due to the type of delamination introduced in the structure. As it can be seen by NDI C-Scan Ultrasonic Testing result of COPV calibration sample, inserting a delamination creates a gap between two adjacent plies. This gap tends to close due to radial expansion of the inner layers caused by internal pressure. When the two plies on each side of the gap are finally in contact, both inner and outer plies expand radially together and the COPV starts to exhibit the same behavior as the no defect structure in terms of radial expansion per unit internal pressure. Therefore, this kind of delamination between adjacent layers does not change the circumferential stiffness of COPV.

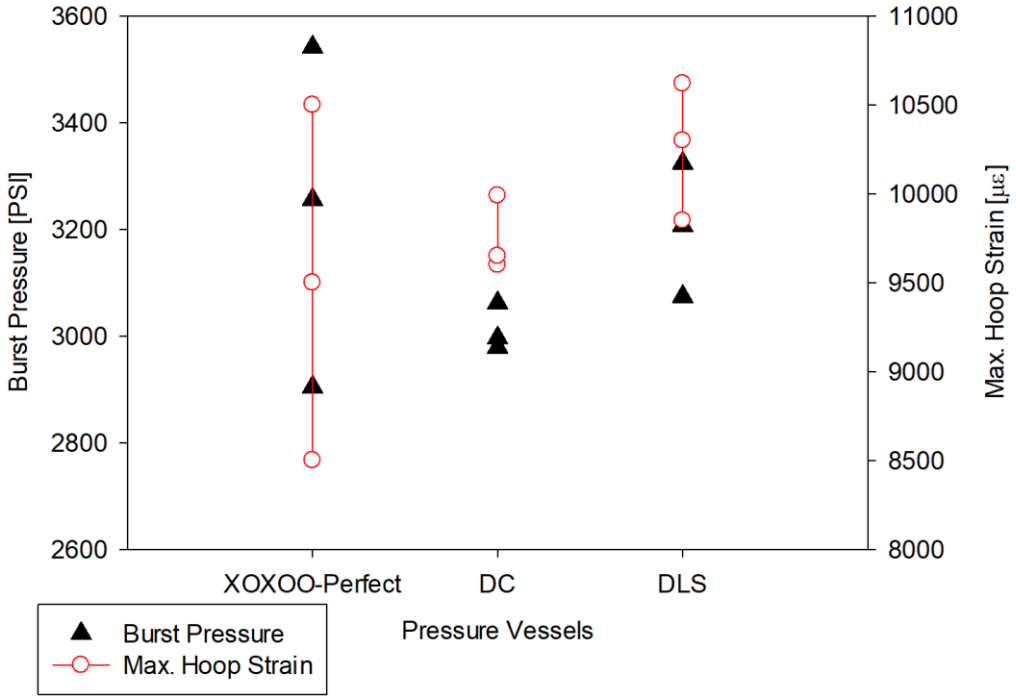

Figure 4.17 Burst pressures and maximum hoop strains for XOXOO layer configuration with delamination

The post-test views of COPVs with delamination are shown in **Hata! Başvuru kaynağı bulunamadı.**. Similar to burst pressure and maximum hoop strain results, the post-test views of the COPVs with delamination are similar with the post-test views of the COPV sample with no artificial defect as shown in Figure 4.18. The

burst mode of both DC and DLS vessels is pure dome damage with boss blowout as observed in the case of XOXOO winding configuration with no artificial defect. The high-speed camera images are not presented for DC and DLS vessels because bursting behavior of these vessels was exactly same with no defect condition. Since the burst was triggered by the helical windings located in the dome, the delamination placed in the cylindrical region did not affect the bursting behavior of the XOXOO windings. Therefore, it is understood that helices in the dome region were still the weakest region of the COPV despite the delamination located in the cylindrical region. Thus, it is concluded that there is no effect of the delamination placed in the cylindrical region on the burst mode, burst pressure and maximum hoop strain for the XOXOO winding that has a 0.99 stress ratio.

Figure 4.18 Burst modes of the XOXOO windings a) DC b) DLS

4.6.2.1.2 Evaluation of XOX DC and DLS burst testing results

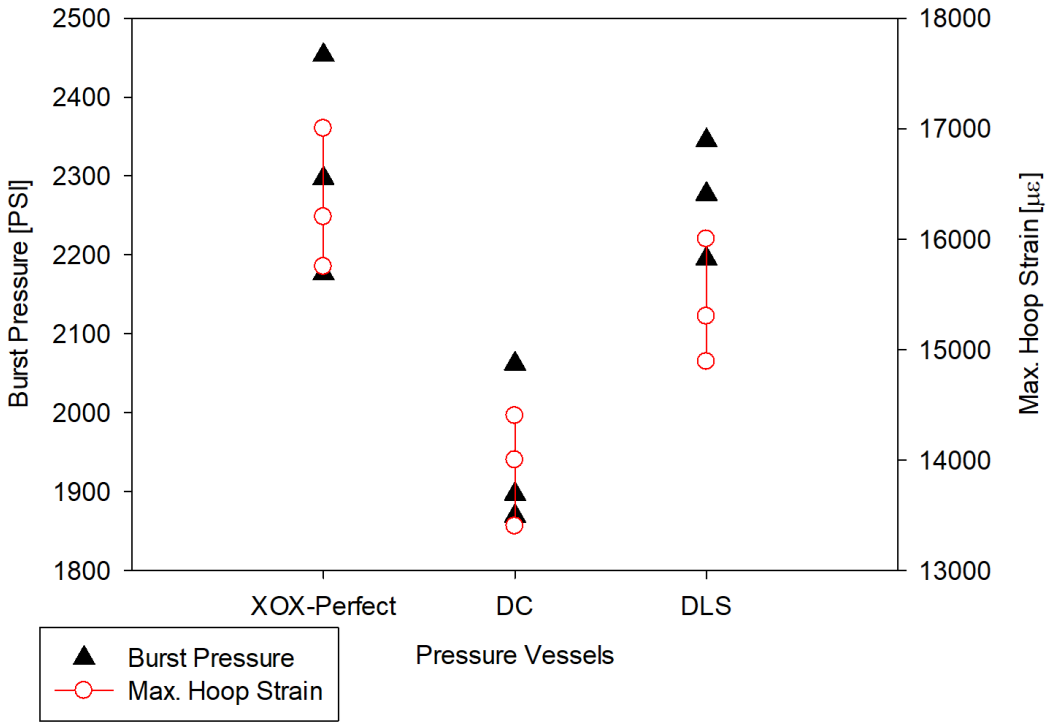

Figure 4.19 Burst pressures and maximum hoop strains for XOX layer configuration with delamination

The burst pressures and maximum hoop strains are presented in Figure 4.19 for the XOX windings with delamination. According to Figure 4.19, there is no significant difference in burst pressure and maximum hoop strain between the COPV with no artificial defect and the DLS COPV as seen before in XOXOO winding. However, the circumferential delamination (DC) reduced the burst pressure and the maximum hoop strain by 15.8% and 14.6% on average respectively, relative to the no defect winding. However, similar decreasing ratios of the burst pressure and maximum hoop strain indicates that the circumferential stiffness of these two COPVs were similar. Therefore, it is concluded that the circumferential stiffness of the vessel did not affected remarkably by the delamination located in the cylindrical region as observed before in the XOXOO winding. Hence, for DC vessel, delamination only reduced the strength of the vessel and for DLS vessel neither stiffness nor strength

were affected. In addition, maximum hoop strain for the DC vessel was 1.44%, which was considerably lower than the fiber strength (1.53%). Therefore, unlike XOX and DLS vessels with no defect, fiber tension failure in the hoop layer may not be expected for DC COPV. Measuring lower maximum hoop strain at the burst pressure than the fiber strength is a sign of a burst mode in which matrix induced failure in the hoop layer or failure of the helices in the dome region may be the main cause of the burst. Therefore, an investigation of post-test views and high-speed camera images is needed to understand the burst behavior of the DC vessel better.

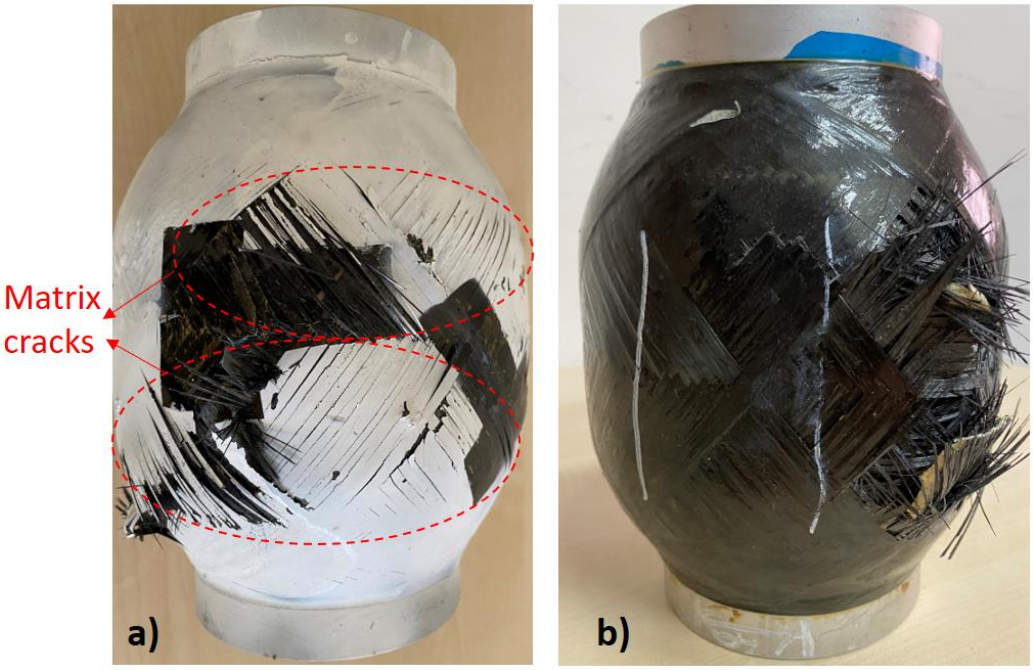

Figure 4.20 Burst modes of the XOX windings a) DC b) DLS

From the presented post-test views in Figure 4.20 (b), it is seen that the burst mode of the DLS vessel is very similar that of the no defect vessel as shown in Figure 3c. Hoop tension failure at the cylindrical region caused this vessel to burst as explained for the vessel with no defect. From the post-test images, an explosive bursting was observed with outwardly protruding fibers for the DLS vessel similar with the COPV with no defect. However, the burst mode of the DC vessel seems moderate with matrix cracks in a wide region (see Figure 4.20 (a)). In addition, a clear hollow region

was not observed in the cylindrical region for the DC vessel. This observation is in agreement with the maximum hoop strain results in which 1.44% maximum hoop strain was obtained for the DC vessel. Therefore, it is understood that the DC vessel burst at a pressure in which fibers in the hoop layer could not reach the maximum fiber tension strength. Observing moderate bursting from the post-test view and measuring lower maximum hoop strain than the no defect vessel show that a premature failure (most likely a matrix-dominant failure or helical failure) occurred in the DC vessel. Obtaining dissimilar burst mode with the no defect COPV and DLS vessels increases importance of the high-speed camera images of DC vessel to better understand the bursting behavior of this vessel.

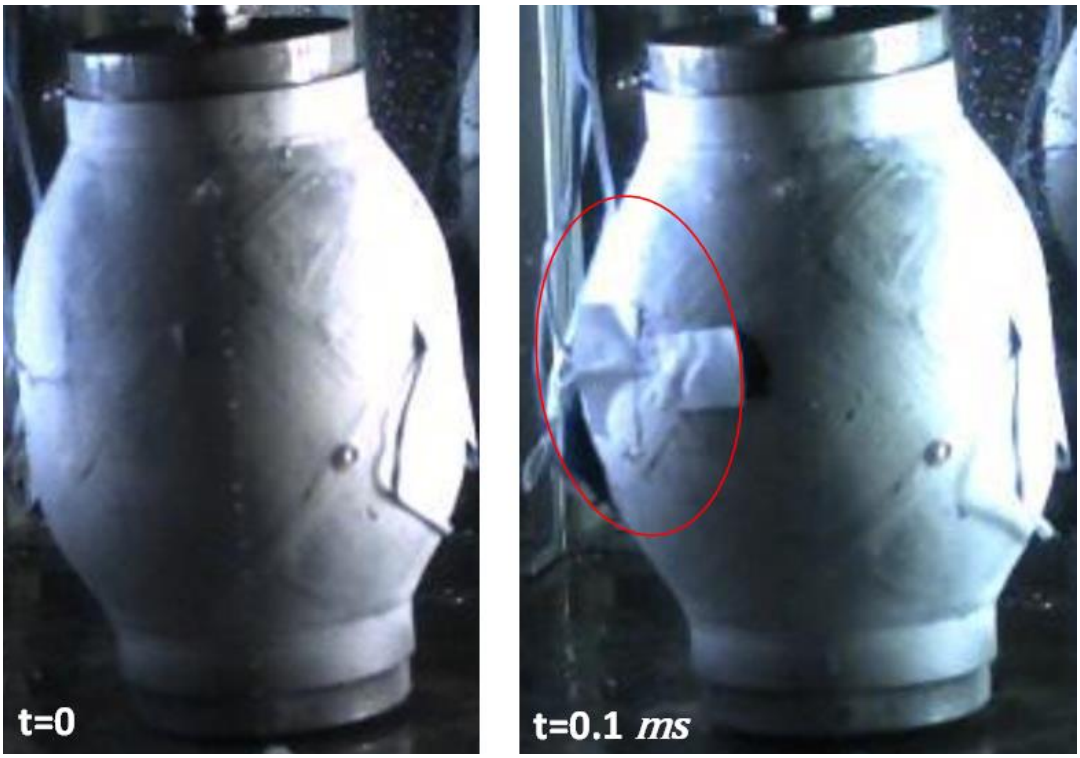

Figure 4.21 High speed camera images of XOX DC sample

The high-speed camera images of the DC vessel are shown in Figure 4.21 to better understand the bursting behavior. According to images, no fluid leakage was observed despite a sudden increase in volume. The cylindrical region expanded suddenly in radial direction (marked with red circle) while the domes were distorted

to maintain the structural continuity between this expanded section and rather stiff polar cap where almost no deformation was permitted. This observation indicates that a failure occurred in the vessel, but it was not yet the final failure to burst the vessel.

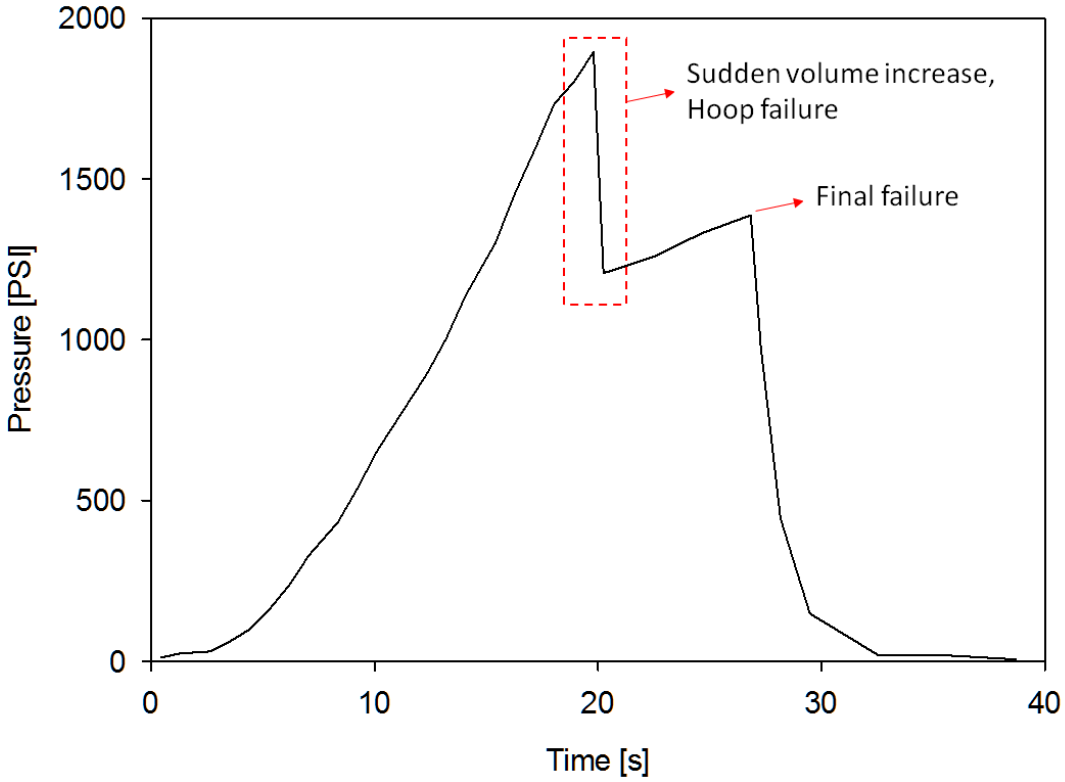

Figure 4.22 Pressure vs. time graph of XOX DC sample

In addition to observing sudden volume increase from high-speed camera images, it can also be seen from Figure 4.22 that the sudden increase in volume was accompanied by pressure drop of 1890 *psi* to approximately 1200 *psi*. The sudden expansion of the cylindrical section that did not immediately result in structural collapse may only be explained by the failure of the hoop layer. However, the maximum hoop strain at 1890 *psi* was measured 1.38%, which was lower than the fiber tension strength (1.53%). Therefore, it is concluded that the vessel burst before the fibers in the hoop layer could reach the fiber tension strength as discussed before. Although the hoop layer located in the middle failed, the vessel could still carry

pressure solely by the helical layers. When the pressure increased again to 1300 *psi*, the helical windings also failed and the vessel burst. Thus, it can be concluded that the reason for the moderate bursting behavior of the DC vessel was the progressive failure that occurred first in the hoop layer and later in the helical layers which lead to the post-test view shown in Figure 4.20 (a).

The XOX winding with circumferential delamination (DC) has a stress ratio of 0.33 like XOX winding with no defect. However, the hoop layer in the DC vessel failed prematurely at 1.38% maximum hoop strain. Although the DC vessel had the same stress ratio as the no defect winding, the circumferential delamination caused a 14.6% lower maximum hoop strain than COPV with no defect. Inserting a circumferential delamination between the hoop and helical layers created a large free surface on top of the hoop layer. It is thought that this free surface enabled the matrix-induced failures in the hoop layer as observed in (70), which eventually lead to this multi-step premature failure. To confirm this comment, XXO winding with no delamination was manufactured and subjected to burst testing. Thus, comparison of the results between XOX and XXO windings with no artificial defect may clarify the free surface effect on the strength of the hoop layer.

4.6.2.1.3 Burst testing of XXO layer configuration

The average burst pressure measured from the test for XXO layer configuration with no defect was 1640 *psi*. Therefore, it is obtained that changing only the location of the hoop layer caused a 28.6% decrease in burst pressure relative to the no defect XOX vessel. Thus, the effect of positioning the hoop layer as a free surface on the burst pressure was more evident according to the XXO winding test result.

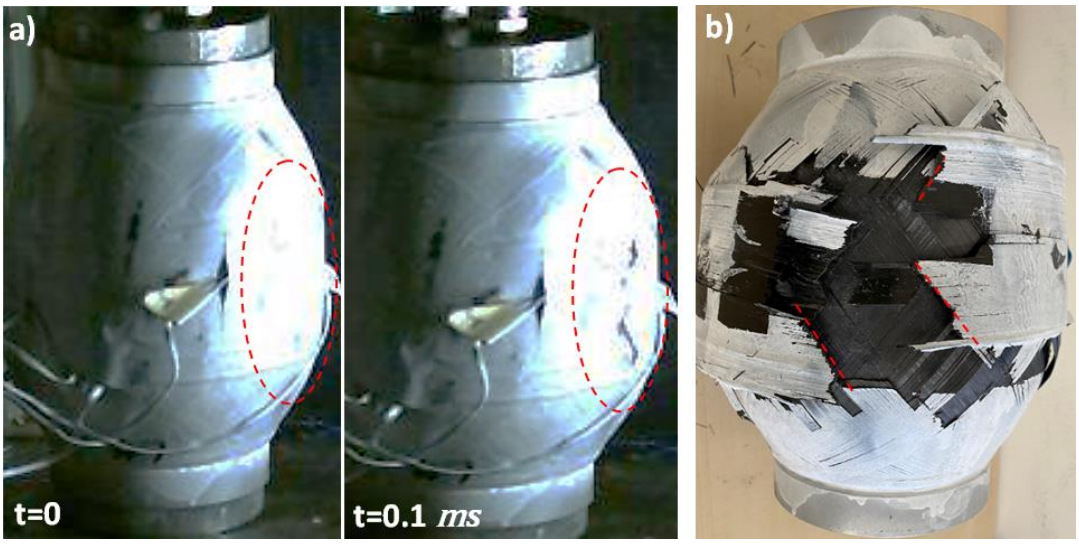

Figure 4.23 (a) High-speed camera images and (b) fracture surface of XXO with no defect

The high-speed camera images are shown in Figure 4.23 (a) and the post-test view of the XXO winding are shown in Figure 4.23 (b). It can be observed that the failure initiated in the hoop layer located outer layer of the COPV. The maximum hoop strain was measured 1.3% that was quite lower than the fiber tension strength (1.53%). Thus, the no defect XXO winding confirmed decreasing of the burst pressure of XOX-DC winding in which the hoop layer could not reach the fiber tension strength due to the free surface effect. Therefore, considering the hoop failure strains of XOX-DC (1.34%-1.44%) and XXO (1.3%) vessels, it can be concluded that the hoop failure may be expected above approximately 1.3% hoop strain due to free surface effect.

4.6.2.2 Effect of the spaced winding on the bursting behavior

Another possible manufacturing defect studied in this paper is spaced winding, which may occur due to the slippage of the epoxy impregnated fiber bands during the winding process. The manufacturing defect of spaced winding was classified in three types; spaced winding of helices (SWX), hoop (SWO), and both of the helices

and hoop (SWXO). As previously considered for delamination, these defects are considered for XOXOO and XOX windings that had unsafe and safe failure modes, respectively.

4.6.2.2.1 Evaluation of spaced winding XOXOO burst testing results

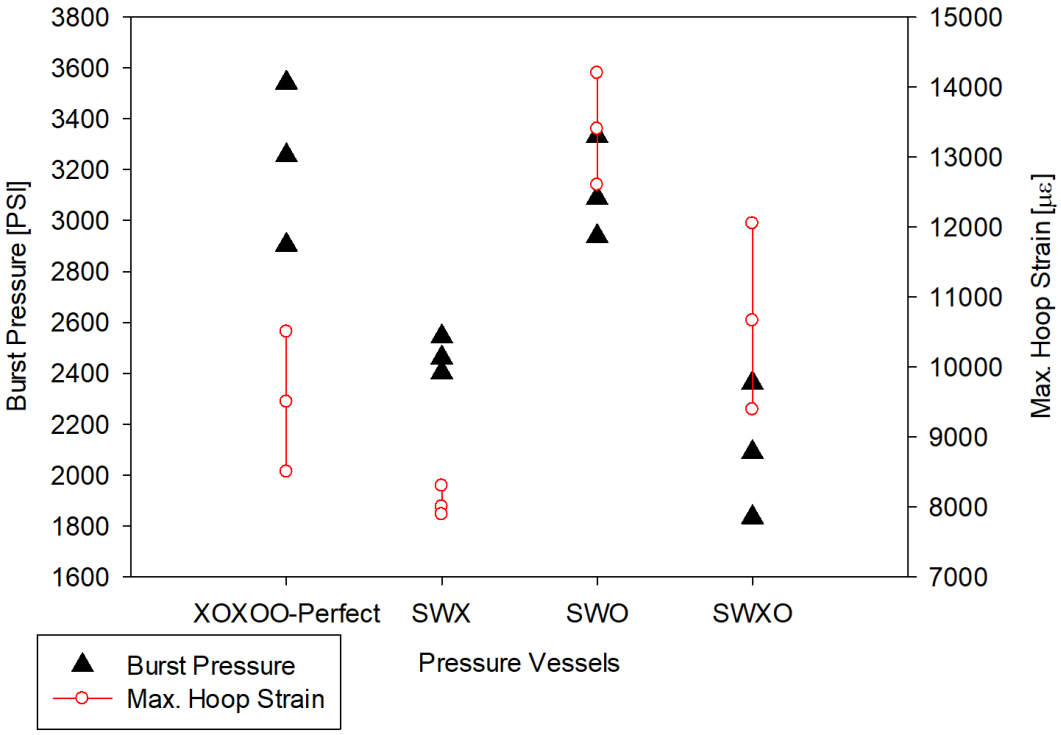

Figure 4.24 Burst pressure and maximum hoop strains for spaced winding XOXOO COPVs

The burst pressure and maximum hoop strain results for the XOXOO windings are presented in Figure 4.24. Since the burst pressure varied across vessels with various spaced windings, measured strain values were normalized per burst pressure in order to compare stiffness values of COPV configurations. Normalized strain values in terms of *με/psi* are presented in Table 4.11. The normalized strain values provide insight on if the discrepancy in measured strains were due to the change in burst pressure or due to the effect of spaced winding.

Table 4.11 The ratio of the maximum hoop strain over burst pressure for the XOXOO winding configurations

Winding Configuration	***Normalized Hoop Strain [με/psi]***
XOXOO (No defect)	2.95
SWX	3.08
SWO	4.36
SWXO	5.27

Figure 4.24 indicates that the spaced winding reduced the burst pressure by 23.6% and 35.2% on average for the SWX and SWXO vessels, respectively, relative to the COPV with no defect. However, winding the hoop layer with space (SWO) did not seem to affect the burst pressure in comparison with the no defect vessel.

The maximum hoop strain of the SWX vessel is declined by 15.1% on average relative to the no defect vessel as seen in Figure 4.24. On the other hand, from Table 4.11, a 4.4% increase of the normalized strain relative to the no defect vessel implies that the spaced windings of the helices had little effect on the circumferential stiffness of the vessel. This means that decreasing of the burst pressure was the main reason for measuring low hoop strain. The maximum hoop strain of the SWO vessel increased approximately by 38.9% relative to the no defect vessel despite having similar burst pressures. A 48% rise of the normalized strain seen in Table 4.11 also clarifies that the maximum strain increased as the circumferential stiffness reduced due to the spaced winding of the hoop layer. In addition, although 1.42% measured maximum hoop strain of the SWO vessel was lower than the fiber tension strength (1.53%), the failure of the outmost hoop layers may be seen due to the free surface effect discussed before. A premature hoop failure has been previously observed above 1.3% hoop strain in XOX-DC and XXO vessels. Therefore, it can be expected that the bursting behavior of the SWO vessel may differ from the XOXOO vessel with no defect. SWXO vessel had lower burst pressure than the vessel with no defect

although the maximum hoop strain of the SWXO increased by 12.6% relative to the vessel with no defect. This caused a 78.6% increase in normalized strain relative to the no defect vessel as seen Table 4.6. Therefore, considering both types of spaced winding XOXOO vessels, it can be concluded that the main reason for the reduction of the circumferential stiffness was spaced winding of hoops but not helices.

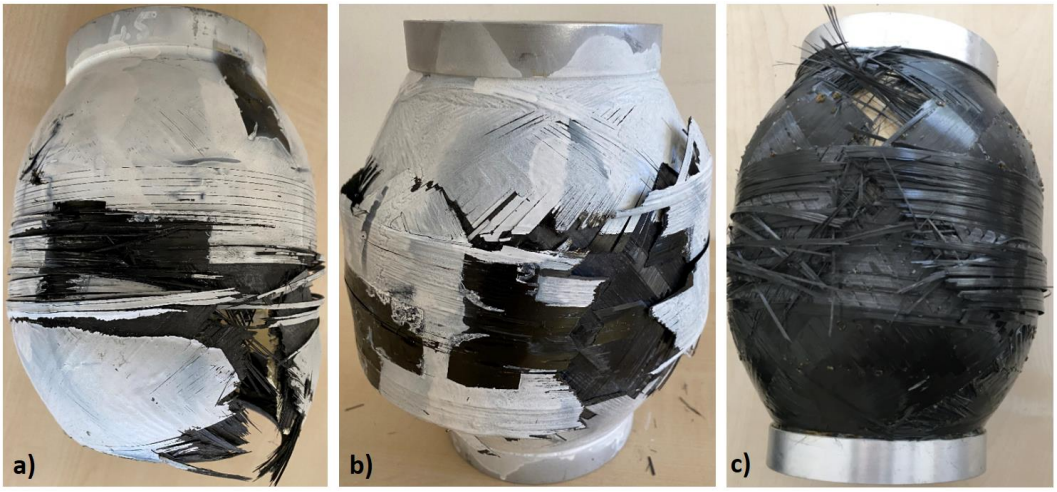

Figure 4.25 Burst modes of the XOXOO vessels a) SWX, b) SWO and c) SWXO

The post-test views of the spaced wound XOXOO vessels are presented in Figure 4.25. According to the post-test views, both of the dome and cylindrical regions seems to be damaged for the SWX and SWXO vessels. Therefore, examination of the high-speed camera data is needed to determine whether the bursting initiated from the dome region or the cylindrical region. In fact, since the measured maximum hoop strain of the SWX vessel was even lower than that of the no defect vessel, the failure initiation may be expected to be in the dome region like the no defect vessel. However, measured 1.2% maximum hoop strain of SWXO vessel makes the investigation of high-speed camera images crucial to gain a deeper understanding of the bursting behavior of this vessel. Unlike the SWX and SWXO vessels, the burst mode of the SWO vessel was different from the other vessels according to Figure 4.25. The two outer hoop layers appear to be separated from the helical layer. In addition, unlike the no defect and other spaced wound vessels, for SWO vessels damage occurred only at the cylindrical region but not at the dome. Considering the

approximately 1.42% maximum hoop strain result and the post-test views together, the main cause of the failure is thought to be hoop failure at the cylindrical region for the SWO vessel, similar to the XXO vessel with no defect.

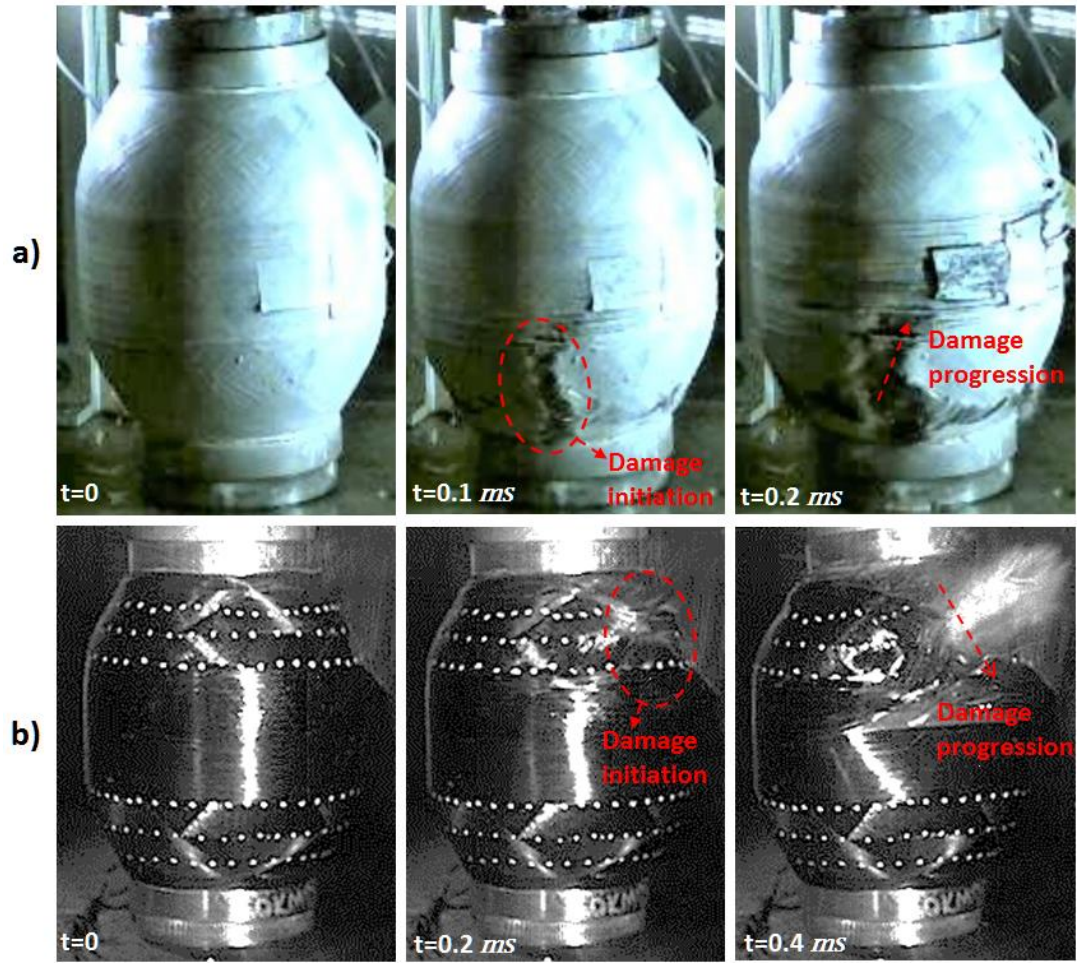

Figure 4.26 High-speed camera images of the XOXOO vessels a) SWX, b) SWXO

In order to determine the initial damage location for SWX and SWXO vessels, high-speed camera images were investigated. The high-speed camera images of the XOXOO SWX and SWXO vessels are presented in Figure 4.26 (a) and Figure 4.26 (b), respectively. From Figure 4.26, it is observed that the damage initiated from the helices located in the dome region for both of XOXOO SWX and SWXO vessels. The location of burst initiation of these vessels was similar with the no defect XOXOO vessel. Reduction in the burst pressure of SWX and SWXO vessels relative

to the no defect one is attributed to strength reduction of helices caused by the spaced winding at the dome region. Thus, it is concluded that even with the reduction of strength and circumferential stiffness of the cylindrical section via spaced hoop and helical windings, dome region was still the weakest point of SWX and SWXO vessels as seen in the no defect vessel. However, reason for propagation of damage through the cylindrical region is thought due to the weakened strengths of spaced wound of helices and hoops for SWX and SWXO vessels.

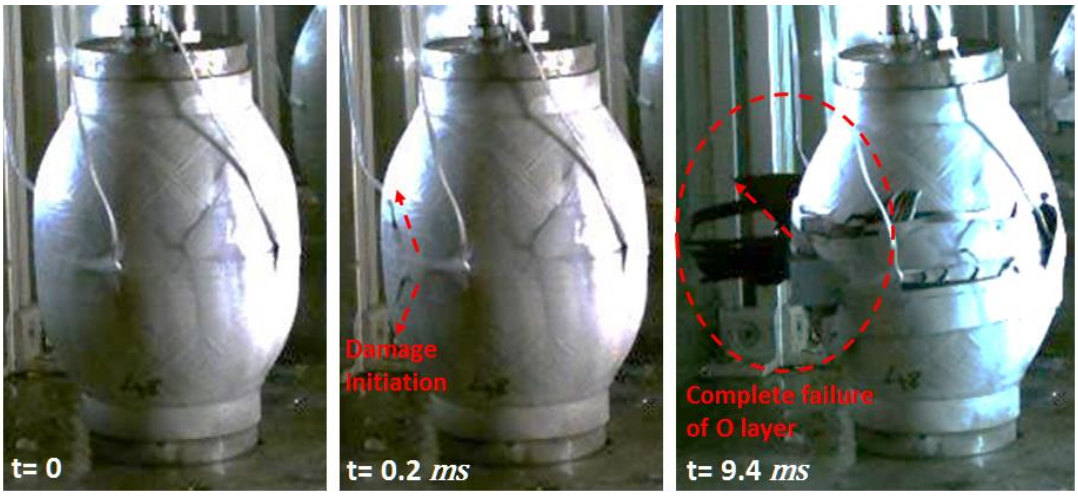

Figure 4.27 High-speed camera images of the XOXOO - SWO vessel

The high-speed camera images of the XOXOO – SWO vessel, which exhibited different burst mode from other spaced wound XOXOO vessels in the post-test views, are shown in Figure 4.27. Damage initiation and propagation at the hoop layers can be clearly seen from the camera images. Complete failure of the outer hoop layers at the burst pressure can also be observed in the last image. It is understood from the high-speed camera images that the damage of the outer hoop layers was main cause of bursting of the vessel. After failure of the outer hoop layers, remaining XOX layers could not carry the pressure and final failure occurred. Thus, the high-speed camera images confirmed that winding only hoops with space caused a 1.42% maximum hoop strain and so the location of burst initiation shifted from dome to cylindrical region for SWO vessel. Due to free surface effect discussed before, the outmost hoop layers failed before they reached the maximum fiber

elongation. In addition, observing failure of outmost hoop layers and first water leakage in different locations shows that first and final failures occurred due to two different damage mechanisms. After failure of outmost hoop layers, the remaining part of vessel burst at different location of the cylindrical region.

4.6.2.2.2 Evaluation of spaced winding XOX burst testing results

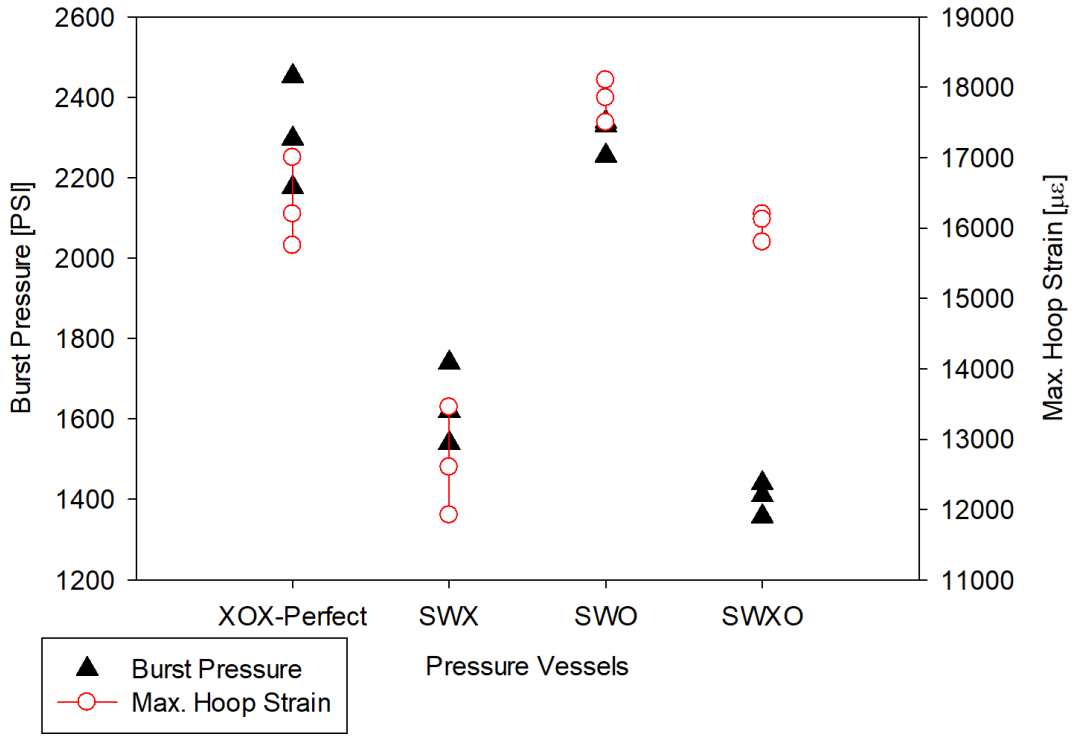

Figure 4.28 Burst pressures and maximum hoop strains for the XOX spaced windings

Winding only the helices with space (SWX) decreased the burst pressure by 29.2% for the XOX winding as shown in Figure 4.28. The burst pressure dropped by 39.2% relative to the no defect vessel due to winding the hoop with space in addition to the helices (SWXO). However, it can be clearly seen from Figure 4.28 that winding only the hoop with space (SWO) had little effect on the burst pressure. Thus, it can be concluded that reason for decreasing of burst pressure was spaced winding of helices but not hoop.

Table 4.12 The ratio of the maximum hoop strain over burst pressure for the XOX winding configurations

Winding Configuration	***Normalized Hoop Strain [με/psi]***
XOX (No defect)	7.06
SWX	7.65
SWO	8.03
SWXO	11.3

The reduction of maximum hoop strain for the SWX vessel relative to no defect XOX vessel was 22.2%, similar with the burst pressure. However, the normalized hoop strain of the SWX vessels was 8.3% higher than that of the no defect vessel as shown in Table 4.12. This implies that winding the helices with space caused a stiffness reduction in the circumferential direction. While the reduction in circumferential stiffness due to spaced wound helices also contributed a bit, the main reason for the reduction of maximum hoop strain was the reduction of burst pressure for the SWX vessel. In addition, measured 1.34% maximum hoop strain of the SWX vessel was considerably lower than the fiber strength (1.53%). Unlike no defect XOX vessels, measuring lower hoop strain than the fiber strength at the burst pressure may indicate that the no defect and SWX vessels exhibited different damage mechanism. Despite having similar burst pressure with the no defect vessel the maximum hoop strain of the SWO vessel was slightly higher than the no defect XOX vessel. Thus, according to Table 4.12, the normalized hoop strain of SWO vessel is approximately 14% higher than that of the no defect XOX vessel due to winding of hoop layer with space. Therefore, considering the results of SWX and SWO vessels, it can be concluded that winding only hoop layer with space had much more effect on circumferential stiffness than winding only helices with space. Despite having quite lower than burst pressure than the no defect XOX vessel, SWXO vessel had similar maximum hoop strain with the no defect vessel. Thus, winding of both helices and

hoop layers with space increased the normalized hoop strain 60% relative to the no defect XOX vessel.

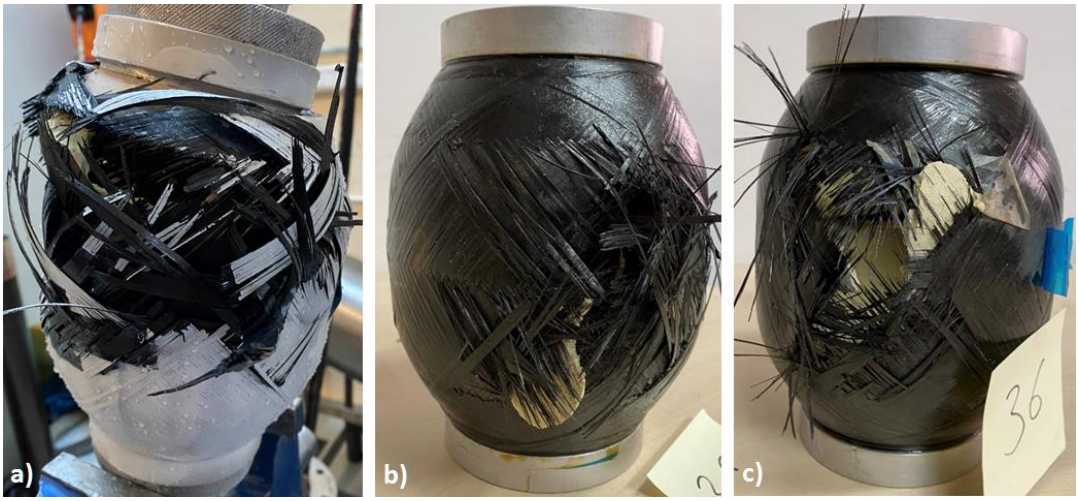

Figure 4.29 Burst modes of the XOX vessels a) SWX, b) SWO and c) SWXO

According to the fracture surfaces presented in Figure 4.29, the burst mode of the SWX vessel was dome and cylindrical region failure, while XOX vessel with no defect had a hoop failure in the cylindrical region only as shown in Figure 4.13 (c). Therefore, investigation of high-speed camera images was needed to determine the location of damage initiation for the SWX vessel. In fact, occurrence of damage in dome was already expected due to low measured maximum hoop strain of the vessel as seen before in the perfect XOXOO vessel. Therefore, winding the helices with space could transform the burst mode from the hoop failure in the cylindrical region to helical failure at the dome region. There is no difference observed between the SWO vessel and XOX COPV with no defect in terms of the post-test views. Thus, it is concluded that winding only the hoop with space (SWO) did not effect the burst mode for the XOX winding. Thus, the spaced wound hoop layer located in the cylindrical region was still weakest region of the vessel. While the SWXO vessel had 39.2% lower burst pressure than the perfect vessel, burst modes of these two vessels were same due to high measured maximum hoop strain as shown in Figure 4.29 (c). It is understood from the burst mode of SWXO vessel that despite winding

of both helices and hoop layers with space, strength of the cylindrical region was still lower than the dome region.

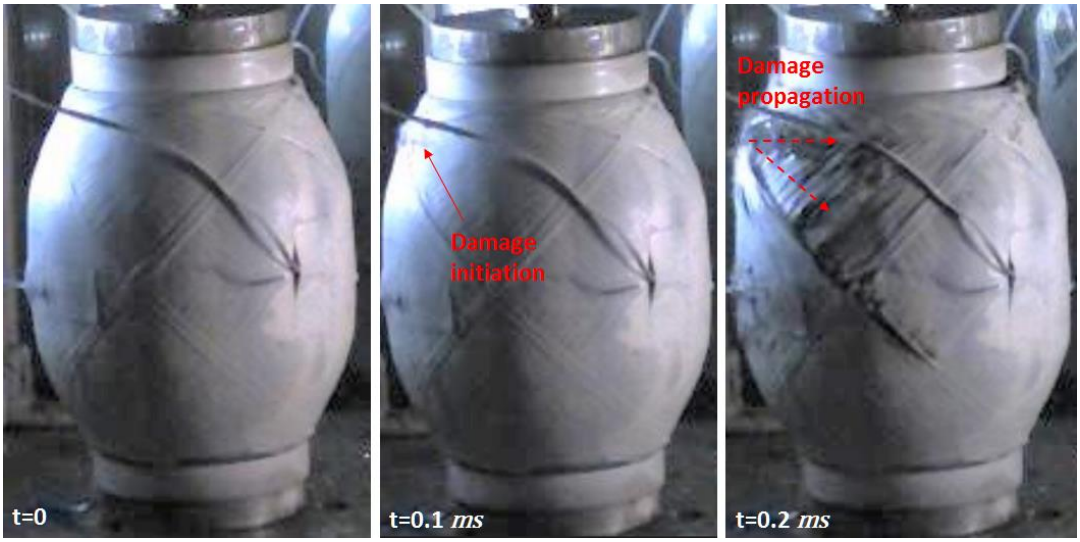

Figure 4.30 High-speed camera images of the XOX - SWX vessel

Presenting of high-speed camera images for SWO and SWXO vessels is not necessary because burst modes and damage mechanisms of these vessels were similar with the perfect XOX vessel discussed in detail before. From the high-speed camera images presented in Figure 4.30, the damage initiation of the SWX vessel was apparently seen at the dome region. The propagation of the damage through the cylindrical and dome regions can also be observed from 0.2 ms after the damage initiation. It is thought for this vessel that winding of the helices with space caused an excessive reduction in the strength of the helices located in the dome region, which was lower than the tensile strength of the hoop layer, and so bursting of the vessel earlier than the perfect vessel.

When the radial cross-section of winding layers in COPV samples with no defect and SW COPV samples are observed in optical microscope, it is seen that SW vessels do not contain large resin-rich areas. Instead, the fibers tend to migrate to the vacancies and decreasing the thickness of the layer in both hoop and helical layers. This phenomenon causes the decrease in the burst pressure of SW COPV samples

proportional with the decrease in the thicknesses of the layers caused by shortening of circuit number for helical winding. Burst pressure results are given in Table 4.13.

Table 4.13 Comparison of Burst Pressure Results of COPV Samples

Stress Ratio	***Sample Type***	***Defect Conf.***	***Avg. BP (psi)***	***Avg. ε (%)***	***Burst Region***	***Discussion for Burst Pressure (BP)***
0.99	No defect	N/A	3234	0,96	Dome	BP 27% less than theoretical
0.66		N/A	3322	1,38	Dome + Cylinder	Almost same with theoretical
0.33		N/A	2309	1,63	Cylinder	BP 16% higher than theoretical
0.99	Delamination	DC	3012	0,97	Dome	Almost same BP with no defect
		DLS	3202	1,03	Dome	Almost same BP with no defect
	Spaced Winding	SWX	2470	0,81	Dome	BP 27% less than no defect
		SWO	3119	1,60	Cylinder	Almost same BP with no defect
		SWXO	2095	1,07	Dome	BP 35% less than no defect
0.33	Delamination	DC	1943	1,39	Cylinder	BP 16% less than no defect
		DLS	2272	1,54	Cylinder	Almost same BP with no defect
	Spaced Winding	SWX	1633	1,27	Dome	BP 29% less than no defect
		SWO	2308	1,78	Cylinder	Almost same BP with no defect
		SWXO	1403	1,60	Cylinder	BP 39% less than no defect

When the burst pressures are evaluated, it is seen that spaced winding causes a certain reduction especially when X layer thickness decreases due to the lower circuit number of winding. Except from DC in 0.33 stress ratio, other delamination types do not decrease BP of COPV samples. When max. hoop strain results is; lower than 1.38% dome failure occurs, higher than 1.38% cylindrical failure is observed.

CHAPTER 5

CONCLUSION

The effects of manufacturing defects on the bursting behavior were investigated for composite overwrapped pressure vessels with various stress ratios. Delamination and spaced winding were considered as manufacturing defects. These defects were studied for COPVs with safe and unsafe burst modes. The findings of this study are summarized as follows;

- Material characterization testing such as tensile testing (in longitudinal and transverse direction), fiber volume fraction determination testing of carbon/epoxy composite coupons are covered in this study. The test results are evaluated and the scattering of the results considered acceptable to be used in the calculation of laminate configuration of COPV.
- At the burst testings it is observed that 0.33 stress ratio vessel has safe (cylindrical region) failure mode where 0.99 stress ration vessel has unsafe (dome region). On the other hand, 0.66 stress ratio caused a mixed mode failure in which both dome and cylindrical regions were damaged. XOXOO vessels has burst pressures 25% lower than the theoretical burst pressures where XOX has 16% higher burst pressures than theoretical. OXOX has an average burst pressure value is almost same with the theoretical. Since maximum hoop strain is measured highest at 0.33 stress ratio XOX vessel, it can be said that safe failure mode is the most effective COPV design in terms of fiber strength.
- Layer thicknesses are measured in optical microscope. It is observed that measured values are consistent with the theoretical ones that are used in the calculations for both COPV with no defect and spaced winding COPV samples when circuit number of winding considered. Decrease in the burst

pressure in SW COPV samples is directly correlated with the decrease in the layer thickness. Fiber migration to the vacancies during curing prevents the occurrence of large resin-rich areas.

- Fracture surfaces of XOX COPV are examined in SEM. In-plane shear failure of epoxy resin and tensile failure of fibers are corroborated with SEM images obtained in the literature.
- The bursting behavior was not affected by delamination inserted in the cylindrical region for the XOXOO COPV with 0.99 stress ratio. However, a circumferential delamination reduced the burst pressure of the XOX COPV with 0.33 stress ratio due to free surface effect. The effect of locating the hoop layer as free surface on bursting behavior was confirmed by testing perfect XXO vessel. Thus, importance of stacking sequence on bursting behavior was emphasized for pressure vessels with low stress ratios. In addition, unlike XOX vessel with local delamination (XOX-DLS), observing a reduction in burst pressure for XOX vessel with global delamination (XOX-DC) indicates importance of defect size on bursting behavior.
- Winding only the hoops with space reduced the circumferential stiffness and transformed the burst location from dome to cylindrical region for XOXOO winding. The burst pressure of the vessel with spaced wound helices was found to be less than the XOXOO vessel. No effect was observed for winding the helices with space on burst mode.
- For XOX vessel, winding only the helices with space not only decreased the burst pressure but also changed the safe burst mode to unsafe. Winding only the hoop with space did not affect the burst pressure and burst mode. However, winding the hoop with space in addition to the helices decreased the burst pressure but did not change the burst mode. Therefore, the spaced winding as a manufacturing defect may be evaluated as detrimental effect and should be avoided.

Considering all experimental and visual data obtained by this study, COPV layer configuration and manufacturing defects have certain influence on the burst

pressures and fracture surfaces of composite overwrapped pressure vessels. Influence of manufacturing defects parameters such as defect type, location and size on burst pressure of COPVs has been covered with this study. Structural analysis tools could be improved by experimental data obtained from this study and acceptance limits of manufacturing defects could be determined before manufacturing of COPVs.

REFERENCES

1. BERTIN, Maxime, et al. One year OSIRHYS IV project synthesis: mechanical behaviour of 700 bar type iv high pressure vessel code qualification. In: 15th European conference on composite materials. 2012. p. 8 p.

2. VASILIEV, Valery V.; MOROZOV, Evgeny V. Advanced mechanics of composite materials and structural elements. Newnes, 2013.

3. SHEN, Frank C. A filament-wound structure technology overview. Materials Chemistry and Physics, 1995, 42.2: 96-100.

4. PETERS, Stanley T. (ed.). Composite filament winding. ASM International, 2011.

5. ROJAS, E. Vargas, et al. Unified approach of filament winding applied to complex shape mandrels. Composite Structures, 2014, 116: 805-813.

6. RANA, Sohel; FANGUEIRO, Raul (ed.). Advanced composite materials for aerospace engineering: Processing, properties and applications. Woodhead Publishing, 2016.

7. COHEN, D. Influence of filament winding parameters on composite vessel quality and strength. Composites Part A: Applied Science and Manufacturing, 1997, 28.12: 1035-1047.

8. BANERJEE, A., et al. Model and experimental study of fiber motion in wet filament winding. Composites Part A: Applied science and manufacturing, 1998, 29.3: 251-263.

9. PANDITA, S. D., et al. Clean wet-filament winding–Part 1: design concept and simulations. Journal of composite materials, 2013, 47.3: 379-390.

10. BRATUKHIN, A. G.; BOGOLYUBOV, V. S. (ed.). Composite manufacturing technology. Springer Science & Business Media, 1994 .p.119.

11. ROUSSEAU, J.; PERREUX, D.; VERDIERE, N. The influence of winding patterns on the damage behaviour of filament-wound pipes. Composites Science and Technology, 1999, 59.9: 1439-1449.

12. MERTINY, P.; ELLYIN, F. Influence of the filament winding tension on physical and mechanical properties of reinforced composites. Composites Part A: Applied Science and Manufacturing, 2002, 33.12: 1615-1622.

13. ZHANG, Shi-jie; WANG, Ru-min; LIAO, Ying-qiang. A comparative study of two kinds of T800 carbon fibers produced by different spinning methods for the production of filament-wound pressure vessels. New Carbon Materials, 2019, 34.6: 578-586.

14. COHEN, David; MANTELL, Susan C.; ZHAO, Liyang. The effect of fiber volume fraction on filament wound composite pressure vessel strength. Composites Part B: Engineering, 2001, 32.5: 413-429.

15. ZU, Lei, et al. Design and analysis of filament-wound composite pressure vessels based on non-geodesic winding. Composite Structures, 2019, 207: 41-52.

16. RAFIEE, Roham; TORABI, Mohammad Ali. Stochastic prediction of burst pressure in composite pressure vessels. Composite Structures, 2018, 185: 573-583.

17. HARADA, Shunsuke, et al. A simplified method for predicting burst pressure of type III filament-wound CFRP composite vessels considering the inhomogeneity of fiber packing. Composite Structures, 2018, 190: 79-90.

18. MADHAVI, M.; RAO, K. V. J.; RAO, K. Narayana. Design and Analysis of Filament Wound Composite Pressure Vessel with Integrated-end Domes. Defence science journal, 2009, 59.1.

19. NEBE, Martin, et al. Experimental and analytical analysis on the stacking sequence of composite pressure vessels. Composite Structures, 2020, 247: 112429.

20. MCLAUGHLAN, Pat B.; FORTH, Scott C.; GRIMES-LEDESMA, Lorie. Composite overwrapped pressure vessels: a primer. National Aeronautics and Space Administration, Johnson Space Center, 2011.

21. ISO 11439:2013 : gas cylindersehigh pressure cylinders forthe on-board storage of natural gas as a fuel for automotivevehicles. Geneva, Switzerland: International StandardsOrganisation (ISO); 2013.

22. FOWLER, Calum P.; ORIFICI, Adrian C.; WANG, Chun H. A review of toroidal composite pressure vessel optimisation and damage tolerant design for high pressure gaseous fuel storage. International Journal of Hydrogen Energy, 2016, 41.47: 22067-22089.

23. MARTINS, L. A. L.; BASTIAN, F. L.; NETTO, T. A. The effect of stress ratio on the fracture morphology of filament wound composite tubes. Materials & Design, 2013, 49: 471-484.

24. MARTINS, Luiz AL; BASTIAN, Fernando L.; NETTO, Theodoro A. Structural and functional failure pressure of filament wound composite tubes. Materials & Design (1980-2015), 2012, 36: 779-787.

25. ELLYIN, F., et al. The behavior of multidirectional filament wound fibreglass/epoxy tubulars under biaxial loading. Composites Part A: Applied Science and Manufacturing, 1997, 28.9-10: 781-790.

26. MEIJER, Garret; ELLYIN, Fernand. A failure envelope for±60 filament wound glass fibre reinforced epoxy tubulars. Composites Part A: Applied Science and Manufacturing, 2008, 39.3: 555-564.

27. KRISHNAN, Pranesh, et al. Effects of winding angle on the behaviour of glass/epoxy pipes under multiaxial cyclic loading. Materials & Design, 2015, 88: 196-206.

28. HAMED, A. F., et al. Effects of winding angles on the strength of filament wound composite tubes subjected to different loading modes. Polymers and Polymer Composites, 2007, 15.3: 199-206.

29. AFRATHIM, Afthab; KARUPPANAN, Saravanan; PATIL, Santosh S. Burst strength analysis of thin composite pressure vessels. Materials Today: Proceedings, 2021, 44: 3115-3120.

30. LIN, Song, et al. Progressive damage analysis for multiscale modelling of composite pressure vessels based on Puck failure criterion. Composite Structures, 2021, 255: 113046.

31. RAFIEE, Roham; TORABI, Mohammad Ali; MALEKI, Sattar. Investigating structural failure of a filament-wound composite tube subjected to internal pressure: experimental and theoretical evaluation. Polymer Testing, 2018, 67: 322-330.

32. WU, Q. G., et al. Stress and damage analyses of composite overwrapped pressure vessel. Procedia Engineering, 2015, 130: 32-40.

33. GREENHALGH, E.; HILEY, M. Fractography of polymer composites: current status and future issues. 2008.

34. BLANC-VANNET, P. Burst pressure reduction of various thermoset composite pressure vessels after impact on the cylindrical part. Composite Structures, 2017, 160: 706-711.

35. PERILLO, Giovanni, et al. Numerical/experimental impact events on filament wound composite pressure vessel. Composites Part B: Engineering, 2015, 69: 406-417.

36. RAJESH, Singuru; SURESH, Gamini; MOHAN, R. Chandra. A review on material selection and fabrication of composite solid rocket motor (SRM) casing. Int. J Mech. Solid, 2017, 9.1: 125-138.

37. TENDEN, S.; FOSSUMSTUEN, K. IM Improvement of Rocket Motor by Composite Motor Case. Applied Vehicle Technology Panel (A VT) Fall, 2002.

38. MIL-HDBK-17F The composite materials handbook; Vol. 2FWest Conshohocken, PA: ASTM International, 2002.

39. WEERTS, Ruben AJ, et al. A methodological approach to model composite overwrapped pressure vessels under impact conditions. Composite Structures, 2021, 276: 114482.

40. STANDARD, A. S. T. M. D3039/D 3039M-08, 2008," Standard Test Method for Tensile Properties of Polymer Matrix Composite Materials", ASTM International, West Conshohocken, PA, 2008, DOI: 10.1520/D3039_D3039M-08.

41. BARBERO, Ever J.; GUTIERREZ, Joaquin M. Determination of basis values from experimental data for fabrics and composites. In: SAMPE 2012 Conference and Exhibition. 2012. p. 21-24.

42. HWANG, Tae-Kyung; KIM, Hyoung-Geun. Experimental and analytical approach for the size effect on the fiber strength of CFRP. Polymer composites, 2013, 34.4: 598-606.

43. ADAMS, Daniel O.; ADAMS, Donald F. Tabbing guide for composite test specimens. Utah Univ Salt Lake City Dept of Mechanical Engineering, 2002.

44. TEST, Standard. Methods for Constituent Content of Composite Materials. ASTM D3171, 9: 77-119.

45. ASTM D1505-98 , Standard Test Methods for Density of Plastic by the Density-Gradient Technique. Philadelphia, PA: American Society for Testing and Materials.1998.

46. DENOST, J.-P. New design concepts for filament-wound pressure vessel with unequal polar openings. In: 18th Joint Propulsion Conference. 1982. p. 1067. In 18th Joint Propulsion Conference. p. p. 1067.

47. YOUDONG, Liang; ZHENQIANG, Zou; GUOZHAO, Wang. An extension of clariaut equation and its application. Applied Mathematics-A Journal of Chinese Universities, 1997, 12.1: 1-14.

48. SO, AGARD-LS I. Design Methods in Solid Rocket Motors. 1988.

49. THESKEN, John C., et al. A theoretical investigation of composite overwrapped pressure vessel (COPV) mechanics applied to NASA full scale tests. 2009.

50. CAMANHO, P. P., et al. Three-dimensional invariant-based failure criteria for fibre-reinforced composites. International Journal of Solids and Structures, 2015, 55: 92-107.

51. RAJA, J.; SELVARAJU, S.; SRIDHAR, R. Modelling and analysis of composite pressure vessel. IJAERD, 2018, 5: 1483.

52. SHEKAR, Indu R; KOTRESH, T.S. Development of Composite Cylinders for Aerospace Applications, Indian Journal of Advances in Chemical Science 3, 2014, 33-37.

53. ERTURAN, Yakup. Development of a structural design methodology for filament winding composite rocket motor case. 2019. Master's Thesis.

54. PETERS, Stanley T.; HUMPHREY, W. Donald; FORAL, Ronald F. Filament winding-Composite structure fabrication. 1991.

55. ABOUDI, Jacob. Mechanics of composite materials: a unified micromechanical approach. Elsevier, 2013.

56. ROYLANCE, David. Introduction to composite materials. Department of material science and engineering, Massachusetts Institute of Technology, Cambridge, 2000.

57. https://tcrcomposites.com/product/product-tow.php. [Online] chrome-extension://efaidnbmnnnibpcajpcglclefindmkaj/viewer.html?pdfurl=https%3A%2F%2Ftcrcomposites.com%2Flib%2FTCR-Tow_042018.pdf&clen=1285232&chunk=true.

58. MALLICK, P. K. Processing of polymer matrix composites. CRC Press, 2017.

59. LAUDER, A. J. Manufacture of rocket motor cases using advanced filament winding processes. Material and Manufacturing Process, 1995, 10.1: 75-87.

60. FAHR, A. Ultrasonic C-scan inspection of composite materials. 1992.

61. SKAAR, Martin Welle. Modeling and testing of impact damage in composite pressure vessels. 2015. Master's Thesis. NTNU.

62. WANG, Zhenyu, et al. Curing Behavior and Thermomechanical Performance of Bioepoxy Resin Synthesized from Vanillyl Alcohol: Effects of the Curing Agent. Polymers, 2021, 13.17: 2891.

63. ROMANO, Fábio Lourenço, et al. Analysis of the coefficient of variation in shear and tensile bond strength tests. Journal of applied oral science, 2005, 13: 243-246.

64. COHEN, David; MANTELL, Susan C.; ZHAO, Liyang. The effect of fiber volume fraction on filament wound composite pressure vessel strength. Composites Part B: Engineering, 2001, 32.5: 413-429.

65. OZASLAN, E., et al. Experimental and numerical investigation of the cylinder-dome transition region of a pressure vessel. Composites Part C: Open Access, 2021, 4: 100119.

66. SHARP, Nathan D.; GOODSELL, Johnathan E.; FAVALORO, Anthony J. Measuring fiber orientation of elliptical fibers from optical microscopy. Journal of Composites Science, 2019, 3.1: 23.

67. SHIN, Yong-Chul; KIM, Seung-Mo. Enhancement of the interlaminar fracture toughness of a carbon-fiber-reinforced polymer using interleaved carbon nanotube buckypaper. Applied Sciences, 2021, 11.15: 6821.

68. KADLEC, M. et al. Fractographic Analysıs Of An Interlaminar Shear Fracture In A Carbon Fibre–Reınforced Epoxy Laminate Enhanced By Carbon Nanotubes. In: 15th European Conference On Composite Materials.2014.

69. NAITO, K., et al. Tensile and flexural properties of single carbon fibres. In: Proceedings of the 17th International Conference on Composite Materials, ICCM-17, Edinburgh, UK. 2009. p. 27-31.

70. SUEMASU, Hiroshi; SAKAJIRI, Ken. A failure mechanism of pressure vessels from filament-wound hoop layer. Journal of composite materials, 2010, 44.6: 657-673.

APPENDICES

A. Calculated COPV Length and Radius Values Corresponding to Winding Angle

Row No	Length position(mm)	Radius (mm)	Winding Angle (degree)		Row No	Length position(mm)	Radius (mm)	Winding Angle (degree)
1	0	47	90		32	81,97	73	40
2	0,06	47,07	86,9		33	84,97	73	40
3	0,32	47,35	83		34	87,97	73	40
4	1,38	48,47	75,8		35	90,97	73	40
5	4,45	51,47	65,9		36	93,97	73	40
6	7,94	54,47	59,6		37	96,97	73	40
7	11,96	57,47	54,7		38	99,97	73	40
8	12,03	57,52	54,7		39	102,97	73	40
9	12,97	58,17	53,8		40	105,97	73	40
10	15,97	60,21	51,2		41	106,03	73	40
11	18,97	62,16	49		42	109,03	72,92	40,1
12	21,97	63,97	47,2		43	112,03	72,68	40,2
13	24,97	65,63	45,6		44	115,03	72,28	40,5
14	27,97	67,12	44,4		45	118,03	71,72	40,9
15	30,97	68,43	43,3		46	121,03	70,99	41,4
16	33,97	69,58	42,4		47	124,03	70,09	42
17	36,97	70,56	41,7		48	127,03	69,03	42,8
18	39,97	71,37	41,1		49	130,03	67,8	43,8
19	42,97	72,02	40,7		50	133,03	66,39	45
20	45,97	72,5	40,3		51	136,03	64,82	46,4
21	48,97	72,82	40,1		52	139,03	63,08	48,1
22	51,97	72,98	40		53	142,03	61,2	50,1
23	54,97	73	40		54	145,03	59,2	52,4
24	57,97	73	40		55	147,28	57,65	54,5
25	60,97	73	40		56	147,52	57,49	54,7
26	63,97	73	40		57	149,62	55,97	57,1
27	66,97	73	40		58	153,36	52,97	62,5
28	69,97	73	40		59	156,63	49,97	70,1
29	72,97	73	40		60	158,83	47,72	80
30	75,97	73	40		61	159,35	47,16	85,3
31	78,97	73	40		62	159,5	47	90